Title

Plant Ecology, Evolution, and Biogeography in Insular Environments

ISBN

9798288861871

Author

Rosenblad, Kyle

Publication Date

2025-05-15

Peer reviewed|Thesis/dissertation

Plant Ecology, Evolution, and Biogeography in Insular Environments

by

Kyle Rosenblad

A dissertation submitted in partial satisfaction of the

requirements for the degree of

Doctor of Philosophy

in

Integrative Biology

in the

Graduate Division

of the

University of California, Berkeley

Committee in charge:

Professor David Ackerly, Chair
Professor Bruce Baldwin
Professor John Battles
Professor Todd Dawson

Spring 2025

Plant Ecology, Evolution, and Biogeography in Insular Environments

Abstract

Plant Ecology, Evolution, and Biogeography in Insular Environments

by

Kyle Rosenblad

Doctor of Philosophy in Integrative Biology

University of California, Berkeley

Professor David Ackerly, Chair

Island-like ("insular") environments are hotspots of rare and threatened biodiversity. These patchy environments differ markedly from their surroundings in one or more key environmental factors. For example, cool north-facing hillslopes receive less energy from the sun than their surrounding landscapes, and wet montane meadows retain more water. Consequently, insular habitats often host unique assemblages of taxa that depend on these distinctive environmental conditions. Many taxa that depend on insular environments have been negatively impacted by human land use change, which has made their habitats even rarer. This conservation challenge is exacerbated by climate change, which may push conditions in some patches beyond the tolerance of their inhabitants (e.g., too warm, too dry, etc.) or bring in new competitors that could outcompete resident taxa. As climate change progresses, it will be crucial to improve our understanding of the factors shaping dynamics of populations, species, and communities in these insular environments. In this dissertation, I focus on responses of plants to spatiotemporal environmental variation among islands and other insular environments. In Chapter 1, I examine how climate change influences tree community composition in hypothesized climatic microrefugia on north-facing hillslopes in the contiguous western United States. Chapter 2 explores how spatial variation in multiple climate variables shapes ecophysiological adaptations to climate for Lemmon's willow (*Salix lemmonii*) in island-like montane meadows of the Sierra Nevada. Chapter 3 shifts the focus to another facet of environmental variation, the biotic environment, and introduces a new method for observational studies of interspecific competition in metacommunities distributed across patches of suitable habitat. In sum, these three chapters provide complementary views on the question of how plant populations, species, and communities respond to spatial and temporal variation in conditions among insular environments.

To my parents and sister for encouraging the nature kid in me.

Table of Contents

Acknowledgments

This work would have been impossible without many forms of support from many people. My advisor, David Ackerly, provided sage advice on all aspects of my work, exciting intellectual freedom, valuable connections to other scientists, and unwavering support throughout my graduate school journey. The Ackerly Lab provided a rich, intellectually diverse environment in which to grow as a scientist. I am grateful for many enriching conversations, scientific and otherwise. I also had the fortune to meet other senior scientists who contributed greatly to my graduate school experience, including Todd Dawson, Bruce Baldwin, Rosemary Gillespie, Kathryn Baer, John Battles, Perry de Valpine, Wayne Sousa, Brent Mishler, Kipling Will, Paul Fine, Jeff Chambers, Ryan Burnett, Al Kovaleski, Jake Grossman, and Rachel Hutchinson. I am grateful to Lydia Smith, Prahlada Papper, and Ilana Stein for teaching me laboratory techniques that were central to my research. I am grateful to Andrew Johnson for helping to resolve a software development problem for Chapter 3. I am grateful to five fantastic undergraduate student research assistants, whose work helped generate the data underlying this dissertation: Evan Shi, Kendall Grajeda-Klingler, Annie Liao, Momo Hlaing, and Maia Supple. I am grateful to the generous funding organizations who put their faith in me: the National Science Foundation, the UC Berkeley Graduate Division, the Philomathia Graduate Fellowship, Sigma Xi, the Garden Club of America, the Northern California Botanists, the Botanical Society of America, and the California Native Plant Society's East Bay and Bristlecone chapters. I am grateful to my friends and family for their love and support across all chapters of my life. Most of all, I am grateful to my wife, Jessica, and our children, Maeve and Fionnuala, who infuse each day with love and inspiration.

Introduction

Insular terrestrial environments, also known as "ecological islands", often contain globally or locally rare taxa, as well as unique assemblages of taxa (Cartwright 2019). These habitats are distinguished from their surrounding landscapes by one or more key environmental characteristics, such as topography (Ackerly et al. 2020), hydrology (McLaughlin et al. 2017), lithology (Walck et al. 1996), or soil chemistry (Harrison & Rajakaruna 2011). Taxa inhabiting these environments are often absent or very rare in the surrounding "matrix" habitat, either because they are poorly adapted to the abiotic conditions, or because they are excluded by negative biotic interactions, e.g., predation or competition (Cartwright et al. 2019, Itescu 2019).

Taxa that depend on insular environments may be especially threatened by climate change (Cartwright 2019). If the climate of a habitat patch becomes unsuitable for its resident taxa (e.g., too hot, too dry, etc.), then the populations in this patch will be at risk of local extinction unless they can evolve rapidly or disperse successfully to another habitat patch with more suitable climatic conditions (Cartwright 2019). However, long distance dispersal is rare in most systems (Gillespie et al. 2012), and genetic diversity, the raw material for evolutionary adaptation, is often limited in isolated populations (Frankham 2015). Furthermore, changing climate conditions in habitat patches may bring an influx of new taxa that could outcompete residents (Schultheis et al. 2010, Cartwright 2019). Thus, without conservation management, climate change could drive population declines or even extinctions among taxa inhabiting insular environments (Cartwright 2019). However, there are important knowledge gaps regarding the ecological, evolutionary, and biogeographic processes shaping these taxa's fates (Cartwright 2019, Itescu 2019). Addressing these knowledge gaps could help improve management strategies.

In this dissertation, I explore the ecological, evolutionary, and biogeographic dynamics of plants occupying insular environments, with an eye toward conservation applications under climate change. I take three complementary approaches, each focused on a different taxonomic level, spatiotemporal scale, and set of biological processes.

In Chapter 1, I explore recent responses of forest tree community composition to changes in climate using recent 10-year repeat-census data from the USDA Forest Service's extensive FIA plot network. I first ask whether warming temperatures have shifted forest community composition in favor of species with warmer climatic niches. Using a Community Temperature Index to characterize community composition, I find that communities have shifted in the predicted direction. However, the rate of community "thermophilization" lags behind the rate of warming by tenfold. I then shift the focus to insular environments, asking whether the thermophilization process has proceeded at a different rate on cool, north-facing hillslopes. These habitats have been hypothesized to function as island-like microrefugia from climate change relative to their surrounding landscapes (Ackerly et al. 2020). Contrary to these predictions, I find that thermophilization has proceeded faster on north-facing hillslopes, and that this process is driven by disproportionate declines in species with cooler climatic niches. These findings show that climate change is outpacing rates of change in community composition for western US forests, and that climate change may erode unique biodiversity occurring on north-

facing hillslopes. This knowledge can help land managers triage species and habitats under climate change.

Chapter 2 continues the focus on plants' responses to spatial climatic variation, but with a narrower geographic and taxonomic scope. I use a common garden experiment to examine how ecophysiological traits in Lemmon's willow (*Salix lemmonii*), a socioecologically important species, respond to gradients in drought and freezing stress across 40 island-like wet meadows in Tahoe National Forest, CA, USA. I also ask whether drought and freezing resistance traits show evidence of a tradeoff, which could constrain adaptive responses to climate change. I find that *S. lemmonii* shows clinal variation in leaf turgor loss point, a measure of drought vulnerability, from -0.95 to -0.74 MPa with increasing spring snowpack. I also show that spring freezing sensitivity increases with minimum May temperature. However, these traits show no tradeoff, as the climate variables that shape them are spatially decoupled in our study region, unlike most of the Sierra Nevada. These findings demonstrate that regions where key climate variables become decoupled could serve as valuable reservoirs of heritable adaptive phenotypic variation, which might be useful sources for assisted gene flow among isolated habitats.

In Chapter 3, I shift the focus to another process influencing the dynamics of plant communities in habitat patches: interspecific competition. Interactions with competitors can strongly influence species' responses to climate change (Alexander et al. 2015). Competition is a particular point of concern for taxa inhabiting insular environments. In some cases, these environments have historically provided refuge for resident taxa from superior competitors inhabiting the surrounding matrix, and climate change could reverse this refuge effect if changing conditions facilitate immigration of new species from the matrix (Debinski & Holt 2001, Schultheis et al. 2010, Cartwright 2019). Thus, an improved understanding of competitive dynamics in habitat patches could facilitate conservation planning as species interactions become reshuffled under climate change. In many cases, the data available for studying interspecific competition include species traits and presence-absence, or abundance, across some number of sites. Most methods applicable in this scenario focus on for competitive niche differentiation, testing whether observed communities show greater trait diversity than "null" communities generated by data-reshuffling algorithms. These methods' performance may be compromised by two key issues: 1- biologically vague null models, and 2- susceptibility to trait correlations that obscure ("confound") key patterns. Here, I introduce a method that does not depend on null models, instead estimating each trait's effect on species' co-occurrence probabilities directly, while controlling for other traits. To compare my method's performance against null model alternatives, I use a simulation study of a hypothetical metacommunity, in which species with varying functional traits compete for resources across isolated patches of habitat. I show that my method outperforms 48 null model methods in detecting competitive niche differentiation. In an empirical example, I demonstrate that trees in Payette National Forest (USA) exhibit competitive niche differentiation driven by height. I detect this effect by controlling for wood density, a "convergence trait" that is correlated with height. My findings suggest my method may help users detect signals of competitive niche differentiation more accurately, clarify the roles of additional community assembly processes, and make predictions about future community dynamics under climate change.

Chapter 1

Climate change, tree demography, and thermophilization in western US forests

This chapter is reproduced from the following published article:

Rosenblad, K. C., Baer, K. C., & Ackerly, D. D. (2023). Climate change, tree demography, and thermophilization in Western US forests. *Proceedings of the National Academy of Sciences of the United States of America*, **120**(18), e2301754120.

Abstract

Climate change is driving widespread changes in ecological communities. Warming temperatures often shift community composition toward more heat-tolerant taxa. The factors influencing the rate of this "thermophilization" process remain unclear. Using 10-year census data from an extensive forest plot network, we show that mature tree communities of the western US have undergone thermophilization. The mean magnitude of climate warming over the 10-year study interval was 0.32°C, whereas the mean magnitude of thermophilization was 0.039°C. Differential tree mortality was the strongest demographic driver of thermophilization, rather than growth or recruitment. Thermophilization rates are associated with recent changes in temperature and hydrologic variables, as well as topography and disturbance, with insect damage showing the strongest standardized effect on thermophilization rates. On average, thermophilization occurred more rapidly on cool, north-facing hillslopes. Our results demonstrate that warming temperatures are outpacing the composition of western US forest tree communities, and that climate change may erode biodiversity patterns structured by topographic variation.

Introduction

Global climate change is reorganizing ecological communities (Parmesan & Yohe 2003, Scheffers et al. 2016), often in ways that are difficult to anticipate. For example, drought-driven tree mortality rates are increasing, but it remains challenging to predict when, where, and to which species mortality events will occur (Trugman et al. 2021). Successful natural resource management will depend on improved understanding of the factors governing variation in community responses to climate change.

Although community responses to climate change vary, there are likely underlying commonalities in relation to species' functional attributes or climatic niches (Harrison et al.

2020). Warming temperatures often increase the relative abundance of heat-tolerant ("thermophilic") taxa (De Frenne et al. 2013). This "thermophilization" process has been documented across many taxa, regions, and spatial scales (Feeley et al. 2020, Zellweger et al. 2020, Haase et al. 2019). However, thermophilization rates vary widely, and although they are often associated with warming rates, much variation remains unexplained.

Additional factors beyond warming rates could influence thermophilization rates. For example, many organisms, such as plants, exhibit physiological links between their water and temperature regulation mechanisms. Consequently, thermophilization rates may be associated with changes in hydrologic variables (Feeley et al. 2020). Additionally, in forests, canopy disturbance increases penetration of solar radiation into forest understories, which can accelerate changes in climate and community composition (Brice et al. 2019, Davis et al. 2019). Tree species may also be differentially susceptible to biotic factors, such as insect damage, which could influence rates of thermophilization.

Topographic features like hillslope orientation (i.e., slope and aspect) might also modify thermophilization rates. A site's hillslope orientation affects the amount of heat received from the sun, with the warmest climates occurring on equator-facing hillslopes and the coolest climates on pole-facing hillslopes. In turn, plant community composition is shaped strongly by hillslope-mediated microclimatic variation (Ackerly et al. 2020), with warmer-associated species occurring on more equator-facing hillslopes. It is less clear how hillslope orientation might interact with climate change to affect rates of change in community composition over time.

Another key step toward improved understanding of thermophilization is to examine the demographic processes underlying shifts in community composition. The average climatic niche (or "community temperature index") of a community can be quantified as the mean of all co-occurring species' temperature optima, often weighted by a metric of species' abundance. When metrics that account for each organism's size (e.g., basal area) are used, a community's temperature index can be changed by losses (mortality), gains (recruitment), or changes in size (growth) (Feeley et al. 2013, Muscarella et al. 2017). Algebraic decomposition can quantify the contributions of each of these processes to overall thermophilization (Feeley et al. 2013, Muscarella et al. 2017). Quantifying these contributions will be instrumental in predicting the long-term trajectories of ecological communities responding to climate change. For example, recruitment-driven thermophilization indicates that warm-associated propagules are recruiting successfully, which could help stabilize community biomass as climate change progresses. In contrast, mortality-driven thermophilization indicates that cool-associated taxa are being lost and not necessarily replaced by other taxa.

Here, we analyze 10-year changes in tree community composition across 44,992 forest subplots in the western United States from the USDA Forest Service Forest Inventory and Analysis (FIA) data set. Using hierarchical Bayesian models that account for latent spatial processes (Lindgren & Rue 2015), we model the mean temperature indices of tree communities over time as a

function of long-term average climate, recent climate change, topography, multiple forms of disturbance, and other predictors. We use these models to address three questions: 1) Are western US forests undergoing thermophilization? 2) What factors modify thermophilization rates? 3) What are the separate contributions of mortality, growth, and recruitment to thermophilization, and how do these contributions respond to potential thermophilization rate modifiers?

Results

In western US forest subplots, baseline community temperature index is greater in warmer regions (0.564°C community temperature index per 1°C plot mean annual temperature, in a model containing other climate variables), as well as in regions with greater climatic water deficit and precipitation (Fig. 1-2). Because continuous predictors were standardized in our models (mean = 0, standard deviation = 1), their effect sizes can be interpreted as °C per standard deviation in the given predictor, thus allowing for comparisons of effect sizes among predictors with different units.

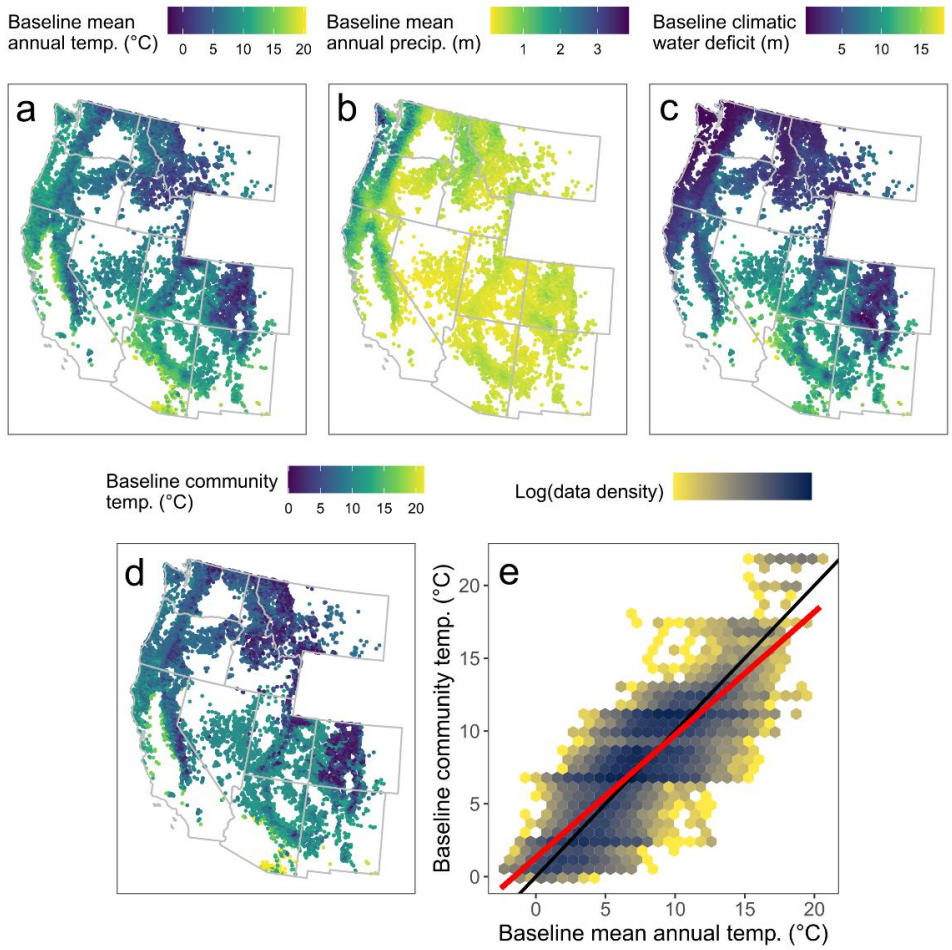

Fig. 1: a) Baseline mean annual temperature from CHELSA's climatology at 30-arcsecond (roughly 1 km) spatial resolution. b) Baseline mean annual precipitation from CHELSA's climatology. c) Baseline climatic water deficit from TerraClimate's

climatology at 1/24-degree (roughly 4 km) spatial resolution. d) Tree community temperature index. In panels a-d, the 4 subplot-scale values for each plot are summarized by a single mean value per plot. e) Tree community temperature index versus baseline mean annual temperature, with hexagons colored by data density. The red trendline, added for illustrative purposes, is generated by simple linear regression (slope = 0.843). The black "one-to-one" line has slope 1 and y-intercept 0.

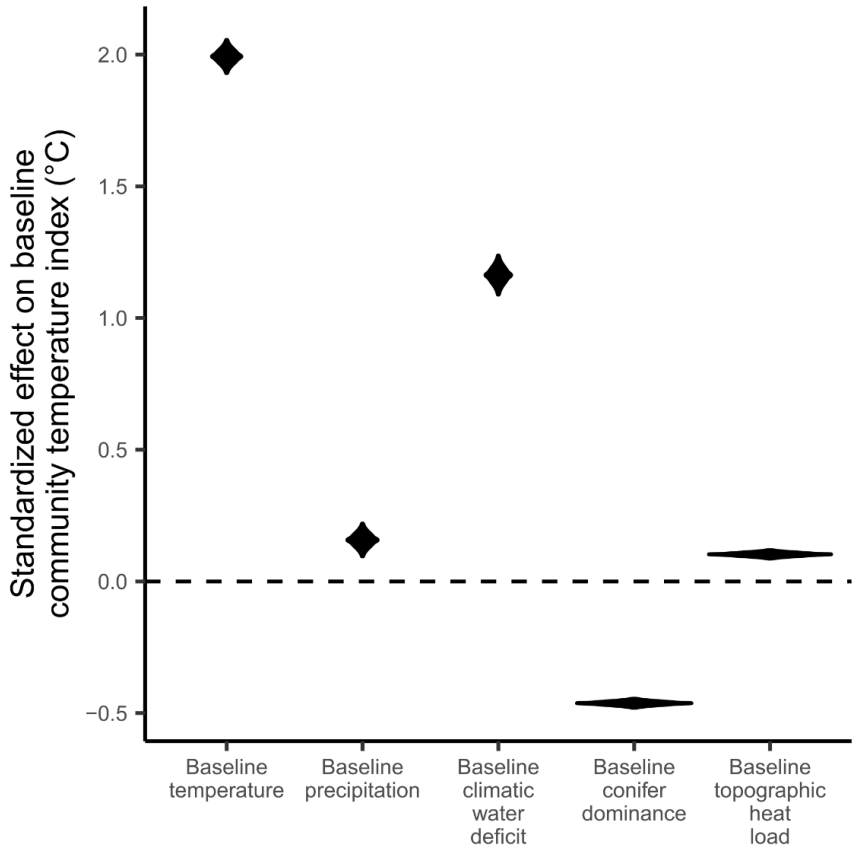

Fig. 2: Violin plot of 95% credible intervals for standardized effects of fixed predictors on baseline community temperature index in western US tree communities. Results come from hierarchical Bayesian regression models of tree community temperature index over time. Violins can be interpreted as smoothed, horizontally symmetrical histograms, with the vertical axis representing parameter values and the horizontal axis representing probability density. The total area of each violin is set to be equal, so shorter and wider violins correspond to model parameters for which the posterior probability density is more concentrated around the mean.

Forested areas in the western US have warmed on average (Fig. 3; mean temperature change = 0.32°C over 10 years). Correspondingly, the average subplot-scale tree community has shifted toward warmer-associated taxa—i.e., undergone thermophilization (Fig. 3-4). Thermophilization rates are greater in plots that warmed more (0.112°C thermophilization per 1°C warming), as well as plots that experienced greater drying, as represented by climatic water deficit and precipitation (Fig. 3-4). The mean observed thermophilization rate in western US forests is 0.00391°C/year, whereas the mean observed rate of macroclimatic warming over the same interval is approximately 0.032°C/year.

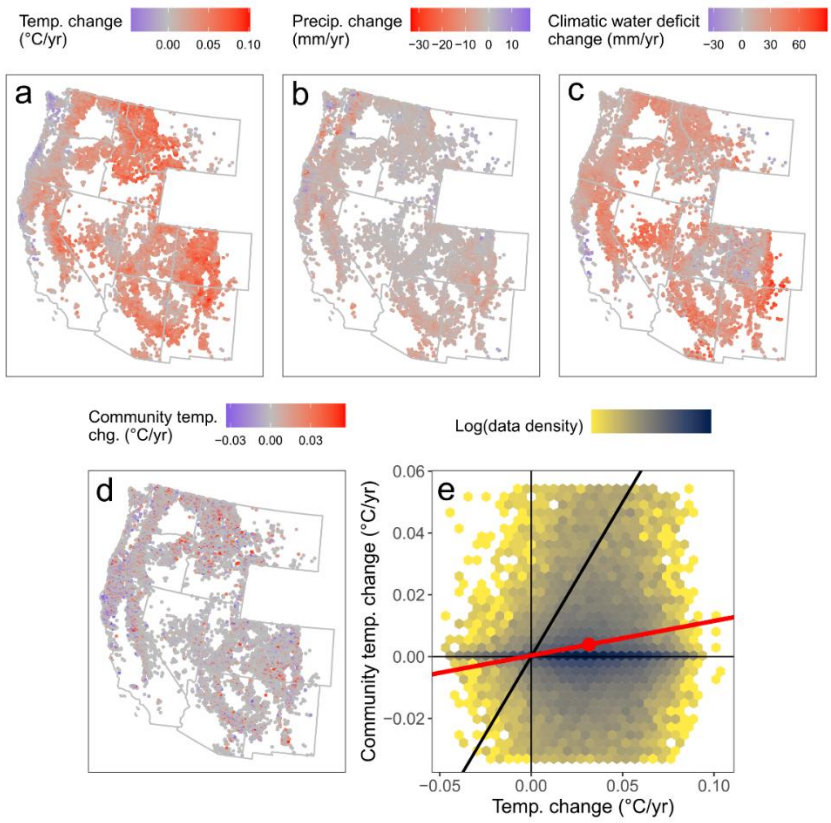

Fig. 3: a) Recent 15-year changes in mean annual temperature from gridMET data at 1/24 arcsecond (roughly 4 km) spatial resolution. b) Recent 15-year changes in mean annual precipitation from gridMET. c) Recent 15-year changes in climatic water deficit from TerraClimate data at 1/24-degree (roughly 4 km) spatial resolution. d) Recent 10-year changes in tree community temperature index. In panels a-d, the 4 subplot-scale values for each plot are summarized by a single mean value per plot. e) Change in tree community temperature index versus change in mean annual temperature. Each point represents one subplot. The red trendline, added for illustrative purposes, is generated by simple linear regression. The red point represents the mean of the x and y variables. The black "one-to-one" line has slope 1 and y-intercept 0. In a-e, points below the 5th percentile or above the 95th percentile of change in community temperature index are omitted to improve pattern visibility and color scale perceptibility.

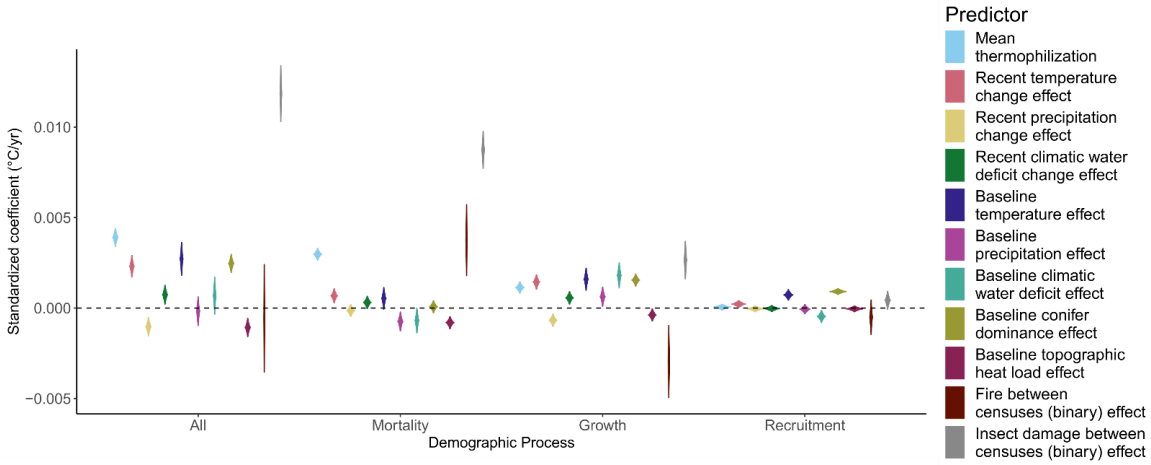

Fig. 4: Violin plots of 95% credible intervals for standardized effects of fixed predictors on the magnitude of thermophilization in western US tree communities. Results come from hierarchical Bayesian regression models of tree community temperature index

over time. Violins can be interpreted as smoothed, horizontally symmetrical histograms, with the vertical axis representing parameter values and the horizontal axis representing probability density. The total area of each violin is set to be equal, so shorter and wider violins correspond to model parameters for which the posterior probability density is more concentrated around the mean. The interval for mean thermophilization represents the effect size for a binary "T1 vs. T2" predictor that distinguishes between repeat tree censuses. The interval shown for each other predictor represent the effect size for the interaction between the named predictor and the "T1 vs. T2" predictor.

The data set comprised 316,519 trees that survived between censuses (mean = 5.6 per subplot), 64,024 that died (1.1 per subplot), and 35,836 that recruited (0.63 per subplot). Per-tree growth and mortality rates are shown in Fig. S1.1. Mortality contributed most to thermophilization, followed by growth, with minimal contributions from recruitment (Fig. 4). In this analysis, recruitment is considered as entry into the 12.7 cm DBH class (diameter at breast height). In a separate analysis of saplings in the 2.5 cm to 12.7 cm DBH class, we found that the contribution to thermophilization of recruitment at the 2.5 cm threshold was also negligible (Fig. S1.2).

Using data from only the portions of each subplot where saplings were recorded (DBH 2.5-12.7 cm), we found that 87% of trees recorded as new 12.7 cm class recruits in the second census had been recorded as saplings in the baseline census. For another 9% of new 12.7 cm class recruits, there was no record of a matching sapling in the baseline census, but there was at least one conspecific seedling with DBH less than 2.5 cm (which are counted but not marked individually). The remaining 4% of new 12.7 cm class recruits had likely not germinated yet at the baseline census.

Mortality-driven and recruitment-driven thermophilization were greater in plots that warmed more (Fig. 4). Growth-driven thermophilization was greater in plots that increased more in temperature and climatic water deficit, as well as plots that decreased more in precipitation (Fig. 4).

Initial community temperature index was greater on warm, south-facing slopes (Fig. 2)—i.e., those with high topographic heat load. Thermophilization was greater on cool, north-facing slopes (Fig. 4). This pattern was driven primarily by mortality (Fig. 4).

Thermophilization was greater at sites where insect damage was observed between surveys (Fig. 4). The effect of this binary predictor on thermophilization rates is stronger than the effect of a one-standard-deviation change in any of our continuous predictors, as well as the effect of our binary fire predictor. Similar patterns appear for mortality-driven and growth-driven thermophilization (Fig. 4).

The 95% credible interval for the net effect of fire on thermophilization rates overlaps zero substantially (Fig. 4). However, fire had opposite effects on mortality-driven and growth-driven thermophilization. In subplots that burned between censuses, mortality-driven thermophilization was stronger than in unburned subplots, whereas growth-driven thermophilization was weaker (Fig. 4).

Thermophilization was greater in conifer-dominated subplots (Fig. 4). This pattern appears in growth-driven thermophilization, as well as in the analysis of recruitment to the 12.7 cm DBH class (Fig. 4).

All effect sizes are shown in Tables S1.1-1.3, including those not shown in figures. These include the "effects" of fire, insect damage, and recent changes in climate variables on baseline community temperature index. It would be incorrect to interpret these associations as direct causes because the events described by these predictors occurred after baseline community temperature index was measured. Instead, they may reflect causal relationships involving unmeasured covariates (Pearl 2009). Mapped predictions from fixed effects only are shown in Fig. S1.3, and mapped random effect values are shown in Fig. S1.4.

Discussion

Our analyses reveal widespread, fine-grained patterns of change in western US forest tree communities. Subplot-scale community composition has shifted in favor of tree taxa with higher temperature niche means (Fig. 3-4). We quantified this thermophilization process using community temperature indices—i.e., weighted averages of species' climatic niche means in each subplot at each time point. Similarly, baseline community temperature indices are higher in plots with higher multi-decadal baseline mean temperatures (Fig. 1-2). These results suggest that the observed changes in forest composition were driven at least in part by recent warming.

Thermophilization in western US forests is also associated with drying conditions. This trend is represented in our analyses by the negative effect of precipitation changes and the positive effect of climatic water deficit changes (Fig. 4), which were modeled alongside the effect of temperature in our hierarchical Bayesian models. (Variance inflation factors for all predictors were less than 5, although some predictors are moderately correlated, with the greatest Pearson correlation of 0.65 occurring between baseline temperature and baseline climatic water deficit.) These patterns are consistent with the hypothesis that tree species from warmer climate zones are better adapted to the increased evaporative demands caused by increasing temperatures. This hypothesis is further supported by the positive association we find between baseline community temperature index and baseline climatic water deficit in our hierarchical Bayesian regression models.

Although most patterns we found are consistent with warming and drying as drivers of thermophilization, some associations suggest more complex processes may have operated during or before our study's timeframe. For example, baseline community temperature index is greater in plots with greater precipitation (Fig. 2). Additionally, although the effect of baseline temperature on baseline community temperature index in our data is near the commonly expected value of 1 in a univariate, OLS linear regression (Fig. 1e), the effect is only 0.564 in our full hierarchical Bayesian regression model, likely reflecting complex causal relationships

among community temperature index and the other climatic variables. While effects of precipitation require further consideration, the strongest effects in our data point to warming and drying as the predominant climatic drivers of thermophilization in western US forests.

Thermophilization rates in western US forests are lagging behind macroclimatic warming rates by roughly tenfold. Our results suggest that western US forests are becoming mismatched with their environments. Should the observed trends continue, macroclimatic temperatures will increase by roughly 3°C on average by the end of the century, whereas the average community temperature index will increase by less than half a degree, thereby adding over 2.5°C in "climatic debt" (Bertrand et al. 2016, Richard et al. 2021). This debt will compound any debt these communities may have already accrued due to earlier anthropogenic climate change, migration lags following glacial retreat (Svenning and Skov 2004), or other factors that may have restricted species' realized climatic niches (Sax et al. 2013). The timeframe of our study coincided with severe drought events in the western US (Crockett & Westerling 2018), so it is possible that the patterns we observed are more extreme than future trends will be. However, recently developed climate models indicate that drought is expected to become increasingly frequent and severe in the western US, and that the timeframe of our study may provide a reasonable preview of upcoming climate change (Crockett & Westerling 2018). Moreover, to the extent that drought accelerated mortality, it could have led to higher rates of thermophilization, notwithstanding the tenfold lag we observed. Disturbances allow for more rapid forest turnover and in some circumstances may allow plant communities to better track changing environments and minimize climate debt (Brice et al. 2019).

The consequences of climatic debt may be particularly severe for western US forests because recent thermophilization has been driven primarily by mortality, with little influence from recruitment to the small-tree size class (Fig. 4) or recruitment of smaller saplings (Fig. S1.2). These patterns indicate that in most subplots, the tree taxa that recruited over the study interval have thermal niches that are no warmer on average than the baseline communities into which they recruited. Instead, thermophilization has mostly resulted from mortality among taxa with the coolest thermal niches. If thermophilization continues to be driven by mortality, then climate change may threaten ecosystem services more strongly than a simple extrapolation of climatic debt might suggest. In this scenario, not only will 3°C of warming occur, but the 0.5°C of thermophilization that occurs in response will be due to losses of the most climatically vulnerable species—not recruitment of warmer-associated species that can cope better with warming conditions. These increasingly maladapted forests would likely decline in their ability to provide ecosystem services, such as carbon sequestration (Aitken et al. 2008).

The lack of evidence we find for recruitment-driven thermophilization contrasts with another recent study, which found that hotspots of fecundity and seedling recruitment for western US tree species are shifting toward cooler, moister regions at a rate roughly commensurate with observed climate change (Sharma et al. 2022). This difference in results between studies might be explained by the difference in demographic scope, as our study does not examine seedling

dynamics directly, instead examining recruitment of saplings and small trees. If this explanation for the discrepancy in results is correct, then mature tree communities could be primed for more rapid recruitment-driven thermophilization in the coming decades as the current cohorts of seedlings mature. Ackerly et al. (2020) predicted that thermophilization driven by seedling recruitment will occur faster on pole-facing hillslopes due to shorter dispersal distances for warmer-associated propagules from communities on adjacent equator-facing hillslopes. Alternatively, our study's contrasting findings may be explained by the difference in the spatial grain of analysis. There may be a lag between the time when the first seedling of a species recruits anywhere within a new macroclimatic zone and the time when conspecifics have spread to a substantial number of forest plots within that new zone. If this explanation is correct, then the species composition of new recruits in western US forests will likely continue to lag behind climate change.

In addition to climatic predictors, recent thermophilization rates in western US forests are associated with several non-climatic predictors. Thermophilization rates are roughly three times greater in subplots with recorded evidence of insect damage (Fig. 4). This is the strongest effect size of all thermophilization "rate modifiers" we considered. There is likely at least an indirect causal link between insect damage and thermophilization because some insects, such as bark beetles, attack drought-stressed trees preferentially (Anderegg et al. 2015). Insect damage could be an indicator of drought patterns occurring at finer spatiotemporal scales than our predictor variables can capture. Additionally, insect damage may have a direct influence on thermophilization if insect-driven canopy loss accelerates microclimatic change in the understory (Stevens et al. 2015, Govaert et al. 2021).

We find little evidence for a net effect of fire on thermophilization rates in western US forests over the 10-year study interval (Fig. 4). However, fire appears to have exerted opposite effects on mortality-driven and growth-driven thermophilization. In subplots that burned between censuses, mortality-driven thermophilization was stronger than in unburned subplots, whereas growth-driven thermophilization was weaker (Fig. 4). A previous study of western US forests found that cool-associated tree taxa have functional traits associated with poor fire tolerance (Stevens et al. 2020), suggesting that fire may disproportionately kill cool-associated taxa. Our results support this prediction. It is unclear why the pattern might be opposite for growth-driven thermophilization. This pattern may reflect features of the postfire environment that disproportionately benefit cool-associated taxa, like decreased competition for moisture, or harm warm-associated taxa, like decreased canopy-mediated thermal buffering during winter (De Frenne et al. 2019). It is also possible that the probability of fire occurring during the census interval was influenced by the balance between growth of cool-associated and warm-associated taxa. Our data on fire occurrence, as well as insect damage, are coarse, and further study is needed on the influence of these processes on thermophilization.

Our analyses indicate that topography influences thermophilization in western US forests. Thermophilization was strongest on cool, pole-facing (i.e., north-facing) hillslopes, and this

pattern is driven by mortality and growth (Fig. 4). We also find that warmer, more equator-facing sites were occupied by warmer-associated tree taxa at baseline (Fig. 2). For example, our data indicate that at 45°N latitude, the expected difference in community temperature index between a community on a 30° north-facing hillslope facing north and a 30° south-facing hillslope is 0.372°C based on our data. However, it is not clear why thermophilization rates are greatest on pole-facing hillslopes. This pattern would be expected if the rates of change in microclimatic conditions—i.e., exposure to climate change (Williams et al. 2008)—vary with hillslope orientation (MacLean et al. 2017, Ashcroft et al. 2009). Alternatively, thermophilization might be faster on pole-facing hillslopes because tree community sensitivity to climate change (as opposed to exposure [Williams et al. 2008]) varies with hillslope orientation. Hillslope orientation could have affected historical disturbance regimes (Moody & Martin 2001), which may have shaped variation in resident tree species' climatic niches (Stevens et al. 2015) and, thus, their sensitivity to climate change.

Because western US tree communities on pole-facing hillslopes are undergoing thermophilization more rapidly than equator-facing neighbors, community temperature indices are becoming more similar between adjacent pole- and equator-facing slopes. In topographically heterogeneous landscapes, this process could drive biotic homogenization—a reduction in spatial turnover in community composition among subplots (Ackerly et al. 2020, McKinney & Lockwood 1999)—as well as declines in landscape-scale species richness. Fig. 5 shows a hypothetical example. This trend could be a bellwether of more pervasive future climate-driven biodiversity loss in topographically heterogeneous landscapes. When biotic homogenization is driven by extirpations, the homogenizing effect of each successive extirpation grows (Rosenblad et al. 2017). More work is needed to explore the extent and consequences of climate-driven homogenization in topographically heterogeneous forests.

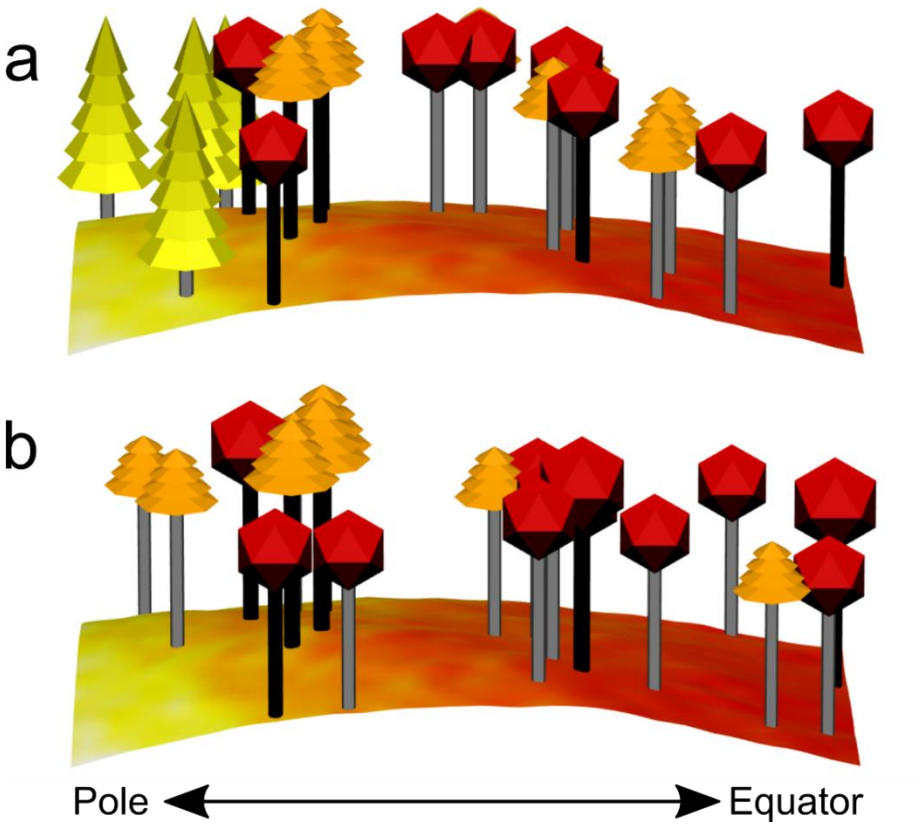

Fig. 5: Before (a) and after (b) views of a topographically heterogeneous landscape occupied by a hypothetical tree community that exemplifies key trends in our data. Effect sizes are magnified for illustrative purposes. Three tree species are shown with three different temperature indices: a low temperature-associated species (5 long crown layers shown in yellow, styled after *Abies*), a medium temperature-associated species (4 short crown layers shown in orange, styled after *Pinus*), and a high temperature-associated species (an icosahedral crown shown in red, styled after deciduous trees). Trees with black trunks were present at both time points. Trees with gray trunks were only observed in one time point, due either to mortality (present in panel a only) or recruitment (present in panel b only). Topographic heat load ranges from low (yellow) on the pole-facing hillslope (left) to high (red) on the equator-facing hillslope (right).

Our study underscores the utility of large data sets with high spatial replication for early detection of biotic responses to climate change, such as thermophilization, accrual of climatic debt, and biotic homogenization. These results could provide a crucial preview of future changes in western US forests that will unfold over longer timescales. We also demonstrate the importance of analyzing the demographic processes underlying thermophilization, showing that western US forests are suffering disproportionately rapid mortality of tree taxa with cool thermal niches, and that new recruits do not have warmer thermal niches than their recipient communities. Additionally, we reveal non-climatic factors that may modify thermophilization rates, including insect attacks and topographic heat load. Our findings elucidate the mechanisms by which ecological communities respond to climate change, as well as highlighting concerning trends in western US forest dynamics that can help inform management strategies.

Materials and Methods

Forest plot data:

We used the USDA Forest Service's (USFS) Forest Inventory and Analysis Program (FIA) plot network (Bechtold & Patterson 2005) to quantify changes in western US forest composition over recent 10-year intervals, with baseline plot censuses occurring from 2000 through 2008 and resurveys from 2010 to 2018. FIA uses a randomized systematic sampling approach in which plots are randomly located within hexagonal grid cells of approximately 2428 hectares. We used data collected solely from Phase 2 FIA plots classified as forested (≥10% tree canopy cover), excluding plots that were only partially covered by forest, in the following US states: New Mexico, Arizona, California, Nevada, Utah, Colorado, Idaho, Oregon, Washington, and Montana. (Wyoming plots had not been re-censused at the time of data download.) Each plot comprises four circular subplots, each with a radius of 7.32 m. Within each subplot, the diameter at breast height (DBH) of each tree with a DBH of at least 12.7 cm was measured. For all subplots, we disregarded any trees recorded more than 7.32 m from the subplot center so that all sampling units in our analyses were equivalent. In our main analyses, we also disregarded saplings with DBH less than 12.7 cm, which were recorded in 2.07 m microplots within the main plots. We used the sapling data for supplementary analyses described below. Additional data filtering protocols are described in the Supplementary Methods, and all data filtering and preparation steps are shown with comments in our publicly available R code. Forest plots are marked, allowing census protocols to be repeated precisely. Our unit of analysis is the subplot, and our regression models included random effects to account for non-independence among subplots within the same plot (details below). In total, we analyzed data from 44,992 subplots.

Quantifying community temperature index:

We quantified temperature index values for each of the 110 species in the data set using three approaches, which are described in the Supplementary Methods: modeled niche means, modeled niche optima, and simple niche means. These values are calculated in °C and reflect a measure of the mean or optimal value of mean annual temperature for each species across its geographic range in the western United States. (The mgcv R package [Wood 2017] was used for thermal niche modeling, and CHELSA [Karger et al. 2017, 2018] was used for climate data.)

To quantify the mean community temperature index in each subplot's tree community at each timepoint, we calculated the mean temperature index value across all species using each of the three niche modeling methods detailed in the Supplementary Methods, weighted by the basal area of each species.

Regression models of thermophilization:

Our regression models were built in a Bayesian framework using R-INLA. We used community temperature index in one subplot at one time point (either "T1" or "T2") as a response variable (Y_{ijk}). The subscript "i" denotes the i^{th} plot, "j" denotes the j^{th} subplot, and "k" denotes our binary timescale (T1 or T2). We tested for changes over time (i.e., thermophilization) using a

binary "T1 vs. T2" indicator variable as one of our predictors (x_{1k}). Its coefficient (β_1) represents the mean change in community temperature index between censuses, which are 10 years apart for all sites in our data set. A zero value of x_{1k} represents T1, and a one value represents T2.

Fixed effects representing climate in our regression models include baseline mean annual temperature, baseline mean annual precipitation, baseline mean annual climatic water deficit, and temporal changes in the same three variables. These six plot-level variables are denoted by $x_{2i} \ldots x_{7i}$ with coefficients $\beta_2 \ldots \beta_7$. Topographic heat load for each subplot is denoted by x_{8ij} with coefficient β_8, and the binary fire and insect damage variables are denoted by $x_{9ij} \ldots x_{10ij}$ with coefficients $\beta_9 \ldots \beta_{10}$. x_{11ij}, with coefficient β_{11}, denotes the subplot's baseline percent basal area of conifers, which have distinctive temperature and water regulation physiology and represent a large component of western US forests. Each subplot is represented by two observations in the data set (one at T1 and one at T2), and the values for each of the above predictors are equal in each set of paired T1 and T2 observations. Only the value of x_{1k} (the binary T1 vs. T2 indicator) differs, with the T1 observations receiving a zero value. Consequently, the coefficients $\beta_2 \ldots \beta_{11}$ on their own represent their associations with baseline (T1) community temperature indices. Similarly, the y-intercept (β_0) represents the mean of the T1 observations—i.e., the mean baseline community temperature index.

We also included interactions between x_{1k} (the T1 vs. T2 predictor) and each other predictor to test the modifying effects of these predictors on temporal changes in community temperature index (i.e., thermophilization rates). These interactions are denoted by $x_{1k}x_{2i} \ldots x_{1k}x_{11ij}$ with coefficients $\beta_{12} \ldots \beta_{21}$. For example, in the interaction between x_{1k} (the T1 vs. T2 variable) and x_{8ij} (topographic heat load), the coefficient (β_{18}) represents the mean effect of topographic heat load on thermophilization rates.

Random effects in our regression models include a subplot-level normally distributed random effect (v_{ij}), as is typically used in linear mixed effects modeling, and a plot-level spatially covarying random effect u_i. The plot-level spatial random effect is modeled using a Matérn covariance structure in a Gaussian Markov Random Field, which is computed as the solution to a stochastic partial differential equation using the finite element method (Lindgren et al. 2011).

The full model structure is written below:

$$Y_{ijk} \sim N(\mu_{ijk}, \sigma^2)$$

$$\mu_{ijk} = \beta_0 + \beta_1 x_{1k} + \beta_2 x_{2i} + \beta_3 x_{3i} + \beta_4 x_{4i} + \beta_5 x_{5i} + \beta_6 x_{6i} + \beta_7 x_{7i} + \beta_8 x_{8ij} + \beta_9 x_{9ij} + \beta_{10} x_{10ij} + \beta_{11} x_{11ij} + \beta_{12} x_{1k} x_{2i} + \ldots + \beta_{21} x_{1k} x_{11ij} + u_i + v_{ij}$$

$$u_i \sim GMRF(0, \Sigma)$$

$$v_{ij} \sim N(0, d^2)$$

We used R-INLA's default uninformed (i.e., "flat") prior probability distributions for all parameters.

Changes in forest composition (including size distributions) over time reflect three distinct demographic processes: mortality, growth, and recruitment of small individuals into the minimum censused size class. In our analyses, "recruitment" denotes entry into the 12.7 cm and above size class, as smaller individuals were not recorded. Consequently, recruitment rates reflect the combined effects of reproduction (both in situ and dispersal from outside the plot), germination and seedling establishment, and seedling and sapling growth to reach this size threshold.

To quantify the contributions of each demographic process to thermophilization, we repeated the regression analysis described above with three additional versions of the community temperature index response variable (Feeley et al. 2013, Muscarella et al. 2017), Y_{ijk}. The predictors and the T1 values of Y_{ijk} are unchanged in all models, whereas the T2 values of Y_{ijk} represent the effects of different demographic processes. In the "recruitment" model, all individuals that recruited between censuses are included at their observed diameter at breast height (DBH) values, any trees that died are treated as still alive using the DBH observed in the first census, and any trees that survived are fixed at zero net growth—i.e., their DBH for the second census is equal to the value observed in the first census. In the "growth" model, all individuals that recruited between censuses are omitted in the second census, all individuals that survived are included with their observed T1 and T2 DBH values, and mortality is ignored as described above. In the "mortality" model, new recruits are ignored as described above, net growth for surviving trees is fixed at zero as described above, and any trees that died are recognized as absent in the second census. Fig. 6 shows a visual example of our analytical approach to isolating the effects of the three demographic processes.

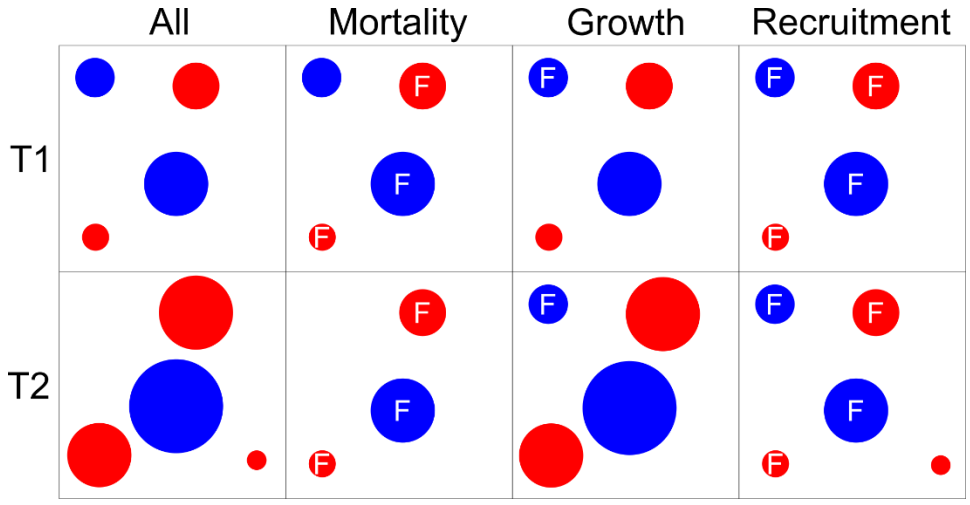

Fig. 6: Schematic of our approach to isolating each demographic process's contribution to changes in tree community temperature index. Circles represent trees of two species (red and blue) as considered by each of four analytical methods, which

are represented by the four columns. The T1 community is considered the same way in all columns, whereas the T2 community differs. Trees marked with "F" are considered to have remained at fixed size between censuses. In the "All" column, all demographic processes (mortality, growth, and recruitment) are considered. In this example, one individual dies, three grow, and one recruits into the community. In the "Mortality" column, the effects of growth and recruitment are excluded, such that any trees present at both time points are held at constant size, and any trees that recruited are ignored. In the "Growth" column, the effects of mortality and recruitment are excluded, such that all trees that died are considered to have survived (but not grown) and all trees that recruited are ignored. In the "Recruitment" column, the effects of mortality and growth are excluded, such that all trees present at the first time point are considered to have remained present at constant size.

We built a separate version of the "recruitment" model for the sapling data (DBH 2.5 cm to 12.7 cm) to explore the sensitivity of our results to the 12.7 cm DBH recruitment threshold. Community weighted niche means were computed as described above, except only trees in the sapling class were considered. The model structure was identical to that described above.

All continuous predictors were centered and scaled (mean 0, standard deviation 1). Each model was built twice; once with dummy coding for binary predictors (presence or absence of fire and insect damage), and once with weighted effect coding for these predictors. Weighted effect coding of categorical predictors produces, for each category, an estimate of the deviation from the population mean, while accounting for differences in numbers of observations among categories (Te Grotenhuis et al. 2017). We included this second coding scheme to obtain estimates of population mean thermophilization.

Among the three versions of community temperature index we generated (see Supplementary Methods), Pearson correlation values are all greater than 0.95 (Fig. S1.5). For simplicity, the main results presented here represent only the "modeled niche mean".

Status of new recruits:

We used the sapling data (DBH 2.5 cm to 12.7 cm), along with the FIA seedling data set (DBH less than 2.5 cm), to check the status of each new recruit to the 12.7 cm DBH class at the baseline census: present as a sapling, likely present as a seedling (although individual seedlings were not marked), or not yet germinated.

Data sources for predictors:

Our mean annual temperature and mean annual precipitation predictors, which we used to quantify broad, macroclimatic variation among climate zones, were extracted from CHELSA's 1981-2010 climatologies (Karger et al. 2017, 2018). We used the temperature change and precipitation change predictors to quantify climate change over a time interval relevant to the observed changes in vegetation. For each plot, we extracted daily temperature and precipitation data at 4 km resolution from gridMET (Abatzoglou 2013) and calculated the difference in mean values between two time intervals, where t is the year of the first census: t-19 through t-5, and t-4 to t+10. These sliding-window measures average over short-term interannual variability to quantify climate change over a 15-year interval, rather than the 10-year interval between tree

censuses, and begin earlier to account for potential lagged effects of climate on vegetation (Evers et al. 2021).

Baseline climatic water deficit (CWD), as well as recent changes in climatic water deficit, were computed from TerraClimate data (Abatzoglou et al. 2018). Annual climatic water deficit was computed as the sum of positive monthly climatic water deficits, where deficit equals potential evapotranspiration (PET) minus actual evapotranspiration (AET).

In the publicly available FIA data set, plot geographic coordinates are subject to a "fuzzing and swapping" protocol designed to prevent unauthorized site access and ensure confidentiality of private data (Bechtold & Patterson 2005). "Fuzzing", which applies to all plots, displaces plot coordinates by up to 0.8 km in a random direction in most cases, or up to 1.6 km for a small subset of plots. "Swapping", which only affects up to 20% of plots on private land, trades coordinates between plots on private land in the same county. We assume that fuzzing and swapping introduced random noise into our extracted climate data, but not systematic bias.

The remainder of our predictors are generated from within the FIA data set. Topographic heat load is calculated from slope and aspect, which were measured by field crews for each subplot, as well as latitude, which is provided in fuzzed and swapped form as described above (McCune & Keon 2002). This variable is a measure of the extent to which energy from the sun warms each microsite. Fire damage and insect damage are binary predictors recorded by field crews that indicate whether each type of damage was observed to have affected at least 25% of the vegetation in each subplot between censuses (or 50% of an individual species' damage count).

Software:

We used R software for all data processing, analysis, and visualization, including the following packages: raster (Hijmans 2020), R-INLA (Rue et al. 2009), mgcv (Wood 2017), ggplot2 (Wickham 2016), patchwork (Pedersen 2020), ncdf4 (Pierce 2019), foreach (Microsoft & Weston 2020a), doParallel (Microsoft & Weston 2020b), rgdal (Bivand et al. 2021), spData (Bivand et al. 2020), sf (Pebesma 2018), adehabitatHR (Calenge 2006), rgeos (Bivand & Rundel 2020), usdm (Naimi et al. 2014), and rcartocolor (Nowosad 2018).

Transition to Chapter 2

In Chapter 1, I explored responses of forest tree communities to recent climate change across the western US, asking whether cool north-facing hillslopes function as microclimatic refugia for cool-associated taxa. I found that cooler-associated taxa were, in fact, disproportionately lost from these north-facing microhabitats. Chapter 2 narrows the focus geographically and taxonomically, while continuing to examine responses of plants to spatial variation in climate across insular habitats. Here, I use a common garden to examine how intraspecific variation in ecophysiological traits for Lemmon's willow (*Salix lemmonii*) relates to gradients in drought and freezing stress among island-like meadows in California's Sierra Nevada.

Chapter 2

Climatic variation allows montane willows to escape an adaptive trade-off

This chapter is reproduced from the following published article:

Rosenblad, K.C. and Ackerly, D.D. (2024), Climatic variation allows montane willows to escape an adaptive trade-off. New Phytol, 244: 265-276. https://doi.org/10.1111/nph.20028

Abstract

Adaptive responses to climate change, based on heritable variation in stress tolerance, may be important for plant population persistence. It is unclear which populations will mount the strongest future adaptive responses. It may be fruitful to identify populations that have escaped tradeoffs among performance traits, which can hinder adaptation. Barring strong genetic constraints, the extent of tradeoffs may depend on spatial relationships among climate variables shaping different traits. Here, we test for climate-driven ecotypic variation and tradeoffs among drought and freezing sensitivity, and growth, for Lemmon's willow (*Salix lemmonii*) in a common garden study of 90 genotypes from 38 sites in the Sierra Nevada, USA. *S. lemmonii* exhibits ecotypic variation in leaf turgor loss point, a measure of drought sensitivity, from -0.95 to -0.74 MPa along a gradient of spring snowpack. We also find variation in spring freezing sensitivity with minimum May temperature. However, we find no tradeoff, as the climatic gradients shaping these traits are spatially uncorrelated in our study region, despite being negatively correlated across the Sierra Nevada. Species may escape adaptive tradeoffs in geographic regions where climate variables are spatially decoupled. These regions may represent valuable reservoirs of heritable adaptive phenotypic variation.

Introduction

Different populations of the same species can exhibit varying, sometimes counterintuitive responses to climate change (Compagnoni et al. 2021, Oldfather & Ackerly 2021, Leites et al. 2023, Perret et al. 2024). This variation may result partly from genetic variation among populations, with some harboring stronger adaptive potential than others (Hoffmann & Sgrò 2011, Alberto et al. 2013). However, for many species, it is unclear which populations are best positioned to mount adaptive responses to future climate change. Identifying these populations would be valuable for conservation, restoration, and assisted gene flow, whereby new genotypes are introduced in vulnerable populations to boost population mean fitness (Aitken et al. 2013).

Spatial patterns of adaptive potential might be clarified by exploring how climate shapes tradeoffs among performance traits (Antonovics 1976, Schluter 1996, Fletcher et al. 2022, Terasaki Hart & Wang 2024). Climate change exposes organisms to multiple forms of abiotic stress (Anderegg et al. 2019, Zohner et al. 2020, Doughty et al. 2023), and tradeoffs can greatly impede adaptation to these stressors (Antonovics 1976, Walsh & Blows 2009, Kelly et al. 2016). For example, population mean drought sensitivity might decrease along a gradient from cooler to warmer locations, whereas freezing sensitivity might increase (Laanisto & Niinemets 2015, Rueda et al. 2017, McCulloh et al. 2023, Pavanetto et al. 2024). This tradeoff could hinder future adaptive responses if climate change intensifies both drought-driven and freezing-driven selection. (Although global mean temperatures are increasing, the changing seasonality of freezing events is making them more dangerous for some taxa [Zohner et al. 2020].) In this example, genotypes conferring low sensitivity to both drought and freezing are rare or absent. Consequently, if drought-induced and freezing-induced selection intensify, populations will struggle to adapt and persist unless genotypes conferring resistance to both stressors are produced sufficiently fast. Generating such genotypes requires introduction of novel alleles or realignment of genetic correlations, both of which may be prohibitively slow (Etterson & Shaw 2001, Hellman & Pineda-Krch 2007, Walsh & Blows 2009). Additionally, even if only one climatic stressor will impose strong future selection—e.g., drought—another may drive strong selection in the present—e.g., freezing—and assisted gene flow efforts must avoid maladaptation to both present and future conditions (Aitken et al. 2013). Lastly, stress resistance can trade off with other important performance traits like growth (Montwé et al. 2015, Piper & Fajardo 2023, Visakorpi et al. 2024). Thus, populations that do not exhibit tradeoffs may constitute valuable sources for assisted gene flow. It remains unclear where populations that have avoided tradeoffs might be found.

Adaptive tradeoffs in performance traits can result from a spectrum of genomic mechanisms, which vary in prospects for escape (Garland 2014). At one extreme is antagonistic pleiotropy, whereby a single genetic locus affects one trait positively (with respect to fitness) and another trait negatively (Caspari 1950), possibly due to an organismal-level physiological tradeoff (Bloom et al. 1985). For example, one allele might confer low drought sensitivity and high freezing sensitivity, and an alternative allele might confer the opposite. This tradeoff is inescapable without introduction of a new allele (e.g., via mutation). At the opposite extreme, adaptive tradeoffs can result from spatially correlated selection gradients acting on unlinked loci (Anderson et al. 2011, Anderson et al. 2013) without any intrinsic physiological tradeoff. For example, in hot, dry environments, an allele that decreases drought sensitivity might be strongly adaptive, whereas an allele at another locus that decreases freezing sensitivity might be neutral. In cold, snowy environments, this selection pattern might be reversed. Consequently, drought and freezing sensitivity are expected to vary in opposite directions among these environments (Garland 2014). In principle, this tradeoff could be avoided in an environment that has selected for resistance to both stressors (e.g., very cold and dry). However, such environments may be unavailable. This example illustrates that when performance traits are free of strong genetic constraints (e.g., antagonistic pleiotropy), the strength of tradeoffs among populations or ecotypes may depend at least partly on spatial variation in climate.

Here, we quantify climate-driven ecotypic variation in drought and freezing sensitivity, as well as growth, for Lemmon's willow (*Salix lemmonii*), a socially and ecologically important species in Tahoe National Forest, USA (Anderson 2013, Vernon et al. 2019). Our common garden study comprises 90 genotypes collected from 38 provenance sites. As a measure of drought sensitivity, we characterize ecotypic variation in leaf turgor loss point (Ψ_{TLP}) using pressure-volume curves. We quantify variation in spring freezing sensitivity with a post-freeze shoot viability experiment. Using a suite of climate variables (April snowpack, minimum May temperature, and actual evapotranspiration), we characterize the climatic gradient shaping each trait. April snowpack (an indicator of growing season moisture availability) and minimum May temperatures are negatively associated across *S. lemmonii*'s Sierra Nevada-wide range, suggesting that natural selection could have shaped an adaptive tradeoff between adaptations to summer drought and spring freezes. However, these variables are spatially decoupled in Tahoe National Forest (Fig. 1), suggesting that natural selection may be less likely to produce a tradeoff in this region. Finally, we test for population-level tradeoffs among traits, and we explore the management implications of our results.

Materials & Methods

Study system:

Salix lemmonii Bebb is a widespread, abundant woody shrub in western North America (Argus 2007). In the high Sierra Nevada and southern Cascade ranges, *S. lemmonii* primarily occupies wet montane meadows and riparian corridors (Argus 2012). It is integral to Indigenous cultural practices (Anderson 2013), provides habitat for endangered wildlife, and features integrally in meadow restoration efforts due to its capacity for rapid growth and streambank stabilization (Vernon et al. 2019). *S. lemmonii* is dioecious and often reproduces from seed, but it can also reproduce clonally from shoot cuttings, facilitating common garden establishment. Field observations from the 2012-2016 Sierra Nevada megadrought suggest that many *S. lemmonii* populations may be vulnerable to intensifying drought under climate change (Burnett, R. pers. comm.). Restoration practitioners are seeking ways to increase resilience of new willow plantings to a more drought-prone future without compromising other important performance traits, like freezing sensitivity or growth (Burnett, R. pers. comm.).

The *Salix lemmonii* genotypes sampled in this study come from 90 individuals in 38 montane meadows across Tahoe National Forest in the northern Sierra Nevada, USA (Fig. 1) occurrences outside Tahoe National Forest are from the Global Biodiversity Information Facility (GBIF 2024). The 38 meadow provenance sites range from 86 to 1,300 mm April 1 snow water equivalent ("spring snowpack"), an indicator of growing season moisture availability, which strongly influences seasonal greening of vegetation in Sierra Nevada meadows (Trujillo et al. 2012, Albano et al. 2019). (We recognize that in other studies, the term "provenance" may refer to sites that are more spatially or climatically disparate than ours. We simply use this term to refer to sites that were sampled for our common garden, with no further implication.) Our provenance sites also range from -0.99 to 3.9 °C in minimum May temperature, which can be a strong predictor of plant populations' sensitivity to spring freezing events (Muffler et al. 2016). Lastly, our provenance sites span 310 to 550 mm in actual evapotranspiration, which is often used as a predictor of plant growth (Aubry-Kientz & Moran 2017). April snowpack and

minimum May temperatures are negatively associated across *S. lemmonii*'s Sierra Nevada-wide range, but they are spatially decoupled in Tahoe National Forest. The least distance between provenance sites is 0.89 km, the greatest is 83 km, and the mean is 32 km.

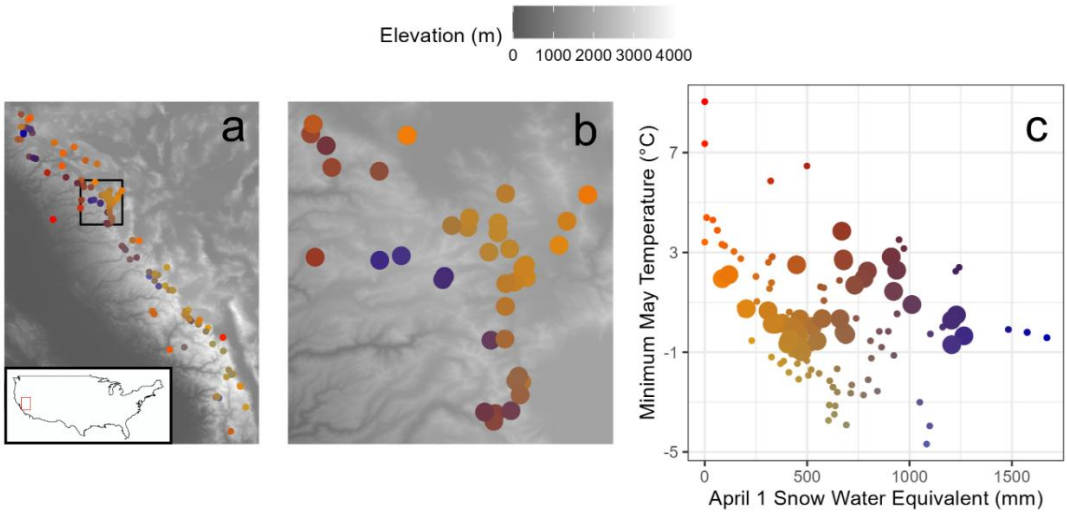

Fig. 1: Study region and climate data from a 1981-2010 climatology generated by the Basin Characterization Model. "m" denotes meters. "mm" denotes millimeters. "°C" denotes degrees Celsius. a) Sierra Nevada, USA. Points are *Salix lemmonii* occurrences. Black bounding box shows our study region in Tahoe National Forest. Inset shows location of Sierra Nevada (red bounding box) in USA. b) Zoomed view of our provenance sites in Tahoe National Forest. c) Two-dimensional color legend for panels a and b. Large points represent provenance sites in Tahoe National Forest. Small points represent occurrences outside Tahoe National Forest. Color varies continuously and two-dimensionally across the panel, with pure red, yellow, blue, and black delineating the four corners—i.e., combinations of extreme values. Red represents the least snowpack and the greatest temperature. Blue represents the opposite. Yellow represents the least observed values of both variables. Black represents the greatest observed values of both variables. Each combination of extremes may not necessarily occur in the data, hence the absence of, e.g., a pure yellow point in the bottom left corner.

Greenhouse common garden:

In October-November 2021, we collected twig cuttings from 1-2 parent plants at each of our 38 provenance sites. Within each of the 38 provenance sites, the plants we selected were spaced approximately evenly across the portion of the site occupied by *Salix lemmonii*. To avoid repeat sampling of a single clone, we only sampled plants separated by 10 meters or more of willow-free ground cover. (Preliminary results from a genomic study of the same individuals suggest this strategy was likely sufficient.) Parent plants were mature and roughly 2-3 m tall. We collected 2-5 twig cuttings from each parent plant to account for the possibility that not all cuttings might be propagated successfully. Each parent plant was tagged so it could be relocated for field measurement of leaf turgor loss point in August 2022. Cuttings were grown in a greenhouse common garden environment in Berkeley, CA. Initial conditions were ambient photoperiod, 25 °C daytime and 20 °C nighttime temperatures, continuous mist application, and a growth medium of 1:1:1 perlite/vermiculite/Sunshine #4 potting mix (Sungro, Agawam, MA). Beginning in December 2021, plants were repotted in 3:3:4 compost/perlite/Sunshine #4, fertilizer was applied weekly (Osmocote slow release 19-6-12), photoperiod was lengthened to 16 hours with supplemental light, mist irrigation ceased, and all plants were watered once daily to field capacity (i.e., until the soil was saturated and excess water drained freely). When necessary, plants were repotted in successively larger pots to ensure that none were pot-bound,

culminating with 3-gallon (11.4 L) pots in September 2022. Each pot size transition occurred on the same date for all plants, ensuring treatment homogeneity.

Drought sensitivity:

We quantified drought sensitivity by measuring the leaf turgor loss point (Ψ_{TLP}). This trait, measured in megapascals (MPa), quantifies the water potential at which a leaf fails to maintain turgor. Beyond this threshold, leaves may exhibit wilting, inability to open stomata, reduced photosynthesis, and other problems with important physiological functions (Lambers & Oliveira 2019). Higher ("less negative") values indicate greater drought sensitivity. We chose this trait because it is known to play an important role in drought stress tolerance for *Salix* and close relatives (Dawson & Bliss 1989, Moran et al. 2023). Additionally, focusing on leaf traits allowed us to assay leaves grown from buds that were set in the greenhouse common garden environment. This approach helps to minimize maternal effects from the clonal parent plants' in situ environments, which might be a greater concern for traits measured in other tissues, like stem hydraulics. We quantified the turgor loss point for common garden plants in July 2022, when they were roughly 1-2 meters tall. For one plant from each provenance site, we estimated the turgor loss point with a pressure-volume curve using the youngest fully expanded leaf on the dominant shoot. We sampled the 38 plants in random order. We followed the method of Tyree & Hammel (1972) to generate pressure-volume curves, and we used Williams et al.'s (2017) algorithm to compute the turgor loss point.

In August 2022, we measured the leaf turgor loss point on 37 of the 38 parent plants in the field (referred to here as 'in situ'). (One in situ parent plant died after we established the greenhouse common garden.) For each plant, we cut off the distal 15 cm of the dominant shoot and recut approximately 1-5 mm off the basal end submerged under water to minimize embolism. We then kept the cut end of the sampled shoot under water, with the full shoot in a dark container for 1-2 days before the sampled tissue arrived in our laboratory. We followed the procedure described above to generate one pressure-volume curve for each plant. Note that this procedure began by cutting a single leaf, which was not submerged, from a roughly 15 cm shoot, of which only several centimeters at the basal end was kept submerged following collection from the field. The goal of this approach was to minimize "plateau effects" that can result from saturated tissue (Parker & Pallardy 1987). We also visually inspected each pressure-volume curve and saw no indication of plateau effects.

Growth:

In September 2022, we separated 80 greenhouse common garden plants into groups of 39 and 41 for drought and control treatments. Note that not all common garden plants were used for growth measurements, as these measurements are destructive and thus prevent inclusion in the subsequent freezing sensitivity assays. Whenever possible, we included multiple replicates of individual genotypes within provenance sites, and for each genotype represented by multiple common garden clones, we included at least one greenhouse plant in the drought and control groups. An exception: one genotype represented by two common garden clones had both clones placed erroneously in the control group. See "Data Analysis" for further details regarding replication. The drought and control groups were subdivided into two spatial blocks each, and these blocks were rotated within the greenhouse room every two weeks. We also reshuffled the

locations of individual plants within blocks every two weeks. (See "Common garden" section for soil details.) Control plants continued receiving the same treatment described above, including daily watering to field capacity. Drought plants received thrice-weekly watering to field capacity for two weeks, then twice-weekly for two weeks, then weekly for the remainder of the experiment, which concluded in November 2022 after 9 weeks. At the conclusion of the drought experiment, we harvested all 80 plants for dry root, shoot, and leaf biomass quantification following Savage & Cavender-Bares (2011).

Freezing sensitivity:

To characterize variation in freezing sensitivity among common garden plants, we exposed new spring shoots from each plant to a range of freezing temperatures (details below) and estimated LT50—i.e., the temperature at which the probability of tissue viability is 50%. We timed the measurements in spring because this is when many temperate zone plants are most vulnerable to freezing (Vitasse et al. 2014, Muffler et al. 2016) and because prior studies of *Salix* indicate they are very resistant to freezing in winter, when they are fully acclimated (Sakai 1970, Savage & Cavender-Bares 2013). We focused on new spring shoots because these tissues are likely among the most vulnerable to freezing (Chamberlain & Wolkovich 2021). We assessed each shoot's post-freeze viability according to its capacity to re-root in well-watered soil. This viability criterion takes advantage of *Salix*'s well-known capacity to re-root from healthy shoot cuttings, thereby providing a less labor-intensive and perhaps more direct measurement of true tissue viability than other methods like differential thermal analysis (DTA) and electrolyte leakage (Grossman 2023). Furthermore, many *Salix* species do not appear to supercool (Neuner et al. 2019), so supercooling-based methods like DTA may be unhelpful for quantifying freeze tolerance in *Salix*.

Before measuring freezing sensitivity, we began inducing winter acclimation in December 2022 by moving all remaining common garden plants from the greenhouse to ambient outdoor conditions in Berkeley, CA, where the mean daily minimum temperature was 6 °C. In January 2023, to further induce winter acclimation in a colder winter environment more similar to Tahoe National Forest, plants were moved to ambient outdoor conditions in Reno, NV, where the mean daily minimum temperature was -6 °C. To induce spring deacclimation, all plants were returned to the greenhouse in Berkeley, CA in April 2023. (Greenhouse conditions are described in the "Common garden" section.)

To assess freezing sensitivity, we sampled and froze four new 15 cm spring shoots from each plant on May 11, 2023. Visual inspection indicated that there was phenological variation among common garden plants—e.g., some had fully expanded leaves, whereas others did not. This was not a problem for our analysis, as our goal was not to compare genotypes' physiology at the same phenological stage. Rather, we aimed to quantify variation in the tissue viability responses of different genotypes to the same freezing event in a common environment, which can result from physiological variation, phenological variation, or both (Grossman 2023). Variation could arise solely from physiological mechanisms—e.g., all genotypes might follow parallel temporal trends in spring deacclimation, with no variation in phenology, and variation in tissue viability could be driven by absolute, time-invariant differences among genotypes in cold-hardiness. Variation in tissue viability could also arise strictly from phenological mechanisms—e.g., all genotypes might

follow the same progression of cold-hardiness levels, but with different timing. Alternatively, phenological and physiological mechanisms could both contribute. Our aim was to integrate across these possible mechanisms and characterize overall tissue viability responses to a spring freezing event.

The set of four shoots for each common garden plant was allocated randomly among four freezing treatment groups: -0.5 °C, -5 °C, -9.5 °C, and -14 °C. Shoots were wrapped in wet cotton balls at the bottom to avoid desiccation and loaded in a Vesta Precision blast chiller in a random (and periodically reshuffled) spatial configuration. Starting at 10 PM, the temperature stepped down by 4.5 °C each hour, starting at the ambient laboratory temperature of approximately 22 °C. We kept each treatment group in the chiller until it had spent one hour at its treatment temperature. After each group was successively removed, we moved them to a 4 °C refrigerator for one hour for a gradual thaw before returning them to the ambient laboratory environment. The following morning, all shoots were planted using the initial propagation protocol described in the "Common garden" section. Shoots were classified as viable if they produced roots within six weeks and inviable if they did not.

With the four shoot viability data points for each plant, we estimated LT50, the temperature at which the probability of tissue viability is 50%, as the midpoint between the coolest temperature with viable shoots and the warmest temperature with non-viable shoots. In one case, in which viability was not completely separated by temperature, we used a least squares logistic regression model of viability versus temperature treatment to estimate the temperature at which the probability of viability was 50%.

Data Analysis:

In total, our study comprises 90 genotypes represented by 129 common garden plants. (39 of the 90 genotypes had two common garden clones that were propagated successfully, and the other 51 were represented by only one common garden plant.) Due to logistical constraints, each of our three phenotypic data sets—drought sensitivity, freezing sensitivity, and growth—contained different numbers of plants (Table S2.1). For our drought sensitivity measurements, we assayed one common garden plant from each of our 38 provenance sites—i.e., 38 common garden plants. Although more replication might have been desirable, we aimed to minimize seasonal variation by completing all measurements in the same month (July 2022), and this was approximately the maximum number of pressure-volume curves we could complete in that time. We took the same approach in measuring each common garden plant's in situ clonal parent plant during August 2022. In allocating plants to the growth and freezing sensitivity measurements, we aimed to strike a balance, as growth measurements (which occurred before freezing sensitivity) are destructive. Based on our observations in situ and in the common garden, we expected growth measurements to be noisier than freezing sensitivity, so we attempted to err on the side of greater replication for growth measurements. The growth data set comprised 50 genotypes represented by 80 common garden plants, which were divided into 39 and 41 between the drought and control treatments, respectively. 30 genotypes were represented by two common garden plants each, and 20 genotypes were represented by one common garden plant each. The 30 genotypes represented by 2 common garden plants each were all divided into one drought plant and one control plant, except for one genotype, for which both common garden plants were erroneously

included in the control group. The freezing sensitivity data set comprised 36 genotypes, each of which was represented by one common garden plant.

For each of our three phenotypic outcome variables measured in the common garden—drought sensitivity, freezing sensitivity, and growth—we built a regression model using climatic predictors to quantify the effects of provenance climate. (Growth was measured under both drought and well-watered control conditions, and these data were analyzed together.) See below for details of each regression model structure. We used three climate variables, represented as means over the period 1981-2010, from the Basin Characterization Model ("BCM"; Flint et al. 2021): April 1 snow water equivalent ("snowpack"), minimum May temperature, and actual evapotranspiration ("AET"). The Basin Characterization Model is optimized for use in California, where our provenance sites occur. Relative to other commonly used climate products, BCM data provide finer spatial resolution, which is useful for capturing small-scale climatic variation in topographically heterogeneous regions like Tahoe National Forest. Below, we provide an a priori justification for each choice of climate variable. We did not explore model selection approaches using additional climate variables because our goal was to test specific hypotheses, not to build an optimal predictive model. Prediction and inference are separate tasks, and model selection tools like AIC can bias inference for the independent variable(s) of interest (Arif & MacNeil 2022). Testing too many climate variables can lead to high "false discovery rates" of patterns that simply occur due to random chance (Roback & Askins 2005). Instead, we defined a priori hypotheses regarding the climatic gradients that we expected to shape each phenotypic outcome variable. All three climate variables were used in each regression, so that the coefficient for each climatic predictor reflects the effect of that variable while holding the others constant.

We used April snowpack because in a recent study, measures of vegetation health and vigor for Sierra Nevada montane meadows (e.g., normalized difference vegetation index) were best predicted by this variable, compared to 16 other variables including precipitation, climatic water deficit, and potential evapotranspiration (Albano et al. 2019). In the Sierra Nevada, most precipitation arrives as snow during winter, and growing season water availability is determined largely by snowmelt (Schoenherr 2017). Consequently, we hypothesized that genotypes' drought sensitivity would increase with provenance snowpack—i.e., environments with low snowpack should select more strongly for low drought sensitivity.

Minimum May temperature was chosen because this variable was the best predictor of sensitivity to a spring freezing event among northern hemisphere woody plant species in a large common garden study (Muffler et al. 2016). Furthermore, our field observations suggest May is the month when plants in our study system are most likely to be growing new shoots. We hypothesized that genotypes' spring freezing sensitivity would increase with provenance minimum May temperatures—i.e., environments with extreme spring cold snaps should select more strongly for low spring freezing sensitivity.

We used actual evapotranspiration (AET) because this variable reflects availability of both energy and water, which are critical for plant growth (Flint et al. 2021). AET exhibits the greatest values in environments that are both warm and wet. For plants subjected to the well-watered

control treatment, we hypothesized that genotypes' common garden biomass accumulation would increase with provenance AET—i.e., environments with high energy and water availability should select for more rapid growth. For plants subjected to the drought treatment, we hypothesized that biomass accumulation would decrease with provenance snowpack, based on the expectation that plants from drier environments would be better able to maintain critical physiological functions throughout the drought.

To quantify the effect of provenance climate on leaf turgor loss point among common garden plants, we used an ordinary least squares (OLS) multiple linear regression with Gaussian errors. As each provenance site was only represented by one genotype, no clustering of errors was expected, and thus no random effects were used.

To quantify the effect of provenance climate on biomass accumulation, we used a maximum likelihood generalized additive mixed model (GAMM) with Gaussian errors. We included a linear term for each climate variable, as well as an intercept term for "treatment" (drought vs. control), as we hypothesized that growth would slow in response to the drought treatment. We included interactions between "treatment" and each climate variable to account for the possibility that provenance climate might influence responses to the drought treatment. To control for differences in the initial sizes of cuttings, we included a thin plate regression spline for initial cutting volume, plus its interaction with "treatment". This approach allows for non-linear effects of initial cutting size on the final biomass measurement. We included a random intercept for "site", as some provenance sites were represented by multiple in situ parent plants (i.e., "genotypes"), leaving open the possibility of clustered errors. We also included a random intercept for "parent plant" (i.e., "genotype"), as some in situ parent plants were represented by two common garden plants (one drought and one control). i.e., in some cases, multiple twigs cloned from the same in situ parent plant were propagated successfully in the common garden and included in the growth study.

To quantify the effect of provenance climate on LT50, the freezing temperature at which the probability of tissue viability is 50%, we used a maximum likelihood linear mixed effects model with Gaussian errors. We included a linear term for each climatic predictor. To account for possible clustered errors, we included a random intercept for "site", as some provenance sites were represented by multiple in situ parent plants.

Our LT50 data have a "binned" distribution (reflecting the midpoints between the four experimental temperatures), which may have strained the robustness of linear mixed effects models to non-Gaussian errors. To address this possibility, we also analyzed our LT50 data using a Bayesian ordinal generalized linear mixed model (GLMM) with a logit link function, in which each LT50 value is treated as an ordered category. This ordered categorical response variable is regarded as a function of a latent continuous variable defined by the linear predictor, which is identical to that of our linear mixed effects model described above. In other words, this model structure treats the true LT50 values as varying continuously (i.e., with infinitely fine resolution) and treats our LT50 measurements as "rounded" versions of the unobserved true values.

Intensifying drought is the facet of climate change regarded by some management practitioners as most threatening to Sierra Nevada willows (Vernon et al. 2019). Consequently, in addition to the analyses testing for effects of climate on common garden phenotypes, we used our greenhouse common garden and in situ drought sensitivity data to assess whether heritable phenotypic variation detected in the greenhouse translates to biologically meaningful phenotypic variation in situ. Toward this aim, we used an ordinary least squares (OLS) simple linear regression with Gaussian errors to quantify the effect of common garden turgor loss point values on in situ values. Common garden phenotypes are assumed to reflect genetic variation (plus environmental noise), so a positive effect of the common garden phenotype on the in situ phenotype would indicate that genetic variation contributes to in situ phenotypic variation.

To visualize the role of climate in determining the extent of adaptive tradeoffs, we reformulated our regression models of drought and freezing sensitivity using z-scaled responses (mean 0, SD 1) and replotted significant effects on the same axes. This approach creates a "common currency" of effect sizes among different traits and helps show more clearly whether they vary in opposite directions along a climatic gradient, creating a tradeoff.

To illustrate how multi-trait phenotypes vary across multi-dimensional climate gradients, we plotted our drought and freezing sensitivity data with a two-dimensional color scale on a grid of spring snowpack and temperature.

To test for direct tradeoffs among traits, irrespective of climate, we built a ranged major axis regression model using provenance site-level mean phenotypes for each possible pairing of traits. Like a principal component analysis (PCA), major axis (MA) regression techniques minimize errors perpendicular to the regression line, rather than the vertical errors that are minimized in ordinary least squares regressions (Legendre 2018). This approach is useful for situations in which both variables of interest are measured with error, and there is no clear independent and dependent variable. "Ranged" major axis regression is the MA method best suited for variables that do not share the same units or scale (Legendre 2018). To account for the binned shape of the LT50 data we also used Kendall's tau tests, which test for rank correlations between variables, irrespective of the functional form of their relationship (Noether 1981). We did not analyze the relationship between final biomass under drought versus control conditions because substantial biomass accumulation occurred before the controlled experiment, when all plants were receiving the same treatment. Consequently, final biomass under drought and control conditions are likely to show a positive association that simply reflects their shared history.

All regression analyses were performed in R (R Core Team 2023). Continuous predictors were z-scaled (mean 0, SD 1). We used the glmmTMB package (Brooks et al. 2017) for linear mixed effects models, gamm4 (Wood & Scheipl 2020) for the GAMM, brms v2.21.0 (Bürkner 2017) for the ordinal GLMM, and lmodel2 (Legendre 2018) for the ranged major axis regression models. Model building and checking steps are shown in our publicly available R code (see Data Availability).

Results

Drought sensitivity & climate:

Genotypes from lower-snowpack provenance sites had less drought-sensitive leaves, as quantified by leaf turgor loss point. The turgor loss point of common garden plants increases (i.e., drought sensitivity increases) by 0.18 MPa per 1,000 mm in April snow water equivalent (Fig. 2a-b, Table S2.2; $p<0.01$). Conditional means range from -0.95 to -0.74 Mpa along the snowpack gradient. Turgor loss point is not associated with provenance minimum May temperature or actual evapotranspiration (Fig. 2b, Table S2.2). For each 1 Mpa increase in the common garden phenotype, the in situ phenotype increases by 0.62 Mpa (Fig. 2c, Table S2.3; $p=0.01$), indicating that genetic variation contributes to in situ phenotypic variation.

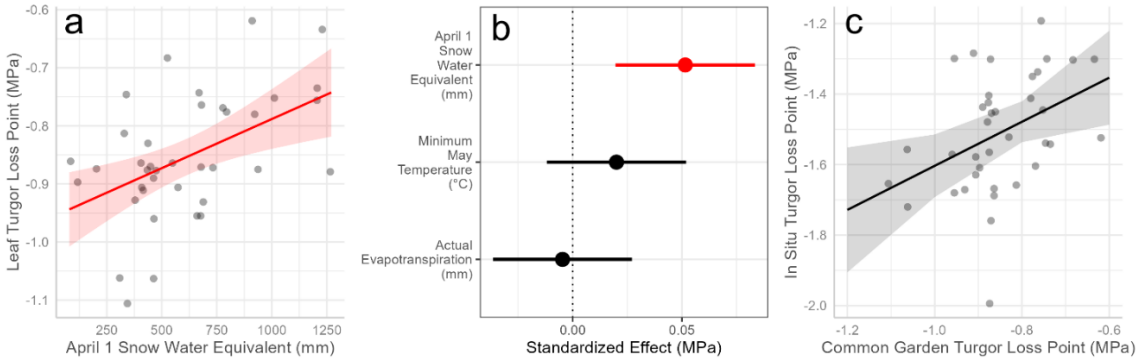

Fig: 2: Results for common garden and in situ studies of leaf turgor loss point, a measure of drought sensitivity, in *Salix lemmonii*. For consistency with Fig. 5, red represents the effect of provenance April snowpack on leaf turgor loss point. "mm" denotes millimeters. "Mpa" denotes megapascals. "°C" denotes degrees Celsius. A) Effect of provenance spring snowpack from multiple linear regression model. Ribbon shows 95% confidence interval. Each point represents one common garden plant from one provenance site. b) 95% confidence intervals for effect sizes of three climatic variables in a multiple linear regression model. C) Effect of common garden phenotypes on in situ phenotypes from simple linear regression model. Each point represents one genotype from one provenance site, which is represented by an in situ parent plant and its common garden clone.

Freezing sensitivity & climate:

Genotypes from colder provenance sites were less sensitive to freezing. Common garden plants' shoot LT50 increases (i.e., freezing sensitivity increases) by 0.60 °C with each 1 °C increase in provenance minimum May temperature (Fig. 3, Table S2.4; $p=0.02$). LT50 is not associated with April snowpack or actual evapotranspiration (Fig. 3b, Table S2.4). When we reanalyzed the data with a Bayesian ordinal logistic GLMM, which may account better for the "binned" shape of the LT50 data, we again found a positive effect of minimum May temperature (95% CI 0.21-3.7) and no effect of the other climate variables (Table S2.5).

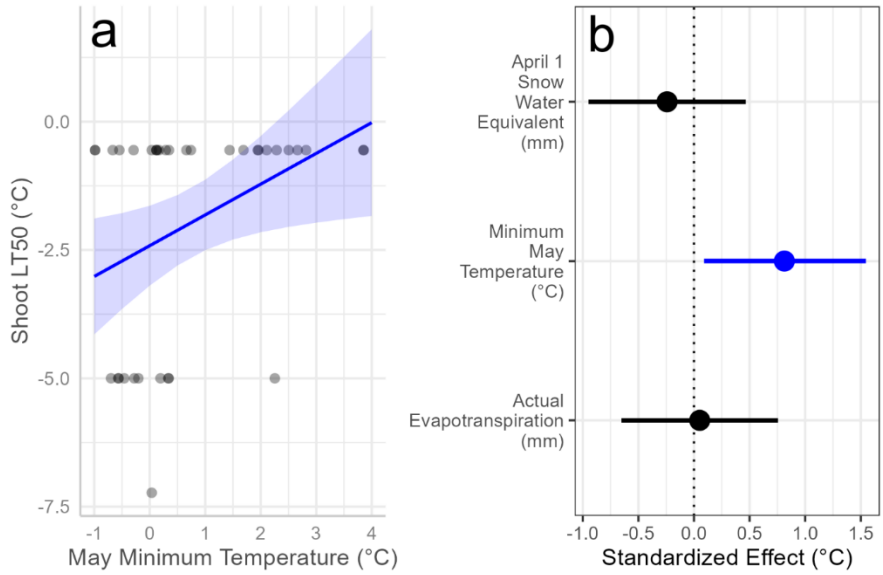

Fig. 3: Results for common garden study of shoot LT50, the freezing temperature at which the probability of tissue viability is 50%, in *Salix lemmonii*. This variable is a measure of freezing sensitivity. "°C" denotes degrees Celsius. "mm" denotes millimeters. For consistency with Fig. 5, blue represents the effect of provenance minimum May temperature on LT50. a) Conditional effect of provenance May minimum temperature from linear mixed effects model. Ribbon shows 95% confidence interval. b) 95% confidence intervals for effect size estimates of three climate variables in a linear mixed effects model. Qualitatively similar results were obtained from an ordinal logistic GLMM, which treats LT50 values as ordered categories to account for the "binned" shape of the data.

Growth & climate:

Biomass accumulation was not associated with any of the climatic variables we tested under drought or well-watered conditions (Fig. 4, Table S2.6). The only significant effect was the overall influence of the drought treatment, which decreased biomass accumulation (Fig. 4, Table S2.6).

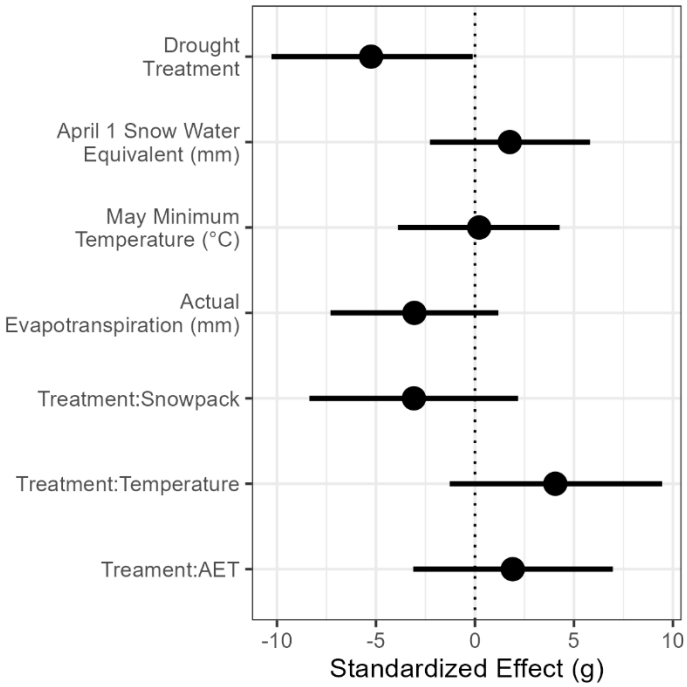

Fig. 4: 95% confidence intervals for effect sizes of provenance climate and drought treatment on common garden biomass accumulation for *Salix lemmonii* in a linear mixed effects model. "°C" denotes degrees Celsius. "mm" denotes millimeters. "AET" is an abbreviation for actual evapotranspiration.

Tradeoffs:

Drought sensitivity increases significantly with spring snowpack, whereas freezing sensitivity exhibits little trend (Fig. 5a). Freezing sensitivity increases significantly with minimum May temperature, whereas drought sensitivity exhibits a weak, nonsignificant positive trend (Fig. 5b). Consequently, in provenance sites with low spring snowpack and minimum temperatures, site-level mean phenotypes are strong in both performance traits (Fig. 5c-d).

No significant negative relationship emerges for any two-trait pairing we analyzed among our four measured traits—drought sensitivity, freezing sensitivity, biomass accumulation under well-watered conditions, and biomass accumulation under drought conditions. This outcome is supported by ranged major axis regressions (Table S2.7) and Kendall's tau tests (Table S2.8).

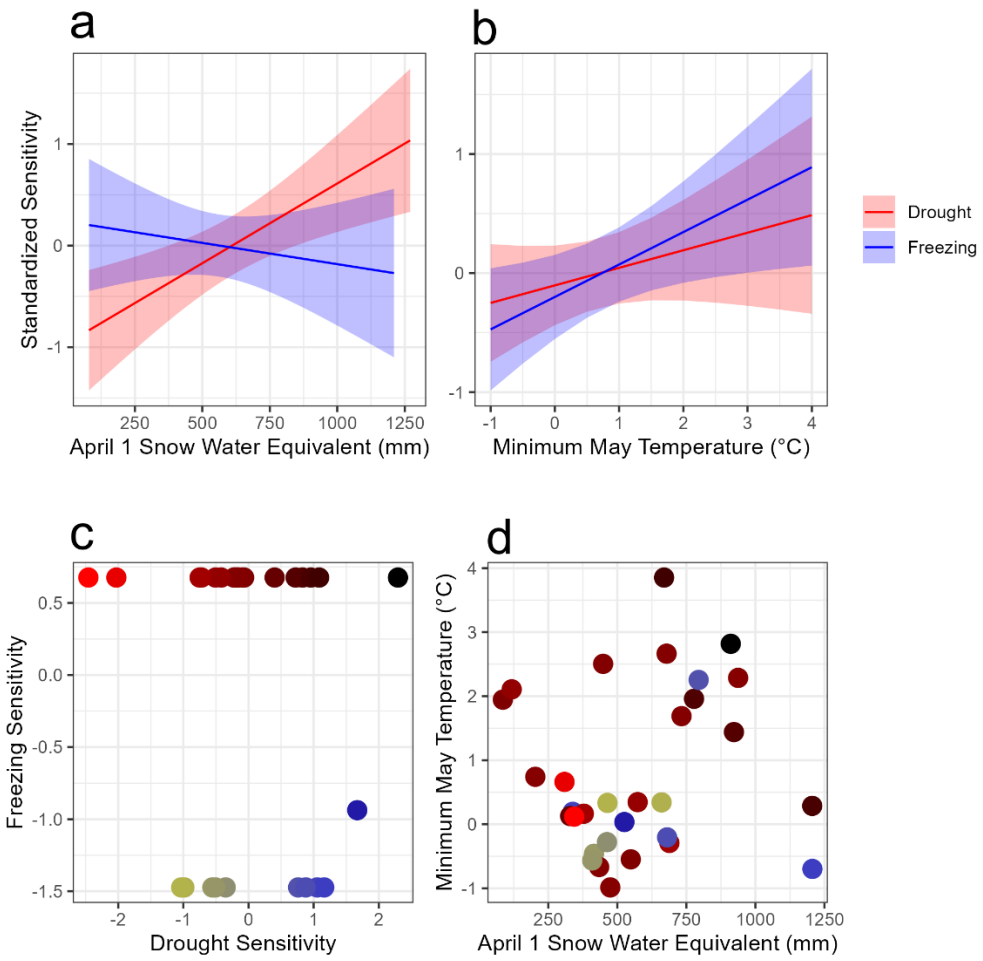

Fig. 5: Responses of drought and freezing sensitivity in *Salix lemmonii* to snowpack and minimum temperature. Drought and freezing sensitivity variables are generated by standardizing leaf turgor loss point and shoot LT50, the freezing temperature at which the probability of tissue viability is 50%. (mean=0, SD=1). "°C" denotes degrees Celsius. "mm" denotes millimeters. a-b) Conditional effects of spring snowpack and minimum temperature on drought and freezing sensitivity from linear mixed effects models. (Points, which would represent mean trait values for provenance sites, are omitted to avoid visual clutter. Site-level mean trait values can be seen as points in Figs. 5c-d and S1.) Ribbons represent 95% confidence intervals. c) Two-dimensional color legend for panel d, in which a two-trait phenotype—drought and freezing sensitivity—is plotted against snowpack and temperature. Color varies continuously and two-dimensionally across the panel, with pure red, yellow, blue, and black delineating the four corners—i.e., combinations of extreme values. Red represents the least drought sensitivity and the greatest freezing sensitivity. Blue represents the opposite. Yellow represents the least observed values of both variables. Black represents the greatest observed values of both variables. Each combination of extremes may not necessarily occur in the data, hence the absence of, e.g., a pure yellow point in the bottom left corner in panel c.

Discussion

Summary:

The results of this investigation show that populations of Lemmon's willow (*Salix lemmonii*) in the northern high Sierra Nevada, USA do not exhibit an adaptive tradeoff between drought and freezing sensitivity. In our common garden, genotypes' drought sensitivity increases with provenance April snowpack, an indicator of growing season soil moisture (Figs. 2, 5). Freezing

sensitivity increases with provenance minimum May temperature (Figs. 3, 5). These climate variables are often negatively correlated (e.g., across the Sierra Nevada-wide realized niche of *S. lemmonii*; Fig. 1), so the trait-environment relationships we found would be expected to produce tradeoffs in regions that exhibit this climatic correlation (Garland 2014). Although drought-freezing tradeoffs are not universal, they occur in many other systems (Laanisto & Niinemets 2015, Rueda et al. 2017, McCulloh et al. 2023). However, in our study domain, April snowpack and minimum May temperature are uncorrelated (see large points in Fig. 1c), and thus we find no tradeoff between drought and freezing sensitivity (Figs. 5a-b). (Note that the existence of individual provenance sites with low mean sensitivity to one stressor and high sensitivity to the other—e.g., the reddest and bluest points in Figs. 5c-d—does not indicate a tradeoff. A tradeoff is an association between traits at the level of the full data set, which we did not find, as Fig. S2.1 also shows.) The absence of a tradeoff suggests weak or absent genetic constraints on this trait pairing (Garland 2014), as well as weak or absent organismal-level physiological tradeoffs (Bloom et al. 1985). Genotypes with relatively low sensitivity to both stressors occur in the coldest, driest provenance sites (yellowest points in Fig. 5c-d). These sites may represent reservoirs of strong adaptive potential under climate change, and assisted gene flow efforts may benefit by using them as sources (Aitken et al. 2013).

Drought sensitivity:

In our drought sensitivity study, genotypes from lower-snowpack sites could withstand stronger drought without wilting. Among plants measured in the common garden, the mean turgor loss point increases (i.e., drought sensitivity increases) by 0.18 MPa with each 1,000 mm increase in provenance April snow water equivalent (Figs. 3a-b; $p<0.01$). Additionally, in situ phenotypes increase by 0.62 Mpa with each 1 Mpa increase in common garden phenotype (Fig. 2c; $p=0.01$). This result indicates that genetic variation contributes substantially to in situ phenotypic variation. The turgor loss point measurements for the in situ parent plants were generally lower (i.e., less drought-sensitive) than the greenhouse common garden measurements. This phenotypic difference may reflect ontogenetic differences (mature plants versus saplings), phenological differences (August versus July), or overall environmental differences, irrespective of season. E.g., the hydrologic regime in the common garden, with daily watering to field capacity, may have provided fewer of the cues that stimulate metabolic investment in osmolytes (Bartlett et al. 2014). Overall, our drought study supports the expectation that wilting-resistant leaves carry greater adaptive value in dry conditions (Dawson & Bliss 1989), and that dry sites harbor genotypes predisposed toward greater wilting resistance—i.e., low drought sensitivity (Soliani et al. 2021, Moran et al. 2023).

Freezing sensitivity:

Our freezing experiment shows that genotypes from provenance sites with colder spring temperatures have less freeze-sensitive shoots. LT50 of new spring shoots in the common garden increases by 0.60 °C with each 1 °C increase in provenance minimum May temperature (Fig. 3; $p=0.02$). LT50 quantifies the temperature treatment at which post-treatment tissue viability is 50%, with greater values indicating greater freezing sensitivity. Our main qualitative result—i.e., LT50 increases with provenance temperature—is robust to reanalysis with an ordinal logistic GLMM, in which each LT50 value is treated as an ordered category. (We performed this analysis to account for the "binned" shape of the LT50 distribution.) All genotypes were assayed

simultaneously, so overall variation in LT50 may reflect both phenological variation (i.e., variation in the timing of spring cold deacclimation) as well as variation in post-deacclimation freezing sensitivity among genotypes that deacclimated quickly (Grossman 2023). Overall, our results support the expectation that freezing resistance carries greater adaptive value in environments that have strong cold snaps in spring, when many plants are most vulnerable (Vitasse et al. 2014, Muffler et al. 2016).

Growth:

Growth did not provide evidence of ecotypic variation or tradeoffs. In our common garden, total biomass accumulation did not vary with provenance climate under drought or control conditions (Fig. 4). When we examined direct relationships among population mean trait values, we also found little evidence for tradeoffs (Fig. S2.1, Tables S2.7-S2.8). It may appear surprising that biomass accumulation among drought-treated plants did not increase with turgor loss point, as our leaf turgor loss point measurements show evidence of local adaptation to hydrologic conditions. Multiple factors might explain this result. First, it is possible that a relationship exists but is too subtle for our sampling design to detect. Second, genotypes with lower leaf turgor loss points (i.e., lesser drought sensitivity) may have had slower average growth rates during their growing season, but their growing seasons may have been longer (Berger et al. 2016). We measured total biomass accumulation over the drought experiment—not shorter-term growth rates—and our observations in the common garden indicate that some drought-treated plants were likely at or approaching dormancy by the conclusion of the growth experiment. These observations suggest that only some drought-treated plants grew throughout the experiment. Tradeoffs between instantaneous growth rates and growing season length are known to promote coexistence among plant species in a Mediterranean climate (Levine et al. 2024) like the Sierra Nevada, and it could be informative for future work to explore the implications of such tradeoffs at the intraspecific level. In addition to these considerations, it is possible that other traits we did not measure, like herbivore defense or other forms of stress tolerance, might form tradeoffs with the traits we measured. However, although tradeoffs among performance traits are well-documented (Grime 1974, Díaz et al. 2016, Visakorpi et al. 2024), they are not ubiquitous. Plants cope with multiple forms of abiotic stress through myriad mechanisms, and some of these mechanisms do not carry zero-sum physiological constraints in relation to growth rates (Savage & Cavender-Bares 2013, Fletcher et al. 2022).

Management implications:

Our findings may help inform conservation strategies for *Salix lemmonii* in the northern high Sierra Nevada and beyond. In the Sierra Nevada, climate change is making drought more frequent and severe (Dettinger et al. 2018). Spring freezing events occur currently, and risks to plants may increase as seasonal and diel temperature fluctuations become more erratic (Arnold et al. 2014). In Tahoe National Forest, we found that the coldest, driest provenance sites disproportionately harbor genotypes with low sensitivity to both drought and freezing. We also found no tradeoffs with growth. Thus, populations at cold, dry sites may be valuable reservoirs of potential to respond adaptively to climate change. ("Cold" refers to minimum May temperatures, which do not necessarily reflect annual mean temperatures.) Although these populations' sensitivity to climate change may be less than others', their future exposure to climate-driven stress may be greater, as their current environments are relatively stressful

(Williams et al. 2008). Consequently, it is unclear whether the balance between exposure and sensitivity will translate to favorable outcomes in situ, although prior research suggests they might (Zohner et al. 2020). Optimal outcomes might be achieved by translocating stress-tolerant genotypes to sites where future exposure will be milder, e.g., snowy sites with equable thermal regimes. Tahoe National Forest contains strong climatic variation within tens of kilometers (Fig. 1), so biologically meaningful translocation might be achievable over distances where legal, ethical, and other difficulties (Schwartz et al. 2012) are minimized. If the combination of low drought and freezing sensitivity we found is exceptional in other parts of the range of *Salix lemmonii*, then longer-distance translocation could also prove fruitful, although ethical, logistical, and ecological mismatch issues may apply (Bucharova 2017, Baldwin 2019).

Conclusions:

Overall, our results suggest that adaptive tradeoffs may be avoided in regions where key climate variables are uncorrelated. Multiple climatic stressors—e.g., drought and freezing—can coincide in certain sites to promote multiple stress adaptations—e.g., the yellowest points in Fig. 5d. The fate of populations in these sites depends not only on their sensitivity to climate change, but also their future exposure, which could be severe given their current exposure. However, regions of uncorrelated climate must also, by definition, contain less stressful sites. Assisted gene flow efforts might achieve the best of both worlds—i.e., low sensitivity and low exposure—by importing genotypes that have escaped adaptive tradeoffs into these less stressful sites. To identify translocation opportunities for other taxa, further investigation is needed regarding the climate variables shaping key performance traits. However, ecotypic trait variation has already been studied extensively for some taxa (Mahony et al. 2019, MacLachlan et al. 2021, Prakash et al. 2022, Capblancq et al. 2022), so the tradeoff-escape concept might be readily applicable in these cases. In general, conservation efforts may benefit by examining how multidimensional climatic gradients shape correlations among adaptive traits, which can have strong, persistent effects on populations' evolutionary trajectories (Schluter 1996, Etter & Shaw 2001, Walsh & Blows 2009, Terasaki Hart & Wang 2024).

Transition to Chapter 3

Chapter 2 focused on *Salix lemmonii* (Lemmon's willow) in island-like montane meadows of California's Sierra Nevada, asking how spatial climatic gradients shape ecotypic variation in key performance traits. Chapter 3 adopts a taxon-agnostic view, pivoting conceptually to focus on interspecific competition among species occupying habitat islands. The goal of this chapter is to introduce a new statistical tool for quantifying the role of interspecific competition in the assembly of communities across habitat patches. In doing so, I introduce a new open-source R package, compnet, which allows any user to implement my method.

Chapter 3

compnet: Bayesian dyadic regression reveals hidden signals of interspecific competition in observational data

Abstract

Quantifying competition's influence on communities is a central goal in ecology. Often, available data include species traits and presence-absence, or abundance, across sites. Most methods test for competitive niche differentiation, asking whether observed communities exhibit greater trait diversity than reshuffled "null" communities. These methods have two limitations: 1- biologically vague null models, and 2- susceptibility to trait correlations that obscure ("confound") key patterns. Here, I introduce a null model-free approach and accompanying R package, compnet, which estimates each trait's effect on species' co-occurrence probabilities while controlling for other traits. I analyze simulated metacommunities, showing that my method outperforms 48 null model methods in detecting competitive niche differentiation. In an empirical example, I show that trees in Payette National Forest (USA) exhibit competitive niche differentiation driven by height. I detect this effect by controlling for wood density, a "convergence trait", thereby demonstrating how my method can also reveal trait convergence patterns.

Introduction

For over a century, ecologists have sought ways to quantify the impact of interspecific competition on communities (Clements 1916, Diamond 1975, Ricklefs & Travis 1980, Connor & Simberloff 1983, Webb et al. 2002, Cornwell & Ackerly 2009). Manipulative experiments can be effective but are frequently infeasible (Adler et al. 2013). Often, only observational data are available, e.g., species abundance or presence-absence across sites, complemented by traits. Most methods used in this scenario focus on competitive niche differentiation, whereby dissimilarity in resource use promotes cooccurrence (de Bello et al. 2021). Null model tests, the standard family of methods, use community-level metrics of functional diversity, e.g., functional richness ("FRic"; Mason et al. 2005, Villéger et al. 2008), dispersion ("FDis"; Laliberte & Legendre 2010), or evenness ("FEve"; Villéger et al. 2008), which are compared to null distributions generated by reshuffling the data (de Bello et al. 2021, Novella-Fernandez et al. 2024, Szeles et al. 2025, Frei et al. 2025). When observed values of the chosen metric are extreme, relative to the null distribution, competitive niche differentiation is inferred as the cause (de Bello et al. 2021). (Mechanisms of niche differentiation can include intra-site microhabitat partitioning, which could be considered distinct from partitioning of consumable resources [Grubb 1977, Poorter 2007, Cornwell & Ackerly 2009].) These methods have two major limitations that could jeopardize their validity: 1- biologically vague null models, which can

misrepresent ecological processes, and 2- inability to control for confounding relationships among intercorrelated traits. Alternative approaches could help and remain underexplored.

Null model methods for studying competition may be compromised by their lack of clear connections to biological processes. The goal of a null model simulation is to approximate the expected distribution of data under two assumptions: 1- competitive niche differentiation is not occurring, and 2- all other processes (e.g., dispersal, habitat filtering) are occurring as they do in the study system (Tokeshi 1986, Gotelli & Graves 1996). Null model permutation algorithms typically lack clear connections to these goals. For instance, null data are often simulated by reshuffling the species-by-site presence-absence matrix while maintaining constant site-level species richness and/or species occurrence frequency (de Bello et al. 2021). This approach has been refined—e.g., by preventing species from being reshuffled to sites outside their inferred habitat niches (Peres-Neto et al. 2001, de Bello et al. 2012), or by specifying distinct roles for classes of traits expected to have different functions (Peres-Neto 2004)—but it remains unclear how reshuffling algorithms can reliably reproduce all intended biological processes while excluding competitive niche differentiation. Consequently, the simulated distributions of the chosen metric may be inappropriate, leading to inflated false positive or false negative rates (Tokeshi 1986). Past simulation studies have tested the performance of various null model methods under a variety of assumptions, yielding mixed results (Mouchet et al. 2010, de Bello 2012, de Bello et al. 2012, Chalmandrier et al. 2013, Botta-Dukát et al. 2016, Götzenberger et al. 2016, Münkemüller et al. 2020). However, there is no readily available alternative, and null model methods remain widely used (e.g., Novella-Fernandez et al. 2024, Szeles et al. 2025, Frei et al. 2025). A null model-free method could help sidestep these issues.

Null model approaches may also be hindered by their inability to account for correlations in multi-trait data. When traits are intercorrelated, as they often are in nature (Barnagaud et al. 2014, Díaz et al. 2016), these approaches may overlook key multi-trait patterns. For example, consider a tree metacommunity. Let tree height be a "divergence trait" that drives competitive niche differentiation (MacArthur & Levins 1967, Stubbs & Wilson 2004). All else being equal, species of disparate heights cooccur more frequently because of decreased overlap in resource use. Let wood density be a "convergence trait" driven by a competitive hierarchy. All else being equal, species of similar wood densities cooccur more frequently because competitively superior low-density species tend to exclude high-density species (Mayfield & Levine 2010). (Other processes can also drive trait convergence, like habitat filtering and dispersal limitation [van der Valk 1981, Cornwell et al. 2006, Münkemüller et al. 2012]). Lastly, let height and wood density be correlated due to the relevant species' evolutionary history (e.g., Felsenstein 1985). In the language of causal inference, there is a backdoor confounding pathway (Pearl 2009, Arif & MacNeil 2023) linking species pairs' height differences, evolutionary history, wood density differences, and co-occurrence probabilities (Fig. 1a). To quantify the effect of height differences on co-occurrence of species pairs, we cannot simply ask how co-occurrence varies with height disparity, as increasing height disparity also means increasing wood density disparity (Fig. 1b). These effects counteract each other (Fig. 1b). However, if we only compare species pairs that are equally disparate in wood density, the expected pattern emerges—i.e., cooccurrence increases with height disparity (Fig. 1c). New methods are needed to reveal such patterns.

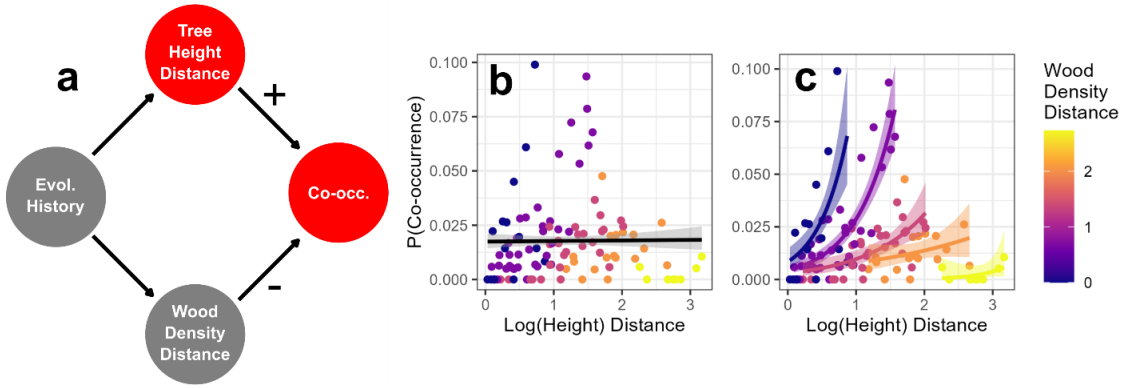

Fig. 1: Hypothetical example of "hidden" competitive niche differentiation in a tree metacommunity. Conditional mean curves are fitted by binomial GLMs for illustrative purposes. a) Diagram depicting causal relationships among variables that describe species pairs in a metacommunity. Distances in tree height and wood density are correlated due to evolutionary history. Pairs that are more disparate in tree height co-occur more often due to reduced resource use overlap. Pairs that are more disparate in wood density co-occur less often due to a competitive hierarchy. b) Naïve estimate of the effect of species' pairs height distances (i.e., absolute value differences) on their probabilities of co-occurrence. The functional "convergence" effect of wood density masks the functional "divergence" effect of tree height. c) Effect of height distance on co-occurrence probability, stratified by wood density distance. The divergence effect of height appears in each stratum—i.e., co-occurrence probability increases with height distance.

The above issues with null model methods—biologically vague null models and susceptibility to confounding—might be alleviated by modeling species co-occurrence probabilities in a regression model. If the model is structured to mimic the hypothesized data-generating process, then null models would be unnecessary, and the goal could shift to modeling the effect of interest directly (Ives & Helmus 2011, McElreath 2020). In the example above, the units of analysis can be species pairs, and the response variable can be the probability of co-occurrence. The predictors can be species' pairwise distances in height and wood density. The coefficient for each predictor can be interpreted as the effect of varying that trait distance while holding the other constant (Harrell 2001). This approach mimics the stratified study design in Fig. 1, which allows us to estimate the effect of height disparities on cooccurrence probabilities while controlling for wood density (Arif & MacNeil 2023). Modeling co-occurrence probabilities of species pairs in an interconnected network may pose technical challenges, as the data could exhibit complex patterns of non-independence (Minhas et al. 2019, White et al. 2024). However, recent advances in dyadic regression, an approach developed in the social sciences, can account for such patterns (Minhas et al. 2019). Ecologists have a valuable opportunity to adapt these methods for the study of interspecific competition.

Here, I introduce a null model-free method for quantifying competitive niche differentiation with species-level presence-absence and trait data. Using species pairs as units of analysis, I adopt a Bayesian dyadic regression approach to estimate the effects of pairwise trait differences on co-occurrence probabilities. I test my method's ability to distinguish metacommunity datasets simulated with versus without competitive niche differentiation, comparing its performance against 48 commonly used null model methods. My simulation study comprises two scenarios regarding interspecific trait variation. In the first scenario, traits are uncorrelated, and in the second scenario, traits have a correlation structure expected to obscure the signal of competitive niche differentiation. The "uncorrelated traits" scenario allows me to test whether my method offers general performance advantages over null model methods, irrespective of trait

correlations. The "correlated traits" scenario allows me to test whether the advantage strengthens when traits are correlated, considering my method's ability to control for confounding among intercorrelated traits. Lastly, in an empirical example, I quantify the effect of differences in tree height and wood density on co-occurrence probabilities of species pairs in Payette National Forest, USA. In demonstrating my method, I introduce the accompanying R package, compnet.

Methods

Statistical framework:

In studies of competitive niche differentiation, the central hypothesis is that dissimilarity between species in resource use promotes cooccurrence (MacArthur & Levins 1967, Cornwell & Ackerly 2009). i.e., for a pair of species, dissimilarity in resource use increases the probability that both species will be present at a site, given that at least one is present ("co-occurrence probability" henceforth). However, comprehensive resource use data are rarely available. Consequently, most studies add an upstream link in the causal chain, specifying one or more suspected "niche differentiation traits" with available data (Cornwell & Ackerly 2009, de Bello et al. 2021). The extended hypothesis states: for a pair of species, dissimilarity in the trait(s) of interest increases dissimilarity in resource use, which increases co-occurrence probability.

This hypothesis translates readily into a regression model. The units of analysis are species pairs or "dyads". The response variable follows a binomial distribution (or related variant; see below). "Successes" are sites occupied by both species, and "trials" are sites occupied by at least one of the pair. For each trait, the relevant predictors are species *i*'s trait value, species *j*'s trait value, and their interaction. This interaction can be multiplicative, such that a negative coefficient signifies attraction of dissimilar species. Alternatively, the interaction term can use an absolute value difference (i.e., a distance), with a positive coefficient signifying attraction of dissimilar species. Categorical traits (e.g., flower color) can also be incorporated. This interaction term takes a 1 value when both species have the same trait value and a 0 when they do not.

If this model is built from data, and residual diagnostics suggest model assumptions were reasonable, then additional features may be unnecessary. However, dyads that share a member may not have independent errors (e.g., species pairs $\{i, j\}$ and $\{i, k\}$; Hoff et al. 2002, White et al. 2024). Higher-order patterns of non-independence can also arise, e.g., "the enemy of my enemy is my friend" (Minhas et al. 2019). Statistical methods typically used in ecology cannot account for these patterns. The dyadic regression approach, developed in the social sciences, can. Species-level effects can be modeled as mean-zero offsets drawn from a univariate normal distribution (Minhas et al. 2019). To account for higher-order non-independence, we can use latent variables representing "unmeasured traits", whose values are inferred from the data. For each species pair, some degree of attraction or repulsion is driven by their inferred values of the unmeasured traits (Minhas et al. 2019).

The full model structure is given below, with notation adapted from Minhas et al. (2019).

$$F_{i\&j} \sim Binomial\left(F_{i\&j} + F_{i|j}, P_{ij}\right)$$

$$Logit\left(P_{ij}\right) = \alpha + \beta_p^T x_{ij} + \beta_s^T \left(x_i + x_j\right) + a_i + a_j + u_i^T \Lambda u_j$$

$$a_1, \ldots a_n \sim i.i.d.N(0, \sigma_a^2)$$

$F_{i\&j}$ is the number of sites where species i and j cooccur. $F_{i|j}$ is the number of sites containing only i or j. P_{ij} is the probability of cooccurrence for species i and j. α is a universal intercept term for the linear predictor. x_{ij} is a vector of pair-level attributes, e.g., trait distance (for a distance interaction model) or the product of species i and j's trait values (for a multiplicative interaction model). β_p^T is a vector of coefficients for pair-level attributes. This is where the coefficient(s) of interest are found in a model of competitive niche differentiation. x_i and x_j are vectors of species-level attributes (i.e., their trait values). β_s^T is a vector of coefficients for species-level attributes. a_i and a_j are unobserved species-level effects drawn from a univariate normal distribution with variance σ_a^2. n is the number of species. u_i is a vector of length K containing species i's values of the K latent variables, and u_j contains species j's values. K, often referred to as the model "rank", is chosen by the user. I follow Hoff (2015) in recommending to start with a model rank of 0 and increase the rank until 'gofstats' diagnostic outputs are acceptable (see below). Λ is a K-by-K matrix specifying the strength of attraction or repulsion between species driven by their positions in the K-dimensional latent space.

In many cases, a binomially distributed response variable (as described above) may be sufficient. However, analysis of ecological data with binomial models often leads to zero inflation (Martin et al. 2005) or overdispersed residuals (Harrison 2015). In the case of overdispersion, beta-binomial likelihood may be required (Harrison 2015), and in the case of zero inflation, a zero-inflated binomial may be required (Martin et al. 2005).

R implementation:

I implement my model in the compnet R package, which also includes functions for diagnosing, summarizing, and visualizing model outputs. My model is implemented in a Bayesian framework using Stan, which is called by buildcompnet(). I also include a diagnostic function called gofstats(), which is adapted from the eponymous function in Hoff et al.'s (2024) 'amen' package. This function helps users assess whether non-independence among dyads has been modeled adequately, or whether a higher model rank may be needed. I also include the postpredsamp() function for easy posterior predictive sampling, a widely favored approach for checking Bayesian model fits (Conn et al. 2018).

Box 1 shows example code, which builds a model of rank 1 from example data using a trait called "ndtrait". Results are then plotted (Fig. 2).

Box 1:

```
# Load and attach package
library(compnet)

# Prep data, use more readable version of trait name
mytraits <- ex_traits[c("ndtrait")]
names(mytraits) <- c("ND Trait")
```

```
# Build model:
mod1 <- buildcompnet(presabs=ex_presabs, spvars_multi_int=mytraits, rank=1)

# Plot results
library(patchwork)
example_violin <- fixedeff_violins(mod=mod1)
example_scatter <- scatter_interaction(mod=mod1, xvar="ND Trait", ymax=0.4)
example_violin + example_scatter
```

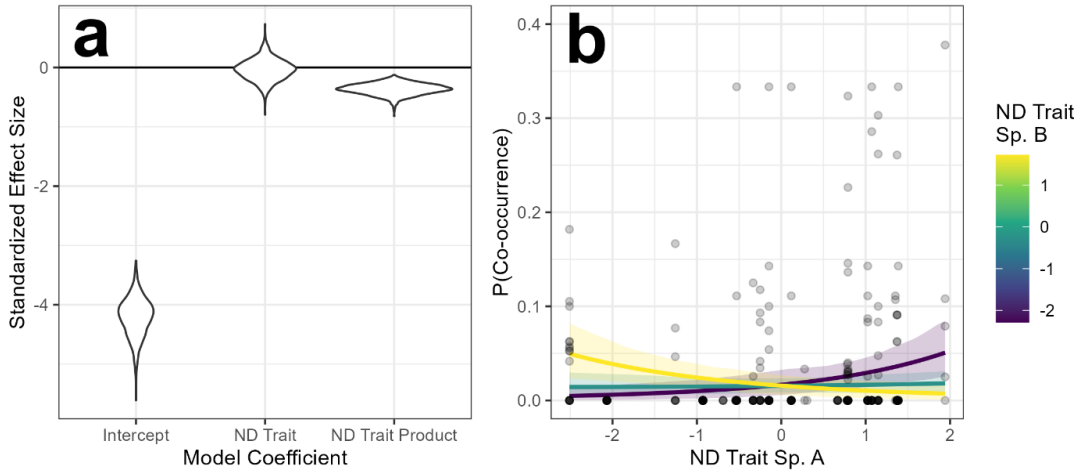

Fig. 2: compnet results for an example simulated metacommunity using a trait called "ND Trait", which drives competitive niche differentiation. Trait units are arbitrary. a) Samples from the posterior probability distributions for standardized effect sizes in a compnet model, including the multiplicative interaction between species' trait values ("ND Trait Product"). A negative coefficient signifies competitive niche differentiation. b) Points represent species pairs. The x axis and the color scale represent possible trait values for an arbitrary pair of species, "A" and "B", respectively. Ribbons represent 95% credible bands for the conditional mean prediction. When one species in a pair has a high value of "ND Trait" (yellow), the probability of co-occurrence decreases with the other species' trait value. When one species has a low "ND Trait" value (purple), co-occurrence probabilities increase with the other species' trait value.

Simulation study:

I used simulated metacommunity data to assess compnet's performance in distinguishing datasets simulated with versus without competitive niche differentiation—i.e., "positive" and "negative" cases. In this test, I compared compnet's performance against 48 null model methods. I ran two versions of the positive-versus-negative comparison: with and without trait correlations that could obscure the signal of interest. The goal of this design is to assess whether compnet has a greater performance advantage when traits are correlated, considering its capacity to control for confounding influences among intercorrelated traits.

My metacommunity simulation framework is adapted from Thompson et al. (2020). I used this model as a starting point because of its explicit, realistic mathematical representation of competitive effects on population growth rates. This feature allowed me to link species' trait values to population growth rates via competitive niche differentiation and competitive hierarchies. (See Appendix 1 for details.) Earlier simulation studies of null models' performance

used simpler, perhaps less realistic models that did not offer a clear path toward incorporating these features (Mouchet et al. 2010, de Bello 2012, de Bello et al. 2012, Chalmandrier et al. 2013, Münkemüller et al. 2015, Botta-Dukát et al. 2016, Götzenberger et al. 2016).

My simulations occur in a spatially explicit landscape over discrete time measured in generations. Ecological processes include competitive niche differentiation, competitive hierarchies, habitat filtering, dispersal, and spatiotemporal variation in the abiotic environment. Species vary in the "competitive niche differentiation trait", which determines differences in resource use, the "competitive hierarchy trait", which determines asymmetries in competitive effects, and the habitat niche optimum. Each run begins with 100 species and 100 habitat patches and concludes after 2,200 generations. I only analyzed simulation runs that concluded with at least 3 extant species and 1 site containing multiple species, as datasets without these features would be uninformative for any analytical method.

Following Thompson et al. (2020), in each simulation run, I assigned all species equal habitat niche breadth and dispersal tendency. Among different runs, I explored a range of values for these parameters, which was adapted from Thompson et al. (2020; see Appendix 1). For interpretability and computational efficiency, I sampled parameter space more sparsely than Thompson et al. (2020), only using integer powers of ten for each parameter (e.g., 0.001, 0.01, 0.1, etc.—see Appendix 1 for details). This approach yielded 20 combinations of habitat niche breadth and dispersal tendency. For each of the four simulation scenarios—i.e., positive or negative case, correlated or uncorrelated traits—I ran 30 simulations at each combination of niche breath and dispersal tendency—i.e., one run for each spatiotemporal landscape (see above). This approach yielded 600 total simulation runs for each of the four scenarios.

In the "uncorrelated traits" version of my simulations, values of each trait that varied among species were drawn from the standard Gaussian distribution (mean 0, variance 1). These were the niche differentiation trait, the competitive hierarchy trait, and the habitat niche optimum. In the "correlated traits" version, trait evolution was simulated prior to the metacommunity simulation via Brownian motion on a randomly generated phylogeny. Variance was 1 for each trait, and covariance was 0 for all trait pairings, except the "niche differentiation trait" and the "competitive hierarchy trait", for which covariance was 0.8. The competitive hierarchy trait is a "convergence trait", which could mask the "divergence" signal of the niche differentiation trait, unless the analytical method used can control for its confounding influence.

For my compnet analyses of simulated metacommunity data, I used a multiplicative interaction term between species' trait values for each dyad. In this model formulation, a negative coefficient value signifies decreasing co-occurrence with increasing trait similarity—i.e., competitive niche differentiation. For consistency and computational efficiency, the model rank (see "Statistical approach" above) was set to 1 for all runs, after analyzing 10 simulated datasets by hand and confirming that model diagnostics were sufficient. I used weakly regularizing Gaussian priors (mean 0, standard deviation 1) for all slope coefficients representing traits effects on cooccurrence (Gelman et al. 2013, McElreath 2020). All traits were centered and scaled for model-building (mean 0, standard deviation 1).

I also analyzed the simulated metacommunity data using 48 null model methods. These comprise all combinations of 3 functional diversity metrics, 8 null model algorithms, and 2 types of community data—presence-absence and abundance. I chose three widely used functional diversity metrics with well-documented theoretical justifications: functional richness ("FRic"; Mason et al. 2005, Villéger et al. 2008), dispersion ("FDis"; Laliberte & Legendre 2010), and evenness ("FEve"; Villéger et al. 2008). Each represents a distinct class of metrics capturing a different facet of functional diversity (Mouchet et al. 2010, de Bello et al. 2021). I used 8 of the 10 null model permutation algorithms used in a recent simulation study with similar goals (Götzenberger et al. 2016): "C1", "C2", "C3", "C4", "C5", "T1", "T3", and "Range". (See Appendix 1 for details.) I omitted Götzenberger et al.'s (2016) "T2" and "T4" because they are only applicable in analyses that aggregate multiple traits.

For each of the 48 null model methods, I used the approach of Cornwell & Ackerly (2009) to test whether each simulated dataset exhibits a significant signal of competitive niche differentiation. Briefly, for each dataset, I generated "standardized effect sizes" of each functional diversity metric for each site via 999 runs of the relevant null model permutation algorithm. I used a Mann-Whitney U test to assess whether the SES values were significantly greater than zero. See Appendix 1 for details.

I applied each method (compnet and the 48 null model methods) to each "positive case" and "negative case" dataset, pooling results across the parameter grid I explored (see above). I used the results to assess how frequently each method correctly or incorrectly detected a signal of competitive niche differentiation. To define "detection" of a niche differentiation effect, I used one-sided tests with an "alpha" level of 5%. For the frequentist null model methods, this was a one-tailed Mann-Whitney U test of site-level "standardized effect sizes" ("SES"; see above), using a p-value threshold of 0.05. For my Bayesian method, I tested whether more than 95% of the posterior samples for my model parameter of interest—i.e., the multiplicative interaction between species' trait values—were negative. Although significance testing is not usually a priority in Bayesian statistics (McElreath 2020), I took this approach to create a common currency for comparison with the frequentist null model methods.

Some datasets were only analyzable by a subset of methods. For example, some simulation runs ended with no communities containing more than 2 species, which is insufficient for computing functional evenness (Villéger et al. 2008). Consequently, I scaled each method's success rate according to the proportion of datasets it could analyze among the pool of datasets that were analyzable by any method. For example, if a method's raw true detection rate was 40%, but this method could only analyze 80% of datasets, then its final true detection rate was the product of these percentages—i.e., 32%. If a method had a raw false detection rate of 10%, then its raw "success rate"—i.e., rate of correct non-detections—was 90%. If only 80% of datasets were analyzable, the adjusted success rate would be the product of these percentages—i.e., 72%. The final false detection rate would be 100% minus this figure—i.e., 28%.

Empirical example:

I applied compnet to 10 tree species from Payette National Forest in the Pacific Northwest, USA. Presence-absence data came from Rosenblad et al. (2023)'s filtered version of the USDA Forest

Service's Forest Inventory and Analysis (FIA) dataset, which excluded cultivated trees and other unsuitable observations. See Rosenblad et al. (2023) for details. I used all 10 tree species recorded in all 152 subplots occurring in Payette National Forest (Idaho). My two traits, downloaded from TRY (Kattge et al. 2011), were maximum height and wood density. Both traits can affect acquisition of resources like light and water in multiple ways (Falster & Westoby 2003, Chave et al. 2009), and thus each could drive competitive niche differentiation, depending on the ecophysiological mechanisms underpinning competition. Height was log-transformed, so that the ratio of two species' heights, rather than their difference, has a consistent meaning.

I ran two versions of my compnet model: one with both traits (height and wood density) and one with only height. The purpose of this approach was to assess whether controlling for wood density helps to reveal the effect of height, as described in the Introduction (Pearl 2009, Arif & MacNeil 2023).

All analyses were conducted in R (R Core Team 2024). In addition to compnet, I used the following packages: sf (Pebesma 2018, Pebesma & Bivand 2024), rtry (Lam et al. 2023), DHARMa (Hartig 2022), ggplot2 (Wickham 2016), patchwork (Pedersen 2024), foreach (Microsoft & Weston 2022), doParallel (Microsoft & Weston 2022), geiger (Harmon et al. 2008), phytools (Revell 2024), vegan (Oksanen et al. 2022), and ggthemes (Arnold 2024).

Results

Simulation study:

I found that compnet exhibits greater true detection rates than leading alternatives, while maintaining false detection rates near the 5% target (Fig. 3). compnet's true detection rates were 47% and 45% in the "uncorrelated traits" and "correlated traits" scenarios, respectively. False detection rates were 5.8% and 3.5%. All presence-absence-based null model methods yielded false detection greater than double the 5% target (Fig. 3a-b). In contrast, in the "uncorrelated traits" scenario, three abundance-based null model methods exhibited false detection rates near the 5% target (Fig. 3c). These methods combine the functional dispersion (FDis) metric with the C1, C3, and C5 null models, yielding false detection rates of 8.7%, 0%, and 0% (Fig. 3c). Among these, C5 yielded the greatest true detection rate at 40%—i.e., 7% below compnet (Fig. 3c). The "correlated traits" scenario yielded similar results, but compnet's advantage in true detection rate increased to 15%—i.e., 45% versus 30% (Fig. 3d). Some null model methods exhibited greater true detection rates than compnet, but their false detection rates were greater than double the 5% target (Fig. 3).

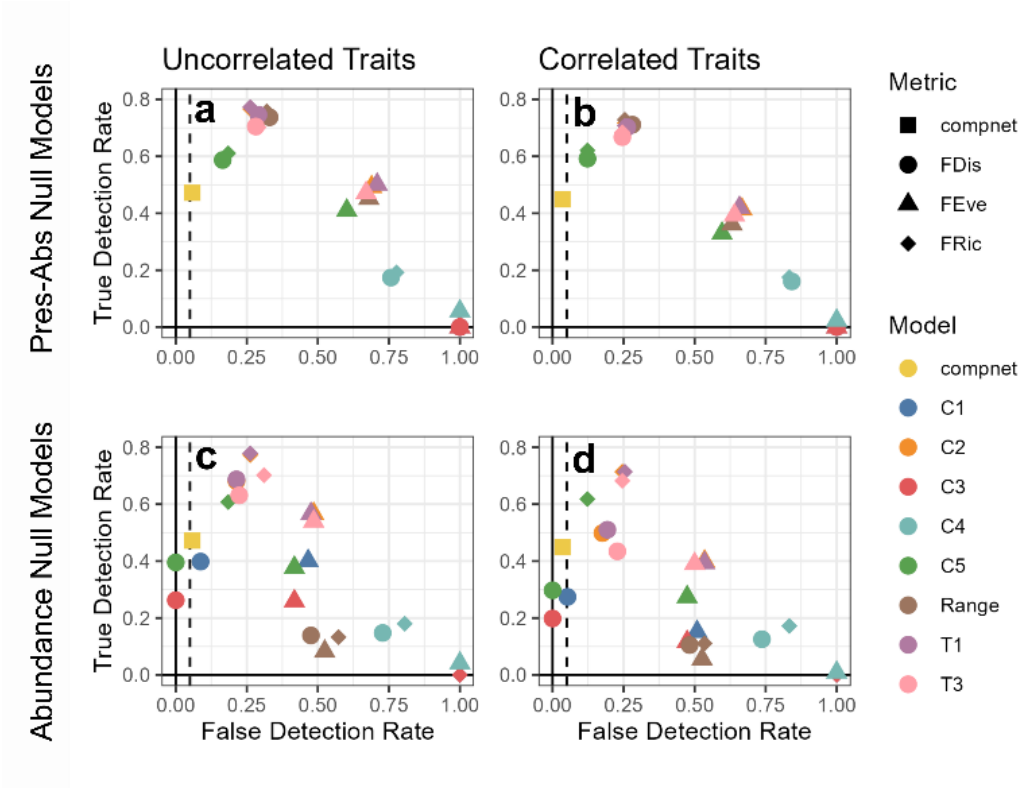

Fig. 3: Simulation study results showing rates of true and false detection of competitive niche differentiation for my method, compnet, and commonly used null model methods. In panels a and b, null model results are based on presence-absence data (i.e., ignoring abundance). In panels c and d, null model results are based on abundance data. Panels a and c are based on metacommunity data simulated with trait correlations. Panels b and d are based on data simulated with trait correlations that mask the signal of competitive niche differentiation. Results for compnet, which only uses presence-absence data, are the same between panels a and c, as well as between panels b and d. Significance is defined by a 5% threshold. The dashed vertical line at 0.05 represents the target false positive rate based on this threshold.

In the "uncorrelated traits" scenario, 339 of 600 "positive case" simulations yielded data suitable for analysis by compnet. 103 of 600 "negative cases" were suitable for compnet. In the "correlated traits" scenario, there were 343 and 114 suitable positive and negative cases, respectively. No dataset was analyzable by a null model method and not by compnet. Some null model methods, such as the combination of the FDis metric and the C5 null model ("FDis/C5")—the top-performing null model method—were usable with the same datasets as compnet. Others were only usable with a subset. e.g, "FRic/C5" was only applicable to 260 of the 339 positive cases with uncorrelated traits. Table S3.1 contains the number of analyzable datasets for each null model method.

True and false detection rates for compnet and "FDis/C5", the leading null model method, varied across the simulation parameter space explored (Fig. S3.1-S3.2). compnet generally performed best at low and medium habitat niche breadth, and FDis/C5 generally performed best at medium habitat niche breadth.

Empirical example:

In my two-trait compnet model for Payette National Forest, I found that tree height is a niche differentiation trait—i.e., tall species co-occur most with short species, and vice versa (Fig. 5a). The standardized interaction effect between species' heights (log transformed) is -0.96 (95% CI -1.76, -0.24). Wood density, which is correlated with height (Pearson correlation 0.83), is a "convergence trait" (Fig. 5b), indicating that species of similar wood density are more likely to co-occur. The standardized effect size for the interaction coefficient between species' wood densities is 0.55 (95% CI -0.21, 1.4). Relative to the two-trait model, the estimated niche differentiation effect for height was attenuated in the single-trait model (Fig. 5c-d; mean effect = -0.54; 95% CI -1.1, -0.11).

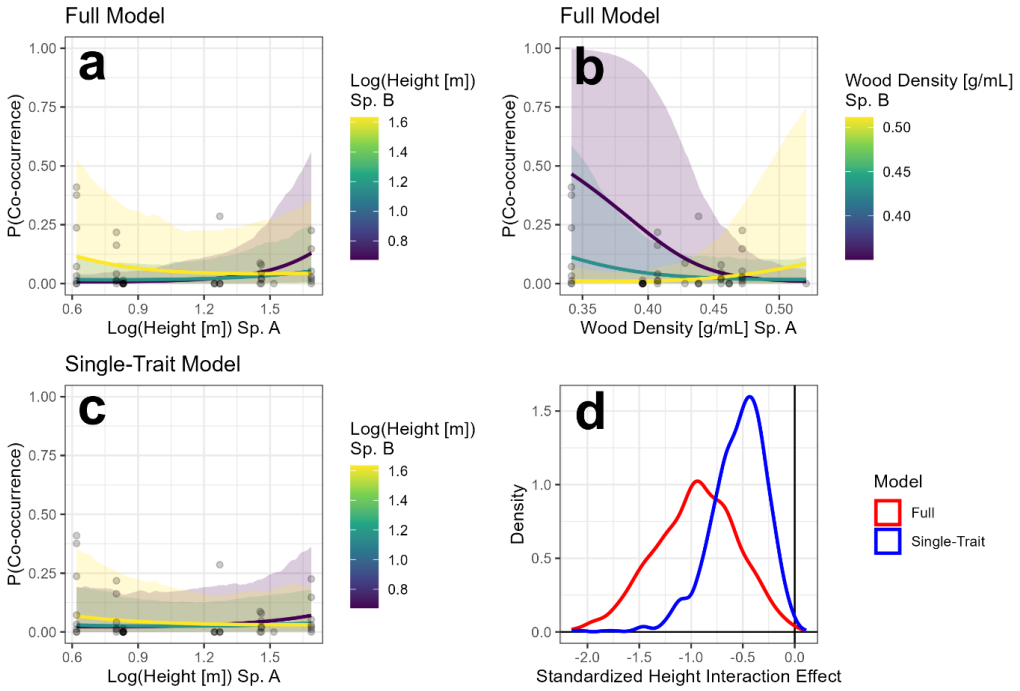

Fig. 4: Effects of tree species' height and wood density on pairwise co-occurrence probabilities in Payette National Forest, USA. Presence-absence data come from the USDA Forest Service FIA program, and height data come from TRY. a-c) Ribbons represent 95% credible bands for the conditional mean prediction. The y-axis represents the probability of co-occurrence in roughly 200 m^2 forest plots. a-b) Results from the model including all measured traits. Points represent species pairs. c) Results from a model including only height. d) Samples from the posterior probability distributions for the standardized interaction effect between species' height values. A negative interaction signifies competitive niche differentiation.

Discussion

Here I introduce compnet, a Bayesian dyadic regression method implemented in R (see Box 1, Fig. 2), which tests for interspecific competition with species traits and presence-absence data. In a simulation study, I show that compnet outperformed 48 null model methods—including 24 that use abundance data—in detecting signals of competitive niche differentiation, while avoiding excessive false detections (Fig. 3). In simulated metacommunity data with uncorrelated species traits, compnet correctly detected competitive niche differentiation in 47% of cases, compared to 40% for the leading null model method (Fig. 3c). For datasets with trait correlations, this detection advantage widened to 45% versus 30% (Fig. 3d). This increased advantage is consistent with the expectation that compnet's relative performance benefits from its ability to

control for confounding among correlated traits. My simulation study also revealed that many null model methods can exhibit problematically high false detection rates (Fig. 3), corroborating past appeals for caution (Mouchet et al. 2010, de Bello 2012, de Bello et al. 2012, Chalmandrier et al. 2013, Botta-Dukát et al. 2016, Götzenberger et al. 2016, Münkemüller et al. 2020). My empirical example further demonstrates compnet's advantages, revealing that tree communities in Payette National Forest (USA) exhibit competitive niche differentiation driven by tree height. The "trait divergence" effect of height is obscured by the "trait convergence" effect of wood density, which compnet controls for in a two-trait model. (This example also shows how compnet can be useful when research goals involve testing for trait convergence.) This new empirical evidence of "hidden" competitive niche differentiation suggests the phenomenon could be more prevalent in nature than previously appreciated. My compnet R package enables any user to implement my method and test for these hidden signals.

My simulation study shows that compnet outperforms null model alternatives even when species traits are uncorrelated (Figs. 3a, 3c). This result suggests compnet offers advantages beyond its ability to account for trait correlations. Of the three null model methods exhibiting false detection rates near the 5% target, the leading method yielded a true detection rate of 40%—i.e., 7% less than compnet (Fig. 3c). This method uses functional dispersion ("FDis"; Laliberte & Legendre 2010) as a functional diversity metric and Götzenberger et al.'s (2016) "C5" as a null model algorithm. An appropriate null model algorithm should approximate the expected distribution of the data under two assumptions: 1- competitive niche differentiation is absent, and 2- all other processes (e.g., dispersal, habitat filtering) are occurring (Tokeshi 1986, Gotelli & Graves 1996). My results suggest null model methods may fail to meet these assumptions, leading to suboptimal performance in detecting competitive niche differentiation. compnet's null model-free approach may help circumvent these issues.

When traits are correlated, compnet outperforms null model methods by a wider margin (Figs. 3b, 3d). This result suggests compnet's ability to account for trait correlations provides an additional performance boost. In my "correlated traits" simulation scenario, the abundance-based "FDis/C5 method" (see above) was again the leading null model approach, but its true detection rate was 30%, only 2/3 of compnet's (Fig. 3d). In this simulation scenario, the trait divergence pattern driven by the "niche differentiation trait" was blurred by the trait convergence effect of the "competitive hierarchy trait" (Pearl 2009, Arif & MacNeil 2023). My compnet models included separate terms for each trait, allowing me to control for the competitive hierarchy trait's confounding influence (Pearl 2009, Arif & MacNeil 2023). (See conceptual illustration in Fig. 1.) In contrast, null model methods include no comparable mechanism. My results suggest this difference between methods may strengthen compnet's performance advantage.

My case study of trees in Payette National Forest (USA) provides new empirical evidence of competitive niche differentiation that is "hidden" by a trait correlation. I show that tree height is a niche differentiation trait, perhaps reflecting partitioning of light resources (Poorter et al. 2005). Wood density exhibits the opposite pattern—i.e., trait convergence. Possible mechanisms include habitat filtering, whereby similar habitats select for similar wood density, a competitive hierarchy, whereby low-density competitively exclude high density species, or dispersal limitation (van der Valk 1981, Cornwell et al. 2006, Mayfield & Levine 2010 Münkemüller et al.

2012). I also show that trait convergence in wood density obscures trait divergence in height. This conclusion is supported by the weaker effect estimate for height in the single-trait model compared to the two-trait model (Fig. 4). This empirical example further illustrates compnet's ability to handle the problem of correlated traits.

In addition to testing for competitive niche differentiation, my method could also help detect patterns of trait convergence. This pattern, whereby species with similar trait values cooccur more often, can indicate habitat filtering, a competitive hierarchy, or dispersal limitation (van der Valk 1981, Cornwell et al. 2006, Mayfield & Levine 2010 Münkemüller et al. 2012). For example, in my case study, compnet revealed that species with similar wood densities are more likely to cooccur. Trait convergence requires care in interpretation due to the diversity of possible mechanisms.

Additionally, my method may help advance the longstanding search for traits underlying coexistence of competing species. Many studies suggest intraspecific competition is stronger than interspecific competition (Adler et al. 2018)—the hallmark of competitive niche differentiation—yet the relationships between functional traits and coexistence remain elusive. A recent theoretical study proposes that these relationships may be too complex to estimate directly (Levine et al. 2024), suggesting that more integrative but labor-intensive "process-informed measurements" ("PIMs"), such as Tilman's (1980) R*, may be required (Levine et al. 2024). Levine et al. (2024) cite past null model studies as evidence that competitive niche differentiation rarely leaves a signal in easily obtainable trait data. However, I show here that compnet can detect signals of competitive niche differentiation that null model methods cannot. Furthermore, compnet's detection advantage is strongest when the traits driving competitive niche differentiation are obscured by correlations with other traits, e.g., traits defining a competitive hierarchy. Intriguingly, prior work suggests correlations between "niche differentiation traits" and "competitive hierarchy traits" may be common (Kraft et al. 2015, Kunstler et al. 2016, Díaz et al. 2016). These results suggest prior null model studies may have missed key patterns that compnet could detect. By controlling for confounding relationships among traits, compnet may offer valuable insights into mechanisms of coexistence when more labor-intensive measurements like PIMs are unavailable.

Conclusion

In this dissertation, I used three different lenses to examine the dynamics of plants in insular environments, with a focus on understanding how climate change may shape their future. This work yielded insights into their basic ecology, evolution, and biogeography, which could also help conservation managers plan strategies for in situ conservation or assisted gene flow.

Chapter 1 yielded several key results regarding responses of western US forests to recent climate change. First, although forests are shifting in composition toward warmer-associated taxa, the rate of this process is slow relative to the rate of warming. This result suggests managers might be able to help forests persist under climate change by helping warmer-associated species become established (Schwartz et al. 2012). This strategy, known as assisted migration, is controversial, but the degree of risk is generally understood to be lower when the geographic scale of the translocation event is small (Richardson et al. 2009). My findings, in conjunction with other recent work, suggest that positive forest conservation outcomes could be achieved via targeted small-scale assisted migration events. This is because, as another recent study showed, tree species in the western US have been successful at immigrating into new large-scale climate zones (i.e., at the scale of hundreds of kilometers) at a rate roughly commensurate with recent changes in climate (Sharma et al. 2022). However, my work suggests that when propagules of a new species reach a new major climate zone, there may be a substantial lag before this species reaches sufficiently high abundance to "fill in" local forest communities. Thus, managers may not necessarily need to move tree species over large distances to help bolster western US forests against climate change. Instead, they may only need to help desired species increase their local abundance more rapidly in newly-reached climate zones through targeted translocation events on the scale of tens of kilometers, rather than hundreds or thousands.

My Chapter 1 results also suggest that in the western US, cool, north-facing hillslopes are unlikely to function effectively as microclimatic refugia, as they are sometimes hypothesized to do (Ackerly et al. 2020). Because pole-facing hillslopes generally receive less solar energy than the surrounding landscape (McCune & Keon 2002), they are often cooler. Consequently, these microsites have been highlighted as good potential places for organisms to escape warming temperatures across the broader landscape (Ackerly et al. 2020). However, recent work has called this hypothesis into question, showing that, for a given landscape in North America, a tree species that occupies north-facing hillslopes is likely to be near the trailing edge of its climatic niche (Ackerly et al. 2020). Thus, these species are likely to be the most vulnerable to climate change among those in the landscape. By analyzing changes in forest community composition over time, I show that not only are north-facing hillslopes losing their most cool-associated taxa—just like other landscape positions—but the rate at which the coolest-associated species are lost is accelerated on north-facing hillslopes. Thus, north-facing hillslopes appear to be "anti-refugia"—i.e., microenvironments that are especially vulnerable to climate change. This finding may help land managers triage conservation strategies, given that cool-associated taxa on north-facing hillslopes appear less likely to persist in situ.

In Chapter 2, I found that Sierra Nevada populations of Lemmon's willow (*Salix lemmonii*) show ecotypic variation in drought and freezing resistance along gradients of exposure to summer drought and spring freezing, respectively. These traits showed no indication of a performance tradeoff. Consequently, genotypes with strong resistance to both abiotic stressors could be sourced from sites that are harsh in both respects—i.e., high drought and freezing exposure. These genotypes could serve as valuable source material for assisted gene flow projects designed to future-proof populations against a future of greater climate-driven abiotic stress. My study region, Tahoe National Forest, harbors steep climatic gradients over just tens of kilometers, so it may be possible to undertake assisted gene flow over a spatial scale at which legal, ethical, and other difficulties (Schwartz et al. 2012) are minimized.

A central message from Chapter 3 is that competitive niche differentiation may play a stronger role in ecological communities than previous results suggest. Functional traits are a key tool for disentangling the ecological processes structuring communities (McGill et al. 2006), but different traits are often intercorrelated across species (Barnagaud et al. 2014, Díaz et al. 2016). Consequently, if two correlated traits shape community dynamics in different ways, they can blur or "confound" each other's signals in the data (Pearl 2009, Arif & MacNeil 2023). My method, compnet, offers new tools for disentangling these types of patterns and revealing signals of competitive niche differentiation that would be missed by other methods. In my empirical example, the signal of competitive niche differentiation, which is driven by tree height, is obscured to other methods by a correlation with wood density. These findings suggest that existing methods for forecasting community dynamics under climate change are likely omitting key interspecific competitive dynamics. My method can help incorporate these dynamics into existing predictive frameworks, thereby improving our ability to forecast community-level responses to climate change across habitat patches.

Overall, this dissertation offers new empirical insights and technical tools that could enhance our ability to predict future plant biodiversity dynamics under climate change. Chapters 1 and 2 also have relevance for planning specific conservation interventions, such as assisted migration and assisted gene flow. These strategies hold potential to lessen the impacts of climate change on biodiversity, as well as the ecosystem services biodiversity provides to humans (Richardson et al. 2009, Schwartz et al. 2012). Nonetheless, as climate change forecasts have become increasingly severe, it has become increasingly clear that, in addition to "climate adaptation" strategies such as those outlined here, reducing greenhouse gas emissions and promoting natural carbon sinks must remain central priorities for humanity (United Nations Environment Programme 2024, Seddon 2022).

Bibliography

Abatzoglou, J.T. (2013) Development of gridded surface meteorological data for ecological applications and modelling. *International Journal of Climatology, 33,* 121-131.

Abatzoglou, J. T. et al. (2018) TerraClimate, a high-resolution global dataset of monthly climate and climatic water balance from 1958–2015. *Scientific Data*, *5,* 170191.

Ackerly, D. D. et al. (2020) Topoclimates, refugia, and biotic responses to climate change. *Frontiers in Ecology and the Environment 18(5),* 288–297.

Adler, P.B., Fajardo, A., Kleinhesselink, A.R. & Kraft, N.J.B. (2013) Trait-based tests of coexistence mechanisms. *Ecology Letters, 16,* 1294–1306.

Adler, P.B., Smull, D., Beard, K.H., Choi, R.T., Furniss, T., Kulmatiski, A. et al. (2018) Competition and coexistence in plant communities: intraspecific competition is stronger than interspecific competition. *Ecology Letters, 21,* 1319-1329.

Aitken, S. N. & Whitlock, M.C. (2013) Assisted gene flow to facilitate local adaptation to climate change. *Annual Review of Ecology, Evolution, and Systematics, 44,* 367–388.

Aitken, S.N., Yeaman, S., Holliday, J.A., Wang, T. and Curtis-McLane, S. (2008) Adaptation, migration or extirpation: climate change outcomes for tree populations. *Evolutionary Applications, 1,* 95-111.

Albano, C.M., McClure, M.L., Gross, S.E., et al. (2019) Spatial patterns of meadow sensitivities to interannual climate variability in the Sierra Nevada. *Ecohydrology*, *12,* e2128.

Alberto, F.J., Aitken, S.N., Alía, R., González-Martínez, S.C., Hänninen, H., Kremer, A., Lefèvre, F., Lenormand, T., Yeaman, S., Whetten, R. & Savolainen, O. (2013) Potential for evolutionary responses to climate change – evidence from tree populations. *Global Change Biology,* 1645-1661.

Alexander, J.M., Diez, J.M. & Levine, J.M. (2015) Novel competitors shape species' responses to climate change. *Nature*, *525,* 515–518.

Anderegg, W.R.L. et al. (2015) Tree mortality from drought, insects, and their interactions in a changing climate. *New Phytologist, 208,* 674-683.

Anderegg, W.R.L., Anderegg, L.D.L., Kerr, K.L., & Trugman, A.T. (2019) Widespread drought-induced tree mortality at dry range edges indicates that climate stress exceeds species' compensating mechanisms. *Global Change Biology, 25*, 3793–3802.

Anderson, J.T., Willis, J.H., & Mitchell-Olds, T. (2011) Evolutionary genetics of plant adaptation. *Trends in Genetics*, 27, 258–266.

Anderson, J.T., Lee, C.-R., Rushworth, C.A., Colautti, R.I., & Mitchell-Olds, T. (2013) Genetic trade-offs and conditional neutrality contribute to local adaptation. *Molecular Ecology, 22,* 699-708.

Anderson, M. K. (2013) Trending the Wild: Native American knowledge and the management of California's natural resources. University of California Press, Berkeley, California, USA.

Antonovics, J. (1976) The nature of limits to natural selection. *Annals of the Missouri Botanical Garden, 63,* 224–247.

Argus, G.W. (2007) *Salix* (*Salicaceae*) distribution maps and a synopsis of their classification in North America, north of Mexico. *Harvard Papers in Botany, 12,* 335–368.

Argus, G.W. (2012) *Salix lemmonii*, in Jepson Flora Project (eds.) Jepson eFlora, https://ucjeps.berkeley.edu/eflora/eflora_display.php?tid=42864, accessed on February 03, 2024.

Arif, S. & MacNeil, M.A. (2022) Predictive models aren't for causal inference. *Ecology Letters, 25,* 1741–1745.

Arif, S. & MacNeil, M.A. (2023) Applying the Structural Causal Model Framework for Observational Causal Inference in Ecology. *Ecological Monographs* 93(1): e1554.

Arnold, J. (2024) _ggthemes: Extra Themes, Scales and Geoms for 'ggplot2'_. R package version 5.1.0, <https://CRAN.R-project.org/package=ggthemes>.

Arnold, C., Ghezzehei, T. A., & Berhe, A.A. (2014) Early spring, severe frost events, and drought induce rapid carbon loss in high elevation meadows. *PLoS ONE, 9*, e106058.

Ashcroft, M.B., Chisholm, L.A., & French, K.O. (2009) Climate change at the landscape scale: predicting fine-grained spatial heterogeneity in warming and potential refugia for vegetation. *Global Change Biology*, *15,* 656-667.

Aubry-Kientz, M. & Moran, E.V. (2017) Climate Impacts on Tree Growth in the Sierra Nevada. *Forests*, *2017*, 8(11):414.

Baldwin, B.G. (2019) Fine-Scale to Flora-Wide Phylogenetic Perspectives on Californian Plant Diversity, Endemism, and Conservation. *Annals of the Missouri Botanical Garden, 104*, 429–440.

Bartlett, M.K., Zhang, Y., Kreidler, N., Sun, S., Ardy, R., Cao, K., & Sack, L. (2014) Global analysis of plasticity in turgor loss point, a key drought tolerance trait. *Ecology Letters 17,* 1580–1590.

Barnagaud, J.-Y., Kissling, W.D., Sandel, B., Eiserhardt, W.L., Şekercioğlu, Ç.H., Enquist, B.J. et al. (2014) Ecological traits influence the phylogenetic structure of bird species co-occurrences worldwide. *Ecology Letters, 17,* 811–820.

Bechtold W.A. & Patterson, P.L. (2005) The Enhanced Forest Inventory and Analysis Program: National Sampling Design and Estimation Procedures. USDA Forest Service, Southern Research Station, Asheville, NC.

de Bello, F. (2012) The quest for trait convergence and divergence in community assembly: are null-models the magic wand? *Global Ecology and Biogeography, 21,* 312-317.

de Bello, F., Price, J. N., Münkemüller, T., Liira, J., Zobel, M., Thuiller, W. et al. (2012). Functional species pool framework to test for biotic effects on community assembly. *Ecology, 93,* 2263–2273.

de Bello, F., Carmona, C. P., Dias, A. T. C., Götzenberger, L., Moretti, M. & Berg, M. P. (2021) Handbook of trait-based ecology. Cambridge Univ. Press.

Berger, J., Palta, J., & Vadez, V. (2016) An integrated framework for crop adaptation to dry environments: Responses to transient and terminal drought. *Plant Science, 253,* 58–67.

Bertrand, R. et al. (2016) Ecological constraints increase the climatic debt in forests. *Nature Communications, 7,* 12643.

Bivand, R., Keitt, T. & Rowlingson, B. (2021) rgdal: Bindings for the 'Geospatial' Data Abstraction Library. R package version 1.5-21. https://CRAN.R-project.org/package=rgdal.

Bivand, R., Nowosad, J., & Lovelace, R. (2020) spData: Datasets for Spatial Analysis. R package version 0.3.8. https://CRAN.R-project.org/package=spData.

Bivand, R. & Rundel, C. (2020) rgeos: Interface to Geometry Engine - Open Source ('GEOS'). R package version 0.5-5. https://CRAN.R-project.org/package=rgeos.

Bloom, A.J., Chapin, F.S., Mooney, H.A. (1985) Resource limitation in plants - an economic analogy. *Annual Review of Ecology and Systematics, 16,* 363–392.

Botta-Dukát, Z. & Czúcz, B. (2016) Testing the ability of functional diversity indices to detect trait convergence and divergence using individual-based simulation. *Methods in Ecology and Evolution, 7,* 114-126.

Brice, M.-H., Cazelles, K., Legendre, P., & Fortin, M.-J. (2019) Disturbances amplify tree community responses to climate change in the temperate–boreal ecotone. *Global Ecology and Biogeography 28,* 1668–1681.

Brooks, M.E., Kristensen, K., van Benthem, K.J., Magnusson, A., Berg, C.W. Nielsen, A. et al. (2017) glmmTMB Balances Speed and Flexibility Among Packages for Zero-inflated Generalized Linear Mixed Modeling. *The R Journal, 9(2),* 378-400.

Bucharova, A. (2017) Assisted migration within species range ignores biotic interactions and lacks evidence. *Restoration Ecology, 25,* 14-18.

Bürkner, P.C. (2017) brms: An R Package for Bayesian Multilevel Models Using Stan. *Journal of Statistical Software, 80(1),* 1-28.

Calenge, C. (2006) The package adehabitat for the R software: a tool for the analysis of space and habitat use by animals. *Ecological Modelling, 197,* 516-519.

Capblancq, T., Lachmuth, S., Fitzpatrick, M.C. & Keller, S.R. (2023) From common gardens to candidate genes: exploring local adaptation to climate in red spruce. *New Phytologist, 237,* 1590-1605.

Cartwright, J. (2019). Ecological islands: Conserving biodiversity hotspots in a changing climate. *Frontiers in Ecology and the Environment, 17,* 331–340.

Caspari, E. (1950) On the selective value of the alleles rt and rt in *Ephestia Kuhniella*. *American Naturalist*, *84(818),* 367–380.

Chalmandrier, L., Münkemüller, T., Gallien, L., de Bello, F., Mazel, F., Lavergne, S. & Thuiller, W. (2013) A family of null models to distinguish between environmental filtering and biotic interactions in functional diversity patterns. *Journal of Vegetation Science, 24,* 853-864.

Chave, J., Coomes, D., Jansen, S., Lewis, S.L., Swenson, N.G., & Zanne, A.E. (2009) Towards a worldwide wood economics spectrum. *Ecology Letters, 12,* 351–366.

Clements, F. E. (1916) Plant succession: an analysis of the development of vegetation. Carnegie Institution of Washington, Washington, D.C., USA.

Compagnoni, A., Levin, S., Childs, D.Z. *et al.* (2021) Herbaceous perennial plants with short generation time have stronger responses to climate anomalies than those with longer generation time. *Nature Communications, 12,* 1824.

Conn, P. B., Johnson, D.S, Williams, P.J., Melin, S. R., & Hooten, M. B. (2018) A guide to Bayesian model checking for ecologists. *Ecological Monographs, 88,* 526–542.

Connor, E. F., & Simberloff, D. (1983) Interspecific competition and species co-occurrence patterns on islands: null models and the evaluation of evidence. *Oikos, 41,* 455–465.

Cornwell, W.K. & Ackerly, D.D. (2009) Community assembly and shifts in the distribution of functional trait values across an environmental gradient in coastal California. *Ecological Monographs*, 79, 109–126.

Crockett, J. L., & Westerling, A. L. (2018) Greater Temperature and Precipitation Extremes Intensify Western U.S. Droughts, Wildfire Severity, and Sierra Nevada Tree Mortality. *Journal of Climate 31(1),* 341-354.

Davis, K. T. et al. (2019) Wildfires and climate change push low-elevation forests across a critical climate threshold for tree regeneration. *Proceedings of the National Academy of Sciences of the United States of America, 116,* 6193–6198.

Dawson, T.E. & Bliss, L.C. (1989) Intraspecific variation in the water relations of *Salix arctica*, an arctic-alpine dwarf willow. *Oecologia*, *79,* 322–331.

Debinski, D.M. & Holt, R.D. (2000) A Survey and Overview of Habitat Fragmentation Experiments. *Conservation Biology, 14,* 342-355.

De Frenne, P. et al. (2013) Microclimate moderates plant responses to macroclimate warming. *Proceedings of the National Academy of Sciences of the United States of America, 110,* 18561–18565.

De Frenne, P. et al. (2019) Global buffering of temperatures under forest canopies. *Nature Ecology and Evolution, 3,* 744–749.

Dettinger, M., Alpert, H., Battles, J.J., Kusel, J., Safford, H., & Fougeres, D. et al. (2018) Sierra Nevada summary report. California's Fourth Climate Change Assessment. California Energy Commission/Natural Resources Agency, Sacramento, California, USA.

Diamond, J. M. (1975) Assembly of species communities. Pages 342–444 *in* M. L. Cody and J. M. Diamond, editors. Ecology and evolution of communities. Harvard University Press, Cambridge, Massachusetts, USA.

Díaz, S., Kattge, J., Cornelissen, J. *et al.* (2016) The global spectrum of plant form and function. *Nature, 529,* 167–171.

Doughty, C.E., Keany, J.M., Wiebe, B.C. et al. (2023) Tropical forests are approaching critical temperature thresholds. *Nature, 621,* 105–111.

Evers, S.M. et al. (2021) Lagged and dormant season climate better predict plant vital rates than climate during the growing season. *Global Change Biology, 27,* 1927-1941.

Falster, D.S. & Westoby, M. (2003) Plant height and evolutionary games. *Trends in Ecology & Evolution, 18,* 337–343.

Feeley, K. J., Bravo-Avila, C., Fadrique, B., Perez, T. M., & Zuleta, D. (2020) Climate-driven changes in the composition of New World plant communities. *Nature Climate Change 10(10),* 965–970.

Feeley, K.J., Hurtado, J., Saatchi, S., Silman, M.R. & Clark, D.B. (2013) Compositional shifts in Costa Rican forests due to climate-driven species migrations. *Global Change Biology, 19,* 3472-3480.

Felsenstein, J. (1985) Phylogenies and the comparative method. *The American Naturalist, 125,* 1–15.

Fletcher, L.R., Scoffoni, C., Farrell, C., Buckley, T.N., Pellegrini, M. & Sack, L. (2022) Testing the association of relative growth rate and adaptation to climate across natural ecotypes of *Arabidopsis*. *New Phytologist, 236,* 413-432.

Flint, L. E., Flint, A. L., & Stern, M. A. (2021) The basin characterization model—A regional water balance software package. Page 85. Report, Reston, VA.

Frankham, R. (2015) Genetic rescue of small inbred populations: Meta-analysis reveals large and consistent benefits of gene flow. *Molecular Ecology, 24,* 2610–2618.

Frei, K., Vojtkó, A. E., Tölgyesi, C., Vojtkó, A., Farkas, T., Erdős, L. et al. (2024) Topographic complexity drives trait composition as well as functional and phylogenetic diversity of understory plant communities in microrefugia: new insights for conservation. *Forest Ecosystems, 11*, 100278.

Garland, T. (2014) Trade-offs. *Current Biology, 24,* R60–R61.

GBIF.org (24 September 2023) GBIF Occurrence Download https://doi.org/10.15468/dl.sxma3d

Gelman, A., Carlin, J. B., Stern, H. S., Dunson, D. B., Vehtari, A., & Rubin, D. B. (2013) Bayesian data analysis. Boca Raton, FL: CRC Press.

Gillespie, R.G., Baldwin, B.G., Waters, J.M., Fraser, C.I., Nikula, R. & Roderick, G.K. (2012) Long-distance dispersal: a framework for hypothesis testing. *Trends in Ecology and Evolution*, 27, 47–56.

Gotelli, N.J. & Graves, G.R. (1996) Null Models in Ecology. Smithsonian Institution Press, Washington, DC, U.S.A.

Götzenberger, L., Botta-Dukát, Z., Lepš, J., Pärtel, M., Zobel, M. & de Bello, F. (2016) Which randomizations detect convergence and divergence in trait-based community assembly? A test of commonly used null models. *Journal of Vegetation Science, 27,* 1275-1287.

Govaert, S. et al. (2021) Rapid thermophilization of understorey plant communities in a 9 year-long temperate forest experiment. *Journal of Ecology, 109,* 2434–2447.

Grime, J. (1974) Vegetation classification by reference to strategies. *Nature, 250,* 26–31.

Grossman, J.J. (2023) Phenological physiology: seasonal patterns of plant stress tolerance in a changing climate. *New Phytologist, 237,* 1508-1524.

Haase, P. et al. (2019) Moderate warming over the past 25 years has already reorganized stream invertebrate communities. *Science of the Total Environment, 658,* 1531–1538.

Harrison, S. & Rajakaruna, N. (2011) Serpentine: The Evolution and Ecology of a Model System. University of California Press, Berkeley.

Harrison, S., Spasojevic, M. J., & Li, D. Climate and plant community diversity in space and time (2020) *Proceedings of the National Academy of Sciences of the United States of America, 117(9),* 4464–4470. https://doi.org/10.1073/pnas.1921724117.

Harmon, L. J., Weir, J.T., Brock, C.D., Glor, R.E., & Challenger, W. (2008) GEIGER: investigating evolutionary radiations. *Bioinformatics, 24,* 129-131.

Harrell Jr., F.E. (2001) Regression modeling strategies. Springer-Verlag. NY: New York.

Hartig, F. (2022) _DHARMa: Residual Diagnostics for Hierarchical (Multi-Level / Mixed) Regression Models_. R package version 0.4.6, <https://CRAN.R-project.org/package=DHARMa>.

Hellmann, J. J. & Pineda-Krch, M. (2007) Constraints and reinforcement on adaptation under climate change: selection of genetically correlated traits. *Biological Conservation, 137*, 599–609.

Hijmans, R.J. (2020) raster: Geographic Data Analysis and Modeling. R package version 3.4-5. https://CRAN.R-project.org/package=raster.

Hoff, P.D. (2015) Dyadic data analysis with AMEN (https://arxiv.org/abs/1506.08237).

Hoff, P.D., Raftery, A.E., & Handcock, M. S. (2002) Latent space approaches to social network analysis. *Journal of the American Statistical Society, 97(460),* 1090–1098.

Hoff, P., Fosdick, B., & Volfovsky, A. (2024). _amen: Additive and Multiplicative Effects Models for Networks and Relational Data_. R package version 1.4.5, <https://CRAN.R-project.org/package=amen>.

Hoffmann, A. & Sgrò, C. (2011) Climate change and evolutionary adaptation. *Nature, 470,* 479–485.

Ives, A.R. & Helmus, M.R. (2011) Generalized linear mixed models for phylogenetic analyses of community structure. *Ecological Monographs, 81,* 511-525.

Karger, D. N. et al. (2017) Climatologies at high resolution for the earth's land surface areas. *Scientific Data 4,* 170122.

Karger, D.N. et al. (2018) Data from: Climatologies at high resolution for the earth's land surface areas. Dryad Digital Repository. http://dx.doi.org/doi:10.5061/dryad.kd1d4.

Kattge, J., Diaz, S., Lavorel, S., Prentic, I.C., Leadley, P., Bonisch, G. et al. (2011) TRY – a global database of plant traits. *Global Change Biology, 17,* 2905-2935.

Kelly, M.W., DeBiasse, M.B., Villela, V.A., Roberts, H.L. & Cecola, C.F. (2016) Adaptation to climate change: trade-offs among responses to multiple stressors in an intertidal crustacean. *Evolutionary Applications, 9,* 1147-1155.

Kraft, N.J.B., Godoy, O. & Levine, J.M. (2015). Plant functional traits and the multidimensional nature of species coexistence. *Proceedings of the National Academy of Sciences of the United States of America, 112,* 797–802.

Kunstler, G., Falster, D., Coomes, D.A., Hui, F., Kooyman, R.M., Laughlin, D.C. et al. (2016). Plant functional traits have globally consistent effects on competition. *Nature, 529,* 204–207.

Laanisto, L. & Niinemets, Ü. (2015) Abiotic polytolerance in woody species. *Global Ecology and Biogeography, 24,* 571-580.

Laliberte, E. & Legendre, P. (2010) A distance-based framework for measuring functional diversity from multiple traits. *Ecology, 91,* 299–305.

Lam, O., Tautenhahn, S., Walther, G., Boenisch, G., Baddam, P., & Kattge, J. (2023). _rtry: Preprocessing Plant Trait Data_. R package version 1.1.0, <https://CRAN.R-project.org/package=rtry>.

Lambers, H. & Oliveira, R.S. (2019) *Plant Physiological Ecology*. Cham, Switz.: Springer. 3rd ed.

Legendre, P. (2018). _lmodel2: Model II Regression_. R package version 1.7-3, https://CRAN.R-project.org/package=lmodel2

Leites, L., & Benito Garzón, M. (2023). Forest tree species adaptation to climate across biomes: Building on the legacy of ecological genetics to anticipate responses to climate change. *Global Change Biology*, 29, 4711–4730. https://doi.org/10.1111/gcb.16711

Levine, J.I., An, R., Kraft, N.J.B., Pacala, S.W., & Levine, J.M. (2024) et al. *Trends in Ecology & Evolution,* 40(2), 147-158.

Levine, J.I., Pacala, S.W. & Levine, J.M. (2024) Competition for time: Evidence for an overlooked, diversity-maintaining competitive mechanism. *Ecology Letters, 27,* e14422.

Lindgren, F., Rue, H. & Lindström, J. (2011) An explicit link between Gaussian fields and Gaussian Markov random fields: the stochastic partial differential equation approach. *Journal of the Royal Statistical Society Series B: Statistical Methodology, 73,* 423-498.

Lindgren, F. & Rue, H. (2015) Bayesian spatial modelling with R-INLA. *Journal of Statistical Software, 63,* 1–25.

MacArthur, R. & Levins, R. (1967) The limiting similarity, convergence, and divergence of coexisting species. *The American Naturalist*, 101, 377–385.

MacLachlan, I.R., McDonald, T.K., Lind, B.M., Rieseberg, L.H., Yeaman, S., & Aitken, S.N. (2021) Genome-wide shifts in climate-related variation underpin responses to selective breeding in a widespread conifer. *Proceedings of the National Academy of Sciences of the United States of America, 118,* e2016900118.

Maclean, I.M.D., Suggitt, A.J., Wilson, R.J., Duffy, J.P., & Bennie, J.J. (2017) Fine-scale climate change: modelling spatial variation in biologically meaningful rates of warming. *Global Change Biology, 23,* 256-268.

Mahony, C.R., MacLachlan, I.R., Lind, B.M., Yoder, J.B., Wang, .T, & Aitken, S.N. (2019) Evaluating genomic data for management of local adaptation in a changing climate: A lodgepole pine case study. *Evolutionary Applications*, *13* 116–131.

Mason, N. W. H., Mouillot, D., Lee, W.G., & Wilson, J.B. (2005) Functional richness, functional evenness and functional divergence: the primary components of functional diversity. *Oikos, 111,* 112–118.

Mayfield, M.M. & Levine, J.M. (2010) Opposing effects of competitive exclusion on the phylogenetic structure of communities. *Ecology Letters, 13,* 1085–1093.

McCulloh, K.A., Augustine, S.P., Goke, A., Jordan, R., Krieg, C.P., O'Keefe, K. et al. (2023) At least it is a dry cold: the global distribution of freeze–thaw and drought stress and the traits that may impart poly-tolerance in conifers. *Tree Physiology*, *43(1),* 1–15.

McCune, B. & Keon, D. (2002) Equations for potential annual direct incident radiation and heat load. *Journal of Vegetation Science, 13,* 603-606.

McElreath, R. (2020) Statistical Rethinking: A Bayesian Course with Examples in R and STAN. CRC Press.

McGill, B.J., Enquist, B.J., Weiher, E., Westoby, M. (2006) Rebuilding community ecology from functional traits. *Trends in Ecology & Evolution 21,* 178–185.

McKinney, M.L. & Lockwood, J.L. (1999(Biotic homogenization: a few winners replacing many losers in the next mass extinction. *Trends in Ecology and Evolution, 14,* 450–453.

McLaughlin, B.C., Ackerly, D.D., Klos, P.Z., Natali, J., Dawson, T.E., & Thompson, S.E. (2017) Hydrologic refugia, plants, and climate change. *Global Change Biology, 23*, 2941-2961.

Microsoft & Weston, S. (2020a) foreach: Provides Foreach Looping Construct. R package version 1.5.1. https://CRAN.R-project.org/package=foreach.

Microsoft & Weston, S. (2020b) doParallel: Foreach Parallel Adaptor for the 'parallel' Package. R package version 1.0.16. https://CRAN.R-project.org/package=doParallel.

Microsoft & Weston, S. (2022) _foreach: Provides Foreach Looping Construct_. R package version 1.5.2, <https://CRAN.R-project.org/package=foreach>.

Microsoft & Weston, S. (2022). _doParallel: Foreach Parallel Adaptor for the 'parallel' Package_. R package version 1.0.17, <https://CRAN.R-project.org/package=doParallel>.

Minhas, S., Hoff, P.D., &Ward, M.D. (2019) Inferential approaches for network analysis: AMEN for latent factor models. *Political Analysis, 27(2),* 208–222.

Monnahan, C. C., Thorson, J.T., & Branch, T.A. (2017) Faster estimation of Bayesian models in ecology using Hamiltonian Monte Carlo. *Methods in Ecology and Evolution, 8,* 339–348.

Montwé, D., Isaac-Renton, M., Hamann, A. & Spiecker, H. (2016) Drought tolerance and growth in populations of a wide-ranging tree species indicate climate change risks for the boreal north. *Global Change Biology*, *22,* 806-815.

Moody, J.A. & Martin, D.A. (2001) Initial hydrologic and geomorphic response following a wildfire in the Colorado Front Range. *Earth Surface Processes and Landforms, 26,* 1049-1070.

Moran, M.E., Aparecido, L.M.T., Koepke, D.F., Cooper, H.F., Doughty, C.E., Gehring, C.A. et al. (2023) Limits of thermal and hydrological tolerance in a foundation tree species (*Populus fremontii*) in the desert southwestern United States. *New Phytologist, 240,* 2298-2311.

Mouchet, M.A., Villéger, S., Mason, N.W.H. & Mouillot, D. (2010) Functional diversity measures: an overview of their redundancy and their ability to discriminate community assembly rules. *Functional Ecology, 24,* 867-876.

Muffler, L., Beierkuhnlein, C., Aas, G., Jentsch, A., Schweiger, A.H., Zohner, C. et al. (2016) Distribution ranges and spring phenology explain late frost sensitivity in 170 woody plants from the Northern Hemisphere. *Global Ecology and Biogeography, 25,* 1061-1071.

Münkemüller, T., de Bello, F., Meynard, C.N., Gravel, D., Lavergne, S., Mouillot, D., Mouquet, N. & Thuiller, W. (2012) From diversity indices to community assembly processes: a test with simulated data. *Ecography, 35,* 468-480.

Münkemüller, T. & Gallien, L. (2015) VirtualCom: a simulation model for eco-evolutionary community assembly and invasion. *Methods in Ecology and Evolution, 6,* 735-743.

Münkemüller, T., Gallien, L., Pollock, L.J., et al. (2020) Dos and don'ts when inferring assembly rules from diversity patterns. *Global Ecology and Biogeography, 29,* 1212–1229.

Muscarella, R. et al. (2017) Demographic drivers of functional composition dynamics. *Ecology 98,* 2743–2750.

Naimi, B., Hamm, N., Groen, T.A., Skidmore, A.K., & Toxopeus, A.G. (2014) Where is positional uncertainty a problem for species distribution modelling. *Ecography, 37,* 191-203.

Neuner, G., Monitzer, K., Kaplenig, D., & Ingruber, J. (2019) Frost survival mechanism of vegetative buds in temperate trees: deep supercooling and extraorgan freezing vs. ice tolerance. *Frontiers in Plant Science, 10,* 537.

Noether, G.E. (1981) Why Kendall Tau? *Teaching Statistics, 3,* 41–43.

Novella-Fernandez, R., Chalmandrier, L., Brandl, R., Pinkert, S., Zeuss, D. & Hof, C. (2024) Trait overdispersion in dragonflies reveals the role and drivers of competition in community assembly across space and season. *Ecography,* e06918.

Nowosad, J. (2018) 'CARTOColors' Palettes. R package version 1.0.0. https://nowosad.github.io/rcartocolor.

Oksanen, J., Simpson, G., Blanchet, F., Kindt, R., Legendre, P., Minchin, P. et al. (2022) _vegan: Community Ecology Package_. R package version 2.6-4, <https://CRAN.R-project.org/package=vegan>.

Oldfather, M.F., Koontz, M.J., Doak, D.F. & Ackerly, D.D. (2021) Range dynamics mediated by compensatory life stage responses to experimental climate manipulations. *Ecology Letters, 24,* 772-780.

Parker, W. & Pallardy, S. (1987) The influence of resaturation method and tissue type on pressure–volume analysis of Quercus alba L. seedlings. *Journal of Experimental Botany, 38,* 535–549.

Parmesan, C. & Yohe, G. (2003) A globally coherent fingerprint of climate change impacts across natural systems. *Nature 421,* 37–42.

Pavanetto, N., Carmona, C. P., Laanisto, L., Niinemets, Ü., & Puglielli, G. (2024). Trait dimensions of abiotic stress tolerance in woody plants of the Northern Hemisphere. *Global Ecology and Biogeography, 33,* 272–285.

Pearl, J. (2009) Causality: Models, Reasoning and Inference. 2nd ed. Cambridge, UK: Cambridge University Press.

Pebesma, E., & Bivand, R. (2023) Spatial Data Science: With Applications in R. Chapman and Hall/CRC. https://doi.org/10.1201/9780429459016

Pebesma, E. (2018) Simple Features for R: Standardized Support for Spatial Vector Data. *The R Journal, 10(1),* 439-446.

Pedersen, T.L. (2020) Patchwork: The Composer of Plots. R package version 1.1.1. https://CRAN.R-project.org/package=patchwork.

Pedersen T (2024) _patchwork: The Composer of Plots_. R package version 1.3.0, <https://CRAN.R-project.org/package=patchwork>.

Peres-Neto, P.R. (2004) Patterns in the co-occurrence of fish species in streams: the role of site suitability, morphology and phylogeny versus species interactions. *Oecologia, 140,* 352–360.

Peres-Neto, P.R., Olden, J.D. & Jackson, D.A. (2001) Environmentally constrained null models: site suitability as occupancy criterion. *Oikos, 93,* 110-120.

Perret, D.L., Evans, M.E.K., & Sax, D.F. (2024) A species' response to spatial climatic variation does not predict its response to climate change. *Proceedings of the National Academy of Sciences of the United States of America, 121,* e2304404120.

Pierce, D. (2019) ncdf4: Interface to Unidata netCDF (Version 4 or Earlier) Format Data Files. R package version 1.17. https://CRAN.R-project.org/package=ncdf4.

Piper, I.F. & Fajardo, A. (2023) Local adaptation to aridity in a widely distributed angiosperm tree species is mediated by seasonal increase of sugars and reduced growth, *Tree Physiology, tpad078.*

Prakash, A., DeYoung, S., Lachmuth, S., Adams, J.L., Johnsen, K., Butnor, J.R. et al. (2022) Genotypic variation and plasticity in climate-adaptive traits after range expansion and fragmentation of red spruce (*Picea rubens* Sarg.). *Philosophical Transactions of the Royal Society B: Biological Sciences, 377,* 20210008.

R Core Team (2023). _R: A Language and Environment for Statistical Computing_. R Foundation for Statistical Computing, Vienna, Austria. <https://www.R-project.org/>.

R Core Team (2024) _R: A Language and Environment for Statistical Computing_. R Foundation for Statistical Computing, Vienna, Austria. <https://www.R-project.org/>.

Revell, L. J. (2024) phytools 2.0: an updated R ecosystem for phylogenetic comparative methods (and other things). *PeerJ, 12,* e16505.

Richard, B. et al. (2021) The climatic debt is growing in the understorey of temperate forests: Stand characteristics matter. *Global Ecology and Biogeography, 30,* 1474–487.

Richardson, D. M., Hellmann, J. J., McLachlan, J., Sax, D. F., Schwartz, M. W., Brennan, J., Gonzalez, P., Root, T., Sala, O., Schneider, S., Ashe, D., Camacho, A., Rappaport Clark, J., Early, R., Etterson, J., et al. (2009) Multidimensional evaluation of managed relocation. *Proceedings of the National Academy of Sciences of the United States of America 106,* 9721–9724.

Ricklefs, R.E. & Travis, J. (1980) A morphological approach to the study of avian community organization. *The Auk*, *97,* 321–338.

Roback, P.J. & Askins, R.A. (2005), Judicious Use of Multiple Hypothesis Tests. *Conservation Biology, 19,* 261-267.

Rosenblad, K. C., K. C. Baer, and D. D. Ackerly. 2023. “Climate Change, Tree Demography, and Thermophilization in Western US Forests.” *Proceedings of the National Academy of Sciences of the United States of America, 120(118),* 1–8.

Rosenblad, K.C. & Sax, D.F. (2017) A new framework for investigating biotic homogenization and exploring future trajectories: oceanic island plant and bird assemblages as a case study. *Ecography 40,* 1040-1049.

Rue, H., Martino, S., & Chopin, N. (2009) Approximate Bayesian inference for latent Gaussian models using integrated nested Laplace approximations (with discussion). *Journal of the Royal Statistical Society, 71(2),* 319-392.

Rueda, M., Godoy, O. & Hawkins, B.A. (2017), Spatial and evolutionary parallelism between shade and drought tolerance explains the distributions of conifers in the conterminous United States. *Global Ecology and Biogeography, 26,* 31-42.

Sakai, A. (1970), Freezing Resistance in Willows from Different Climates. *Ecology, 51,* 485-491.

Savage, J.A. & Cavender-Bares, J.M. (2011) Contrasting drought survival strategies of sympatric willows (genus: *Salix*): consequences for coexistence and habitat specialization, *Tree Physiology*, 31(6), 604–614.

Savage, J.A. & Cavender-Bares, J. (2013) Phenological cues drive an apparent trade-off between freezing tolerance and growth in the family Salicaceae. *Ecology, 94,* 1708-1717.

Sax, D. F., Early, R. and Bellemare, J. (2013) Niche syndromes, species extinction risks, and management under climate change. *Trends in Ecology and Evolution 28,* 517–523.

Scheffers, B. R. et al. (2016) The broad footprint of climate change from genes to biomes to people. *Science 354,* aaf7671.

Schluter, D. (1996) Adaptive radiation along genetic lines of least resistance, *Evolution, 50(5),* 1766–1774.

Schoenherr, A. (2017) A natural history of California. Oakland, California: University of California Press.

Schultheis, E.H., Hopfensperger, K.N., & Brenner, J.C. (2010) Potential impacts of climate change on sphagnum bogs of the southern Appalachian Mountains. *Natural Areas Journal, 30,* 417–24.

Schwartz, M.W., Hellmann, J.J., Jason, M.M., Sax, D.F., Borevitz, J.O., Brennan, J. *et al*. (2012). Managed relocation: integrating the scientific, regulatory, and ethical challenges. *Bioscience, 62,* 732–743.

Seddon, N. (2022). Harnessing the potential of nature-based solutions for mitigating and adapting to climate change. *Science*, *376(6600),* 1410–1416.

Sharma, S. et al. (2022) North American tree migration paced by climate in the West, lagging in the East. *Proceedings of the National Academy of Sciences of the United States of America, 119(3),* e2116691118.

Soliani, C., Mattera, M.G., Marchelli, P. et al. (2021) Different drought-adaptive capacity of a native Patagonian tree species (*Nothofagus pumilio*) resulting from local adaptation. *European Journal of Forest Research, 140,* 1147–1161.

Stan Development Team (2024) RStan: the R interface to Stan. R package version 2.32.6. https://mc-stan.org/.

Stevens, J.T., Kling, M.M., Schwilk, D.W., Varner, J.M., & Kane, J.M. (2020) Biogeography of fire regimes in western U.S. conifer forests: A trait-based approach. *Global Ecology and Biogeography, 29,* 944–955.

Stevens, J.T., Safford, H.D., Harrison, S. & Latimer, A.M. (2015(Forest disturbance accelerates thermophilization of understory plant communities. *Journal of Ecology, 103,* 1253-1263.

Stubbs, W. J. & Wilson, J. B. (2004) Evidence for limiting similarity in a sand dune community. *Journal of Ecology, 92,* 557–567

Svenning, J.-C. & Skov, F. (2004) Limited filling of the potential range in European tree species. *Ecology Letters, 7,* 565-573.

Szeles, J., B-Béres, V., Bozóki, T. et al. (2025) Exploring macroinvertebrate community assembly rules: unraveling the effects of flow intermittency and poor ecological potential on environmental filtering and limiting similarity through functional traits. *Hydrobiologia, 852,* 1825-1846.

Te Grotenhuis, M. et al. (2017) When size matters: Advantages of weighted effect coding in observational studies. *International Journal of Public Health, 62(1),* 163–167.

Terasaki Hart, D. E., & Wang, I. J. (2024) Genomic architecture controls multivariate adaptation to climate change. *Global Change Biology, 30,* e17179.

Thompson, P.L., Guzman, L.M., De Meester, L., Horváth, Z., Ptacnik, R., Vanschoenwinkel, B., Viana, D.S. and Chase, J.M. (2020) A process-based metacommunity framework linking local and regional scale community ecology. *Ecology Letters, 23,* 1314-1329.

Tilman, D. (1980) Resources: A graphical-mechanistic approach to competition and predation. *The American Naturalist, 116,* 362–393.

Tokeshi, M. (1986) Resource utilization, overlap and temporal community dynamics: a null model analysis of an epiphytic chironomid community. *Journal of Animal Ecology, 55,* 491–506.

Trugman, A. T., Anderegg, L. D. L., Anderegg, W. R. L., Das, A. J., & Stephenson, N. L. (2021) Why is tree drought mortality so hard to predict? *Trends in Ecology and Evolution* 36, 1–13.

Trujillo, E., Molotch, N., Goulden, M. et al. (2012) Elevation-dependent influence of snow accumulation on forest greening. *Nature Geosciences, 5,* 705–709.

Tyree, M.T. & Hammel, H.T. (1972) The Measurement of the Turgor Pressure and the Water Relations of Plants by the Pressure-bomb Technique. *Journal of Experimental Botany, 23(1),* 267–282.

United Nations Environment Programme (2024) Emissions Gap Report 2024: No more hot air … please! With a massive gap between rhetoric and reality, countries draft new climate commitments. Nairobi. https://doi.org/10.59117/20.500. 11822/46404.

van der Valk, A. G. (1981) Succession in wetlands—a Gleasonian approach. *Ecology, 62,* 688–696.

Vernon, M.E., Campos, B.R., & Burnett, R.D. (2019) A guide to climate-smart meadow restoration in the Sierra Nevada and southern Cascades. Point Blue Contribution Number 2232. Point Blue Conservation Science, Petaluma.

Villéger, S., Mason, N.W.H. and Mouillot, D. (2008), New multidimensional functional diversity indices for a multifaceted framework in functional ecology. *Ecology, 89,* 2290-2301.

Visakorpi, K., Manzanedo, R. D., Görlich, A. S., Schiendorfer, K., Altermatt Bieger, A., Gates, E., & Hille Ris Lambers, J. (2024) Leaf-level resistance to frost, drought and heat covaries across European temperate tree seedlings. *Journal of Ecology, 00,* 1–16.

Vitasse, Y., Lenz, A., & Körner, C. (2014) The interaction between freezing tolerance and phenology in temperate deciduous trees. *Frontiers in Plant Science, 5,* 541.

Walck, J.L., Baskin, J.M., Baskin C.C., & Francis S.W. (1996) Sandstone rockhouses of the eastern United States, with particular reference to the ecology and evolution of the endemic plant taxa. *Botanical Review 62*, 311–62.

Walsh, B. & Blows, M.W. (2009) Abundant genetic variation plus strong selection = multivariate genetic constraints: a geometric view of adaptation. *Annual Review of Ecology Evolution and Systematics, 40,* 41–59.

Webb, C.O., Ackerly, D.D., McPeek, M.A. & Donoghue, M.J. (2002) Phylogenies and community ecology. *Annual Review of Ecology and Systematics, 33,* 475–505.

White, P. A., Frye, H. A., Slingsby, J. A., Silander, J. A. Jr, & Gelfand, A. E. (2024) Generative spatial generalized dissimilarity mixed modelling (spGDMM): An enhanced approach to modelling beta diversity. *Methods in Ecology and Evolution, 15,* 214–226.

Wickham, H. (2016) ggplot2: Elegant Graphics for Data Analysis. Springer-Verlag New York.

Williams, C.B., Næsborg, R.R., & Dawson, T.E. (2017) Coping with gravity: the foliar water relations of giant sequoia, *Tree Physiology*, *37(10),* 1312–1326.

Williams, S. E., Shoo, L. P., Isaac, J. L., Hoffmann, A. A. & Langham, G. (2008) Towards an integrated framework for assessing the vulnerability of species to climate change. *PLoS Biology, 6,* 2621–2626.

Wood, S. & Scheipl, F. (2020) _gamm4: Generalized Additive Mixed Models using 'mgcv' and 'lme4'_. R package version 0.2-6, <https://CRAN.R-project.org/package=gamm4>.

Wood, S.N. (2017) Generalized Additive Models: An Introduction with R (2nd edition). Chapman and Hall/CRC.

Zellweger, F. et al. (2020) Forest microclimate dynamics drive plant responses to warming. *Science 368(6492),* 772–775.

Zohner, C. M., Mo, L., Renner, S. S., Svenning, J.-C., Vitasse, Y., Benito et al. (2020). Late-spring frost risk between 1959 and 2017 decreased in North America but increased in Europe and Asia. *Proceedings of the National Academy of Sciences of the United States of America*, *117(22),* 12192–12200.

Appendix 1: Supplementary information for Chapter 1

Supplementary Methods

Additional data filtering protocols:

In addition to the data filtering described in the main text, we omitted plots with the following attributes from our analyses: plots with evidence of human-assisted tree regeneration, plots where trees were harvested, plots with evidence of anthropogenic disturbance or treatments, plots where all trees present in the first census died, plots where slope and aspect were not recorded, plots that were not fully surveyed at least twice using FIA's nationally standardized protocol, trees that were recorded but fall outside the standardized plot size, and trees that were suspected of being missed, misidentified, or subject to other complicating events in previous surveys.

Thermal niche modeling:

The niche modeling input data for each method are species occurrence data from FIA plots within the spatial domain described above. In modeling species' thermal niches, we included trees with some attributes that were excluded from the spatiotemporal community comparisons described above: those less than 12.7 cm DBH, more than 7.32 m from the subplot center, recorded in a plot that did not receive a repeat census, recorded in a plot with missing subplots, and recorded in a plot where the habitat status (forested vs. non-forested) changed over time. The purpose of these data filters was to facilitate standardized spatiotemporal comparisons among plots, which was not necessary for niche modeling.

Two thermal niche modeling methods use a smoothing spline regression approach implemented in the mgcv R package (Wood 2017). The response variable is presence or absence of the focal species in each plot, and the predictor is a smooth term for mean annual temperature that uses cubic regression splines. We used a logit link function between predictor and response. For each species, we used the maximum number of knots among smoothing splines supported by the input data. The selection procedure for input data is described below. Smoothing splines were fit by penalized maximum likelihood, where the penalty is a coefficient, lambda (discussed below), multiplied by a "wiggliness" term, the integral over squared second derivatives of the smooth functions. The optimal value of lambda, which determines the balance between under- and over-fitting (or bias and variance), was selected by mgcv's default generalized cross validation (GCV) algorithm.

For each species, regression input data were selected as follows. A minimum convex polygon is circumscribed in geographic space around all plots where the focal species has been recorded as present ("presences"). This polygon is expanded by a buffer that is either 20 km wide or 10% of the maximum distance between any two presences—whichever distance is greater. Then all plots (both presences and absences) within the expanded polygon are selected. (Some species' ranges

extend beyond the western US, and we did not include these portions of their ranges.) Mean annual temperature data for each location were extracted from CHELSA's (Karger et al. 2017, Karger et al. 2018) 30-arcsecond resolution climatologies averaged over the years 1979-2013. We used the output of this regression model to calculate two quantities: the niche optimum and the niche mean. The niche optimum is the temperature at which the probability of presence is greatest. The niche mean is the mean temperature of occurrence, weighted by the probability of occurrence across the domain of the input data. We estimated this quantity for each species by discretizing the temperature domain in increments of 0.01°C. The key difference between the niche mean and the niche optimum is that the mean will be weighted by the frequency of occurrence of different climate types, whereas the optimum is less sensitive to this distribution.

We calculated a third measure of temperature index for each species, a "simple niche mean". This value is the mean temperature of all plots where the focal species has been recorded, weighted by the basal area of the focal species at each of these plots. The basal area values we used are simply the sums of the basal areas of the individual trees present in each subplot. We did not use any of the FIA data set's estimated variables that pertain to larger spatial areas than the plots themselves.

Table S1.1

Predictor	Mean	2.5 Percentile	97.5 Percentile
Mean thermophilization	**0.0391**	**0.0341**	**0.0440**
Intercept	**7.51**	**7.46**	**7.56**
Before vs. after (dummy coding)	**0.0247**	**0.0196**	**0.0299**
Percent conifer	**-0.462**	**-0.479**	**-0.445**
Mean annual temperature (MAT)	**1.99**	**1.93**	**2.06**
Mean annual precipitation (MAP)	**0.157**	**0.0949**	**0.220**
Mean climatic water deficit (CWD)	**1.16**	**0.799**	**1.18**
Fire	0.0452	-0.122	0.212
Insect damage	**-0.312**	**-0.396**	**-0.228**
Change in MAT	**-0.157**	**-0.201**	**-0.113**
Change in MAP	**0.0758**	**0.0421**	**0.110**
Change in CWD	**0.0947**	**0.0596**	**0.130**
Topographic heat load	**0.103**	**0.0867**	**0.119**
Before vs. after: Percent conifer	**0.0247**	**0.0197**	**0.0297**
Before vs. after : MAT	**0.0272**	**0.0181**	**0.0362**
Before vs. after : MAP	-0.00173	-0.00967	0.00620
Before vs. after : CWD	0.00689	-0.00337	0.0171
Before vs. after : Fire	-0.00569	-0.0355	0.0241
Before vs. after : Insect damage	**0.119**	**0.103**	**0.134**
Before vs. after : Change in MAT	**0.0231**	**0.0171**	**0.0291**

Before vs. after : Change in MAP	**-0.0103**	**-0.0153**	**-0.00523**
Before vs. after : Change in CWD	**0.00739**	**0.00223**	**0.0125**
Before vs. after : THL	**-0.0107**	**-0.0158**	**-0.00571**

Means and 95% credible intervals from estimated posterior distributions of fixed effects in hierarchical Bayesian regression models of tree community weighted temperature index over time. Colons denote interaction terms. All terms except mean thermophilization come from a model that used dummy coding for all binary predictors. Mean thermophilization comes from a model that used weighted effect coding for fire and insect damage. Bold text highlights credible intervals that do not overlap zero.

Table S1.2

Model	Predictor	Mean	2.5 %ile	97.5 %ile
Growth	**Mean thermophilization**	**0.0114**	**0.00801**	**0.0148**
Growth	**Intercept**	**7.51**	**7.45**	**7.57**
Growth	**Before vs. after (dummy coding)**	**0.00892**	**0.00537**	**0.0125**
Growth	**Percent conifer**	**-0.477**	**-0.494**	**-0.460**
Growth	**Mean annual temperature (MAT)**	**1.99**	**1.92**	**2.06**
Growth	**Mean annual precipitation (MAP)**	**0.169**	**0.100**	**0.238**
Growth	**Mean climatic water deficit (CWD)**	**1.17**	**1.09**	**1.25**
Growth	Fire	0.0629	-0.116	0.242
Growth	**Insect damage**	**-0.314**	**-0.407**	**-0.224**
Growth	**Change in MAT**	**-0.146**	**-0.194**	**-0.0979**
Growth	**Change in MAP**	**0.0738**	**0.0373**	**0.110**
Growth	**Change in CWD**	**0.0907**	**0.0524**	**0.129**
Growth	**Topographic heat load**	**0.0987**	**0.0826**	**0.115**
Growth	**Before vs. after: Percent conifer**	**0.0153**	**0.0119**	**0.0188**
Growth	**Before vs. after : MAT**	**0.0161**	**0.00985**	**0.0223**
Growth	**Before vs. after : MAP**	**0.00646**	**0.000993**	**0.0119**
Growth	**Before vs. after : CWD**	**0.0181**	**0.0110**	**0.0251**
Growth	**Before vs. after : Fire**	**-0.0298**	**-0.0503**	**-0.00931**
Growth	**Before vs. after : Insect damage**	**0.0266**	**0.0159**	**0.0372**
Growth	**Before vs. after : Change in MAT**	**0.0145**	**0.0104**	**0.0186**
Growth	**Before vs. after : Change in MAP**	**-0.00652**	**-0.0100**	**-0.00305**
Growth	**Before vs. after : Change in CWD**	**0.00563**	**0.00208**	**0.00918**
Growth	**Before vs. after : THL**	**-0.00393**	**-0.00740**	**-0.000483**
Mortality	**Mean thermophilization**	**0.0296**	**0.0265**	**0.0328**
Mortality	**Intercept**	**7.50**	**7.45**	**7.55**
Mortality	**Before vs. after (dummy coding)**	**0.0181**	**0.0146**	**0.0215**
Mortality	**Percent conifer**	**-0.469**	**-0.486**	**-0.451**
Mortality	**Mean annual temperature (MAT)**	**1.98**	**1.91**	**2.05**
Mortality	**Mean annual precipitation (MAP)**	**0.136**	**0.0698**	**0.202**
Mortality	**Mean climatic water deficit (CWD)**	**1.15**	**1.07**	**1.23**
Mortality	Fire	0.0339	-0.154	0.220

Mortality	**Insect damage**	**-0.305**	**-0.400**	**-0.210**
Mortality	**Change in MAT**	**-0.184**	**-0.231**	**-0.138**
Mortality	**Change in MAP**	**0.0820**	**0.0449**	**0.119**
Mortality	**Change in CWD**	**0.0998**	**0.0620**	**0.138**
Mortality	**Topographic heat load**	**0.0965**	**0.0797**	**0.113**
Mortality	Before vs. after: Percent conifer	0.000785	-0.00258	0.00415
Mortality	Before vs. after : MAT	0.00532	-0.000772	0.0114
Mortality	**Before vs. after : MAP**	**-0.00745**	**-0.0128**	**-0.00212**
Mortality	Before vs. after : CWD	-0.00687	-0.0138	1.11E-05
Mortality	**Before vs. after : Fire**	**0.0345**	**0.0145**	**0.0544**
Mortality	**Before vs. after : Insect damage**	**0.0875**	**0.0771**	**0.0979**
Mortality	**Before vs. after : Change in MAT**	**0.00681**	**0.00279**	**0.0108**
Mortality	Before vs. after : Change in MAP	-0.00130	-0.00469	0.00209
Mortality	Before vs. after : Change in CWD	0.00304	-0.000425	0.00650
Mortality	**Before vs. after : THL**	**-0.00817**	**-0.0115**	**-0.00480**
Recruitment	Mean thermophilization	0.000987	-0.000739	0.00271
Recruitment	**Intercept**	**7.51**	**7.45**	**7.58**
Recruitment	Before vs. after (dummy coding)	0.000465	-0.00144	0.00236
Recruitment	**Percent conifer**	**-0.475**	**-0.493**	**-0.457**
Recruitment	**Mean annual temperature (MAT)**	**1.99**	**1.92**	**2.07**
Recruitment	**Mean annual precipitation (MAP)**	**0.170**	**0.0944**	**0.245**
Recruitment	**Mean climatic water deficit (CWD)**	**1.170**	**1.08**	**1.26**
Recruitment	Fire	0.0494	-0.145	0.243
Recruitment	**Insect damage**	**-0.311**	**-0.408**	**-0.214**
Recruitment	**Change in MAT**	**-0.144**	**-0.196**	**-0.0911**
Recruitment	**Change in MAP**	**0.0708**	**0.0312**	**0.110**
Recruitment	**Change in CWD**	**0.0855**	**0.0437**	**0.127**
Recruitment	**Topographic heat load**	**0.0952**	**0.0783**	**0.112**
Recruitment	**Before vs. after: Percent conifer**	**0.00945**	**0.00760**	**0.0113**
Recruitment	**Before vs. after : MAT**	**0.00867**	**0.00532**	**0.0120**
Recruitment	Before vs. after : MAP	8.68E-05	-0.00284	0.00301
Recruitment	**Before vs. after : CWD**	**-0.00530**	**-0.00908**	**-0.00152**
Recruitment	Before vs. after : Fire	-0.00434	-0.0153	0.00662
Recruitment	Before vs. after : Insect damage	0.00522	-0.000474	0.0109
Recruitment	**Before vs. after : Change in MAT**	**0.00340**	**0.00120**	**0.00561**
Recruitment	Before vs. after : Change in MAP	-0.000626	-0.00249	0.00123
Recruitment	Before vs. after : Change in CWD	-0.000500	-0.00240	0.00140
Recruitment	Before vs. after : THL	-0.000282	-0.00213	0.00157

Means and 95% credible intervals from estimated posterior distributions of fixed effects in hierarchical Bayesian regression models of tree community weighted temperature index over time, where effects of individual demographic processes are isolated. "Model" distinguishes three alternate models, each of which reflects the effect on community temperature index of only one demographic mechanism: mortality, growth, or recruitment. Colons denote interaction terms. All terms except mean thermophilization come from a model that used dummy coding for all binary predictors. Mean thermophilization comes from a

model that used weighted effect coding for fire and insect damage. Bold text highlights credible intervals that do not overlap zero.

Table S1.3

Predictor	Mean	2.5 Percentile	97.5 Percentile
Mean thermophilization	0.00208	-0.00151	0.00566
Intercept	**7.35**	**7.28**	**7.41**
Before vs. after (dummy coding)	0.000870	-0.00282	0.00456
Percent conifer	**-0.131**	**-0.165**	**-0.0974**
Mean annual temperature (MAT)	**2.41**	**2.33**	**2.50**
Mean annual precipitation (MAP)	**0.251**	**0.172**	**0.330**
Mean climatic water deficit (CWD)	**0.837**	**0.739**	**0.936**
Fire	0.0863	-0.129	0.302
Insect damage	**-0.152**	**-0.257**	**-0.0476**
Change in MAT	**-0.183**	**-0.239**	**-0.126**
Change in MAP	**0.0859**	**0.0442**	**0.128**
Change in CWD	**0.131**	**0.0855**	**0.177**
Topographic heat load	**0.0754**	**0.0448**	**0.106**
Before vs. after: Percent conifer	**0.00355**	**8.66E-05**	**0.00701**
Before vs. after : MAT	-0.000350	-0.00670	0.00600
Before vs. after : MAP	0.00227	-0.00310	0.00764
Before vs. after : CWD	0.00328	-0.00403	0.0106
Before vs. after : Fire	0.00201	-0.0198	0.0238
Before vs. after : Insect damage	0.00940	-0.000766	0.0196
Before vs. after : Change in MAT	-0.00207	-0.00627	0.00213
Before vs. after : Change in MAP	9.70E-05	-0.00332	0.00351
Before vs. after : Change in CWD	-0.000910	-0.00468	0.00286
Before vs. after : THL	**-0.00347**	**-0.00689**	**-4.27E-05**

Means and 95% credible intervals from estimated posterior distributions of fixed effects in hierarchical Bayesian regression models of sapling community weighted temperature index over time, where the effect of sapling recruitment (as opposed to growth or mortality) is isolated. Saplings are plants with diameter at breast height greater than or equal to 2.5 cm and less than 12.7 cm. Colons denote interaction terms. All terms except mean thermophilization come from a model that used dummy coding for all binary predictors. Mean thermophilization comes from a model that used weighted effect coding for fire and insect damage. Bold text highlights credible intervals that do not overlap zero.

Table S1.4

Predictor	**Mean**	**Standard Deviation**
Mean annual temperature (MAT) (°C)	7.27	3.54
Mean annual precipitation (MAP) (mm)	711	557
Climatic water deficit (CWD) (mm)	5470	3240

Change in MAT (°C)	0.474	0.309
Change in MAP (mm)	-40.7	50.5
Change in CWD (mm)	33.0	22.2
Percent conifer	0.905	0.259
Topographic heat load	0.863	0.139

Summary statistics for continuous predictors in hierarchical Bayesian models of community temperature index over time.

Figure S1.1

Descriptive demography for the trees in the data set. a) Mean 10-year basal area relative growth rates by size class. Growth rate equals the ratio of newly added basal area to initial basal area. b) Mortality rates by size class. Mortality rate equals the number of trees that died in each size class divided by the number of live trees in that size class at the baseline census.

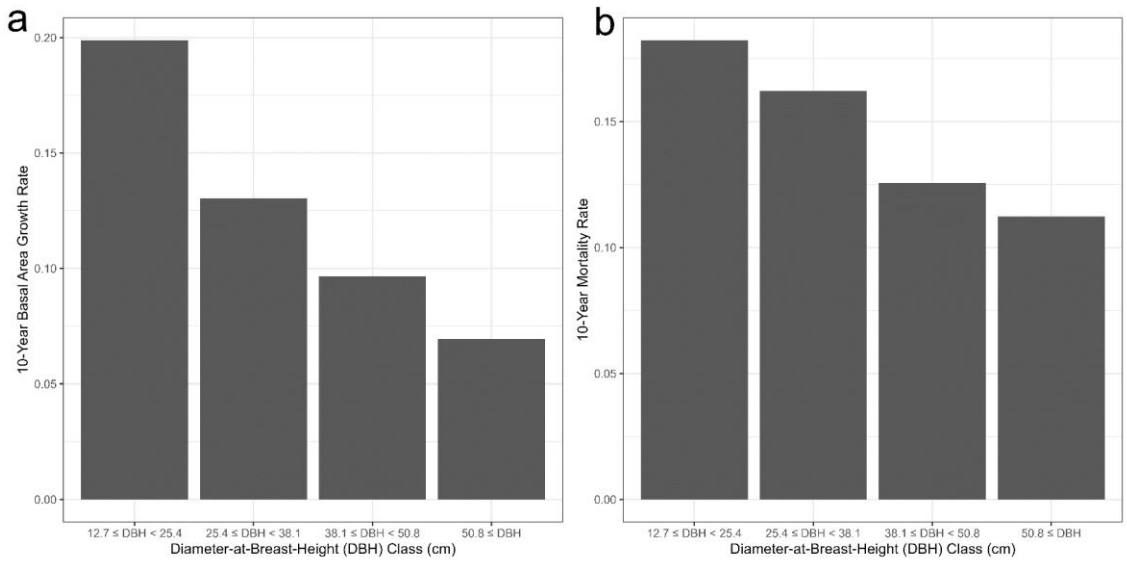

Figure S1.2

Violin plot of 95% credible intervals for standardized effects of fixed predictors on the magnitude of thermophilization in western US sapling communities. Violins can be interpreted as smoothed, horizontally symmetrical histograms, with the vertical axis representing parameter values and the horizontal axis representing probability density. The total area of each violin is set to be equal, so shorter and wider violins correspond to model parameters for which the posterior probability density is more concentrated around the mean. Saplings are plants with diameter at breast height greater than or equal to 2.5 cm and less than 12.7 cm. Results come from hierarchical Bayesian regression models of sapling community temperature index over time, where the effect of sapling recruitment (as opposed to growth or mortality) is isolated. The interval for mean thermophilization represents the effect size for a binary "T1 vs. T2" predictor that distinguishes between repeat tree censuses. The interval shown for each other predictor represent the effect size for the interaction between the named predictor and the "T1 vs. T2" predictor.

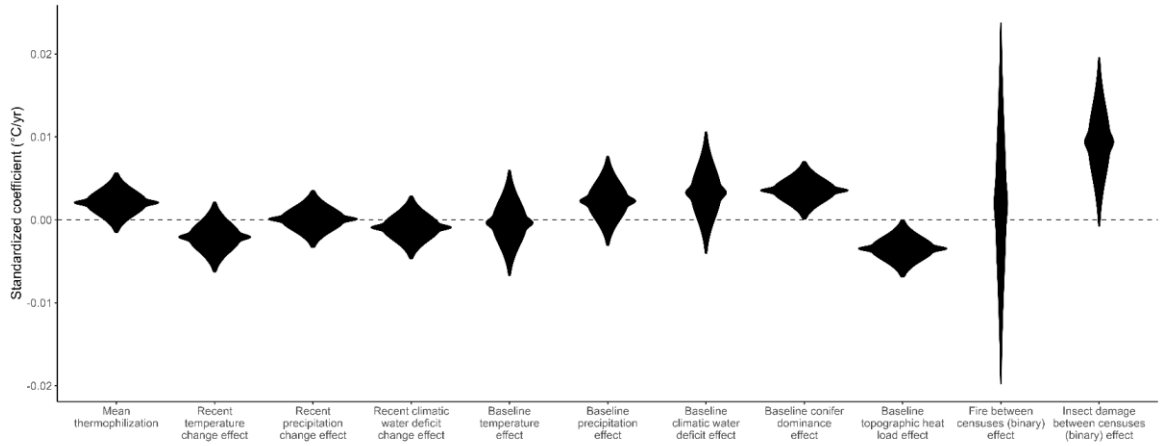

Figure S1.3

Predicted community temperature index values derived from fixed effects only ($X\beta$) in the hierarchical Bayesian regression models that consider all demographic processes together. Values shown are for: a) the baseline census, b) the repeat census, and c) the difference between baseline and repeat censuses.

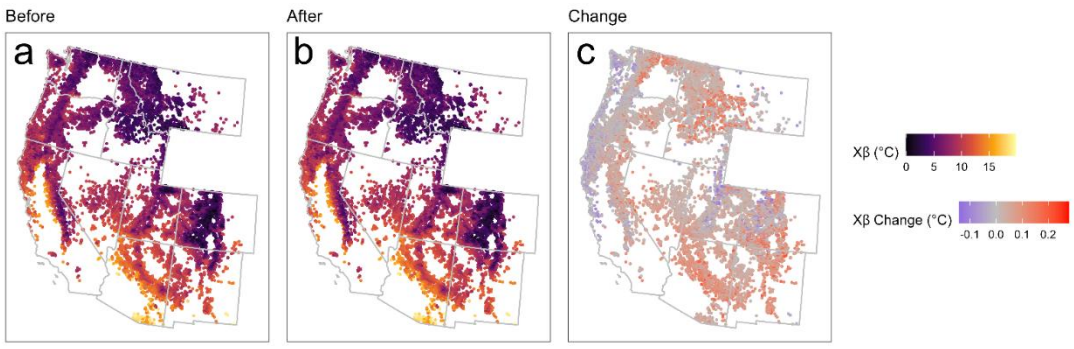

Figure S1.4

Values of random effects in the hierarchical Bayesian regression models that consider all demographic processes together. a) The Gaussian Markov Random Field from which the spatially covarying, plot-level random effect u_i is generated. b) Mean values by plot for the subplot-level, normally distributed random effect v_{ij}.

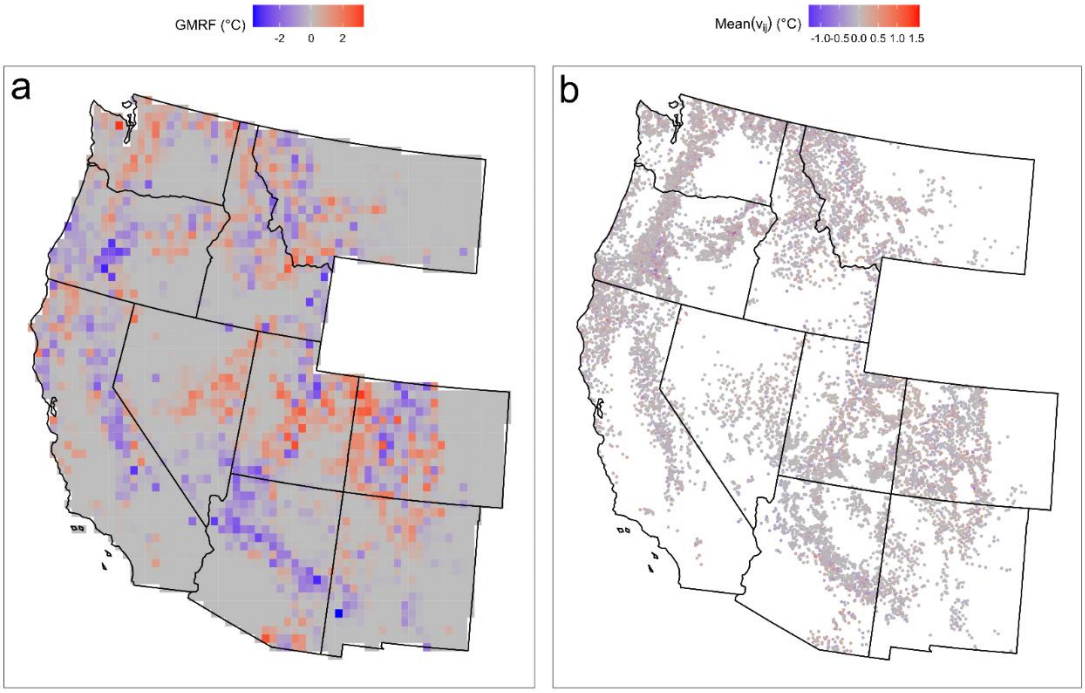

Figure S1.5

Bivariate relationships among the three versions of community temperature index we generated (see Supplementary Methods).

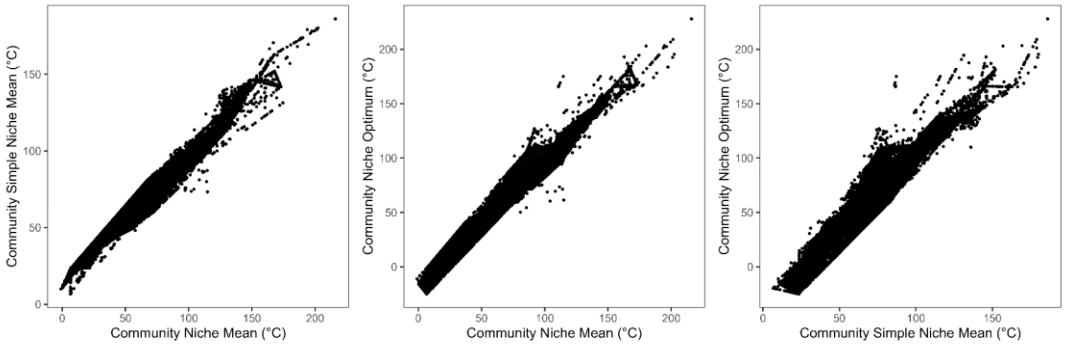

Appendix 2: Supplementary information for Chapter 2

Table S2.1

Data set	Provenance Sites	Genotypes	Replicate clones
Drought sensitivity	38	38	38
Freezing sensitivity	31	36	36
Growth – control	30	40	41
Growth – drought	30	39	39

Summary of replication for each *Salix lemmonii* common garden data set at the levels of provenance site, genotype ("parent plant"), and replicate clone ("cutting" or "common garden plant").

Table S2.2

Coefficient	Estimate	Std. Error	p
Intercept	-0.85	0.015	$> 10^{-15}$
Snowpack	0.052	0.016	0.0024
May Tmin	0.02	0.016	0.21
Actual Evapotranspiration	-0.0047	0.016	0.77

Results from OLS multiple linear regression analysis of common garden turgor loss point data for *Salix lemmonii*. Coefficient estimates represent effect sizes for standardized predictor variables (mean zero, SD 1).

Table S2.3

Coefficient	Estimate	Std. Error	p
Intercept	-0.98	0.21	$> 10^{-4}$
Common Garden Phenotype	0.62	0.24	0.013

Results from OLS linear regression analysis of in situ turgor loss point data for *Salix lemmonii*. Coefficient estimates represent effect sizes for standardized predictor variables (mean zero, SD 1).

Table S2.4

Coefficient	Estimate	Std. Error	p
Intercept	-2.0	0.34	$> 10^{-7}$
Snowpack	-0.24	0.35	0.49
May Tmin	0.81	0.36	0.024
Actual Evapotranspiration	0.051	0.35	0.88

Results from maximum likelihood linear mixed effects model of common garden LT50 data for *Salix lemmonii*. Coefficient estimates represent effect sizes for standardized predictor variables (mean zero, SD 1).

Table S2.5

Coefficient	Estimate	95% CI Lower	95% CI Upper
$Intercept_{Cat1}$	-5.4	-9.1	-2.9
$Intercept_{Cat2}$	-1.5	-3.3	-0.30
Snowpack	-0.37	-1.7	0.91
May Tmin	1.6	0.21	3.7
Actual Evapotranspiration	0.040	-1.2	1.3

Results from Bayesian ordinal logistic GLMM of common garden LT50 data for *Salix lemmonii*. Coefficient estimates represent effect sizes for standardized predictor variables (mean zero, SD 1).

Table S2.6

Coefficient	Estimate	Std. Error	p
Intercept	53	2.3	$<10^{-3}$
Snowpack	1.7	2.2	0.42
May Tmin	0.20	2.2	0.93
Actual Evapotranspiration (AET)	-3.1	2.3	0.19
Drought Treatment	-5.3	2.7	0.06
Drought : Snowpack	-3.1	2.8	0.28
Drought : May Tmin	4.0	2.8	0.17
Drought : AET	1.9	2.7	0.48

Results from maximum likelihood GAMM of common garden biomass accumulation for *Salix lemmonii*. Coefficient estimates represent effect sizes for standardized predictor variables (mean zero, SD 1).

Table S2.7

Trait	Trait	Kendall's tau	p
Drought Sensitivity	Freezing Sensitivity	-0.019	0.90
Drought Sensitivity	Growth, Well-Watered	0.0046	0.97
Drought Sensitivity	Growth, Drought Treatment	0.081	0.53
Freezing Sensitivity	Growth, Well-Watered	0.12	0.49
Freezing Sensitivity	Growth, Drought Treatment	0.21	0.20

Results from Kendall's tau tests of pairwise relationships for population mean trait values for *Salix lemmonii*.

Table S2.8

Trait	Trait	95% CI Lower	95% CI Upper
Drought Sensitivity	Freezing Sensitivity	-0.032	0.016
Drought Sensitivity	Growth, Well-Watered	-0.013	0.011
Drought Sensitivity	Growth, Drought Treatment	-0.022	0.00068
Freezing Sensitivity	Growth, Well-Watered	-1.9	3.2
Freezing Sensitivity	Growth, Drought Treatment	-1.3	4.5

95% confidence intervals for slope terms in ranged major axis regression analyses of pairwise relationships between population mean trait values for *Salix lemmonii*.

Fig. S2.1

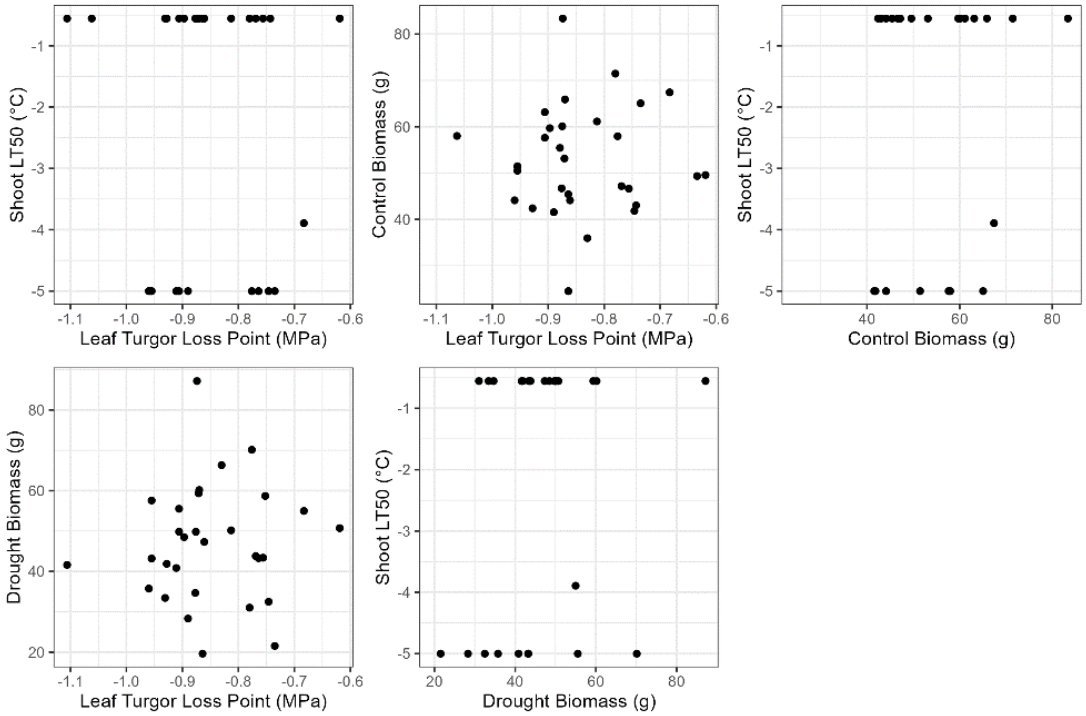

Scatterplots of pairwise relationships among population mean trait values for *Salix lemmonii*. “MPa” denotes megapascals. “°C” denotes degrees Celsius. “mm” denotes millimeters.

Appendix 3: Supplementary information for Chapter 3

Supplementary Methods

Simulated environment:

Each spatiotemporally explicit metacommunity simulation takes place in a square landscape containing 100 randomly placed points or "sites". These sites are discrete patches of inhabitable land surrounded by an uninhabitable matrix. Sites do not have an explicit size or shape, but for the species inhabiting them (see "Simulated species" below), resource limitation is implied by the fact that competition decreases population growth rates. (See "Simulated metacommunity dynamics" below.) As in Thompson et al. (2020), the spatial coordinates of each are drawn from uniform distributions ranging from 1 to 100. Time is represented in 2,000 regular, discrete steps or "generations". The habitat conditions at each site are characterized by a continuous variable, which varies across space and time. To induce realistic spatiotemporal autocorrelation in the habitat variable, I used a spatiotemporal Gaussian process simulation implemented by the sdmTMB_simulate() function in the sdmTMB R package.

Using the above parameter settings, I generated a set of 30 simulated spatiotemporal landscapes, which were used to produce 30 replicate metacommunity simulation runs at each point along the 600-point parameter grid defined by habitat niche breadth and dispersal tendency (see main Methods section).

Simulated species:

Each simulation run begins with 100 species. These species' phylogenetic relationships are simulated using a constant-rates birth-death model implemented by the sim.bdtree() function in the geiger R package. The phylogeny is generated using a stopping criterion of 100 extant species.

For each species, values of three traits are assigned using a macroevolutionary simulation. I simulated these traits via Brownian motion on the simulated phylogeny (see above) using the sim.char() function in the geiger R package. The three traits are the "niche differentiation trait", the "competitive hierarchy trait", and the "habitat niche optimum trait". The niche differentiation trait and the competitive hierarchy trait jointly determine the per capita competitive effect of each species on itself and each other species. Species that differ more in the niche differentiation trait have smaller competitive effects on each other. Species with greater values of the competitive hierarchy trait have stronger competitive effects on others, and others' effects on them are weaker.

The habitat niche optimum trait determines how each species' population growth rates respond to variation in the habitat variable described above. See "Metacommunity dynamics" below for further details on the functional role of each trait.

In all Brownian motion trait simulations, the variance for each trait is set to 1. In the "uncorrelated traits" simulations, covariance for all trait pairings is set to 0. In the "correlated traits" simulations, covariance between the niche differentiation and competitive hierarchy traits is set to 0.8.

Three other traits are held constant among species. Following Thompson et al. (2020), I set r_{max}, the maximum population growth rate for each species, to 5. I selected values of σ and "a", the parameters representing habitat niche breadth and vagility, based on Thompson et al.'s (2020) results, aiming for a combination of parameter values that strikes a balance between maintaining alpha, beta, and gamma diversity—i.e., site-level species richness, among-site species turnover, and landscape-level species richness. I took this approach based on the expectation that a metacommunity dataset is unlikely to yield a signal of competitive niche differentiation if any one of these diversity facets is too low. If alpha diversity is too low, then few species pairs exhibit any cooccurrence, and thus there is little information regarding what trait configurations promote cooccurrence. If beta diversity is too low, then the same species cooccur almost everywhere, and thus cooccurrence rates are high for almost all species pairs, again limiting opportunities to determine what trait configurations promote cooccurrence. Lastly, if gamma diversity is too low, then there are few species in the dataset, limiting statistical power. This approach led me to choose a niche breadth value of 0.5 and a vagility value of 10^{-5}, which yielded relatively high alpha, beta, and gamma diversity in Thompson et al.'s (2020) results. (See the second row of panels in Fig. 4 from Thompson et al. [2020].)

Metacommunity dynamics:

We simulated the abundance of each species at each site for 2,200 generations following the approach of Thompson et al. (2020). In each generation, changes in abundance for a given species at a given site are determined by three processes: immigration from other sites, emigration to other sites, and in situ population growth (or decline), which is driven by the density and traits of competitors, as well as the degree of mismatch between the site's habitat and the species' habitat niche optimum.

As in Thompson et al.'s (2020) equation 1 (shown below), the population size of species i at site x at time t+1 is modeled as the population size before accounting for immigration and emigration, $\text{N-hat}_{ix}(t+1)$ minus emigrating individuals, $E_{ix}(t)$, plus immigrating individuals, $I_{ix}(t)$.

$$N_{ix}(t+1) = \hat{N}_{ix}(t+1) - E_{ix}(t) + I_{ix}(t),$$

Within each site, effects of intraspecific and interspecific competition on population growth rates are modeled using Thompson et al.'s (2020) equation 2, shown below. $N_{ix}(t)$ is the population of species i at site x at time t. r_{ix} is that species' density-independent population growth rate. α_{ij} is the competitive effect of species j on species i. $N_{jx}(t)$ is species j's population size at site x at time (t). In simple terms, each species present at the site depresses other species' population growth rates, as well as its own, based on its population size, as well as the relevant value of α_{ij} (see

below). Stochasticity is introduced by drawing the population size at the next time step from a Poisson distribution. Abundances are forced to be non-negative.

$$\hat{N}_{ix}(t+1) = \text{Poisson}\left(max\left\{N_{ix}(t)\frac{r_{ix}(t)}{1+\sum_{j=1}^{S}\alpha_{ij}N_{jx}(t)}, 0\right\}\right),$$

Density-independent growth for species i at site x at time t follows Thompson et al.'s (2020) equation 3, shown below. The density-independent growth rate increases with r_{max} (the maximum population growth rate for all species) and σ (the niche breadth value for all species) and decreases with the distance between z_i (the species' habitat niche optimum) and $env_x(t)$ (the habitat condition at site x at time t).

$$r_{ix}(t) = r_{max}e^{\left(\frac{z_i - env_x(t)}{2\sigma_i}\right)^2}.$$

Immigration of each species to each site in each generation is modeled according to Thompson et al.'s (2020) equation 4. $E_{iy}(t)$ is emigration of species i from site y at time t, d_x is distance from site y to site x, and L is a parameter determining the decay of dispersal probability with distance. Following Thompson et al. (2020), we use an L value of 0.1.

$$\hat{I}_{ix}(t) = \frac{\sum_{y\neq x}^{M} E_{iy}(t)^{-L_i d_x}}{\sum_{x=1}^{M} E_{ix}(t)}.$$

Alpha, the parameter describing the per-capita competitive effect of each species on each other species (and itself), is computed according to the equation below, in which α_{ij} is the effect of species i on species j, $|m_i - m_j|$ is the distance (always positive) between the two species' values of the niche differentiation trait, and n_i and n_i are the two species' values of the competitive hierarchy trait.

$$\alpha_{ij} = 10^{-5}e^{-(|m_i - m_j| + n_i - n_j)}$$

As described above, for each species at each site, the theoretical maximum growth rate is 5, following Thompson et al. (2020). This is the growth rate a given species would have at a given site when competitors are nonexistent and the species' habitat niche optimum is perfectly matched with the site's habitat.

Null model analyses:

For each of the 48 null model methods, I used the approach of Cornwell & Ackerly (2009) to test whether each simulated dataset exhibits a significant signal of competitive niche differentiation. First, I computed the relevant functional diversity metric for each community in the dataset. I then simulated a null distribution of that metric for each community by recomputing the chosen metric 999 times from "null" datasets produced by the relevant null model permutation algorithm. I then computed a "standardized effect size" ("SES") of each metric for each community by comparing the observed value of the chosen metric against its null distribution, following the commonly used formula, where x is the observed value, μ is the mean of the null distribution, and σ is the standard deviation of the null distribution:

$$SES = (x - \mu)/\sigma$$

Following Cornwell & Ackerly (2009), I used a Mann-Whitney U test to assess whether the SES values were significantly greater than zero.

Table S3.1

Method	Trait Scenario	Positive cases	Negative cases
compnet	Uncorrelated	339	103
fric_c1	Uncorrelated	0	0
fdis_c1	Uncorrelated	338	100
feve_c1	Uncorrelated	323	60
fric_c2	Uncorrelated	299	103
fdis_c2	Uncorrelated	339	103
feve_c2	Uncorrelated	323	60
fric_c3	Uncorrelated	0	0
fdis_c3	Uncorrelated	339	103
feve_c3	Uncorrelated	322	60
fric_c4	Uncorrelated	115	28
fdis_c4	Uncorrelated	183	28
feve_c4	Uncorrelated	81	0
fric_c5	Uncorrelated	260	97
fdis_c5	Uncorrelated	339	103
feve_c5	Uncorrelated	323	60
fric_range	Uncorrelated	87	66
fdis_range	Uncorrelated	96	73
feve_range	Uncorrelated	92	52
fric_t1	Uncorrelated	299	103
fdis_t1	Uncorrelated	339	103
feve_t1	Uncorrelated	323	60
fric_t3	Uncorrelated	292	103
fdis_t3	Uncorrelated	339	103

feve_t3	Uncorrelated	323	60
compnet	Correlated	343	114
fric_c1	Correlated	0	0
fdis_c1	Correlated	341	110
feve_c1	Correlated	282	60
fric_c2	Correlated	321	114
fdis_c2	Correlated	343	114
feve_c2	Correlated	282	60
fric_c3	Correlated	0	0
fdis_c3	Correlated	343	114
feve_c3	Correlated	282	60
fric_c4	Correlated	120	30
fdis_c4	Correlated	164	30
feve_c4	Correlated	58	0
fric_c5	Correlated	291	112
fdis_c5	Correlated	343	114
feve_c5	Correlated	282	60
fric_range	Correlated	86	70
fdis_range	Correlated	94	74
feve_range	Correlated	92	55
fric_t1	Correlated	321	114
fdis_t1	Correlated	343	114
feve_t1	Correlated	282	60
fric_t3	Correlated	311	112
fdis_t3	Correlated	343	114
feve_t3	Correlated	282	60

Summary of replication from simulation study. Values represent the number of analyzable positive case and negative case datasets for each analytical method under each simulation scenario (correlated or uncorrelated species traits).

Figure S1

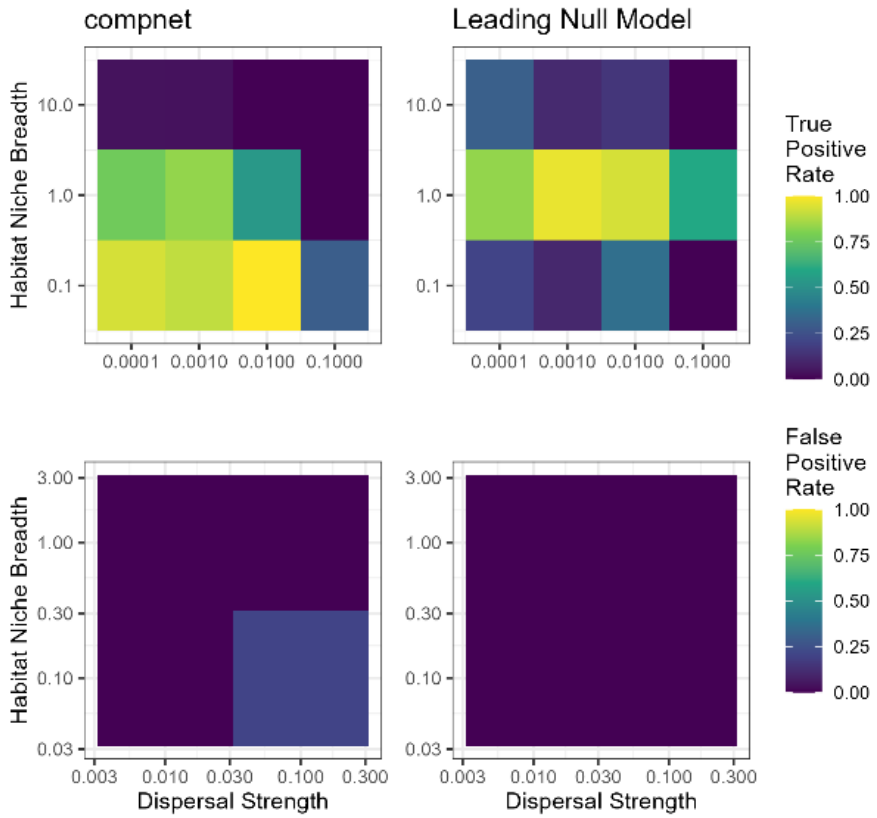

Simulation study results for the uncorrelated traits scenario, summarized by niche breadth and dispersal tendency. The leading null model used the functional dispersion (FDis) metric with the C5 null model permutation algorithm. A "detection" occurs for compnet when over 95% of the posterior samples are less than zero for the interactive effect of species' trait values on cooccurrence. A detection occurs for the null model method when site-level FDis standardized effect sizes ("SES") are significantly greater than zero ($p < 0.05$). The units of habitat niche breadth and dispersal strength are arbitrary.

Figure S2

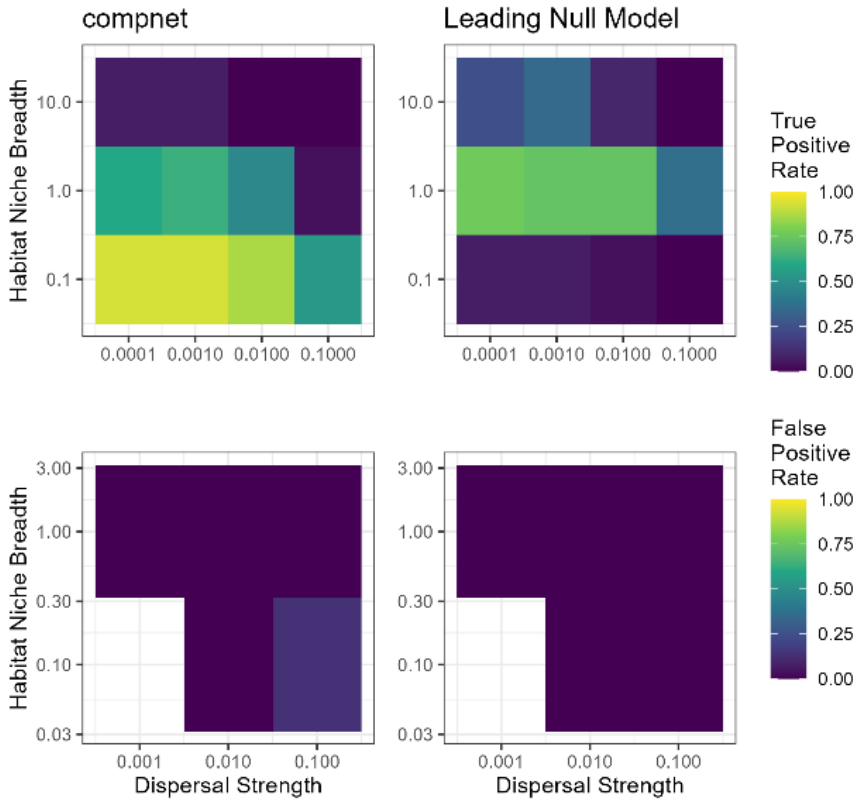

Simulation study results for the correlated traits scenario, summarized by niche breadth and dispersal strength. The leading null model used the functional dispersion (FDis) metric with the C5 null model permutation algorithm. A "detection" occurs for compnet when over 95% of the posterior samples are less than zero for the interactive effect of species' trait values on cooccurrence. A detection occurs for the null model method when site-level FDis standardized effect sizes ("SES") are significantly greater than zero ($p < 0.05$). The units of habitat niche breadth and dispersal strength are arbitrary.